TAMPEREEN TEKNILLINEN YLIOPISTO
TAMPERE UNIVERSITY OF TECHNOLOGY

SANNA KARJALAINEN

STATIC AND DYNAMIC MECHANICAL BEHAVIOR OF BIOMATERIALS IN DRY AND SIMULATED PHYSIOLOGICAL CONDITIONS

Master of Science Thesis

Examiners: Minna Kellomäki
and Kaarlo Paakinaho
Examiner and topic approved in the
Faculty Council of Engineering Sciences
on 9th March 2016

ABSTRACT

SANNA KARJALAINEN: Static and dynamic mechanical behavior of biomaterials in dry and simulated physiological conditions
Tampere University of Technology
Master of Science Thesis, 102 pages
Master's Degree Programme in Material Science
Major: Material Sciences
Examiners: Minna Kellomäki and Kaarlo Paakinaho
Keywords: Static mechanical testing, dynamic mechanical testing, viscoelasticity, biomechanics

Mechanical testing is one of the fundamental procedures when determining the properties of materials. Biomaterials, when used as temporary or permanent replacements of biological tissues inside the human body, demand particularly the characterization of mechanical properties. One of the main requirements is that the biomaterials behave mechanically as similarly to the original tissue and are mechanically compatible with the surrounding tissue after implantation. Since the human body is constantly in motion, the implanted biomaterials are subjected to different fluctuating forces, the prior knowledge of how the biomaterials behave not just during static loading but dynamic as well, is extremely important.

The aim of this thesis was to study the mechanical behavior of different polymer based biomaterials by subjecting them to static and dynamic loadings and also to two different environments, dry ambient laboratory and physiologically simulated condition consisting of aqueous and 37 °C environment. The stress-strain behavior as well as static and dynamic stress relaxation and creep behaviors were considered among other things.

The study revealed that in order to produce reliable mechanical properties of biomaterials intended to be used in the human body, mechanical tests should be conducted in 37°C and at least in aqueous media. Introducing water and warmer environment in tests result in more elastic and flexible behavior of the tested materials. While static tests can be used to determine basic mechanical properties, more extensive knowledge can be obtained by also dynamically loading the samples. Because of the viscoelasticity of polymers, careful design of mechanical tests is important since different parameters such as testing speeds may give different results.

TIIVISTELMÄ

SANNA KARJALAINEN: Biomateriaalien staattinen ja dynaaminen mekaaninen käyttäytyminen kuivassa ja simuloidussa fysiologisessa olosuhteissa
Tampereen teknillinen yliopisto
Diplomityö, 102 sivua
Materiaalitekniikan diplomi-insinöörin tutkinto-ohjelma
Pääaine: Materiaalitekniikka
Tarkastajat: Minna Kellomäki ja Kaarlo Paakinaho
Avainsanat: staattinen mekaaninen koestus, dynaaminen mekaaninen koestus, viskoelastisuus, biomekaniikka

Mekaaninen koestus on yksi olennaisista menettelytavoista määritettäessä materiaalien mekaanisia ominaisuuksia. Biomateriaalit biologisten kudosten tilapäisinä tai pysyvinä korvikkeina ihmiskehossa, vaativat erityisesti mekaanisten ominaisuuksien karakterisointia. Yksi tärkeimmistä edellytyksistä on, että biomateriaalit käyttäytyvät mekaanisesti mahdollisimman samankaltaisesti alkuperäisen kudoksen kanssa ja ovat implantaation jälkeen mekaanisesti yhteensopivia ympäröivän kudoksen kanssa. Koska ihmiskeho on jatkuvassa liikkeessä, implantoidut biomateriaalit altistuvat erilaisille muuttuville voimille, joten tieto miten biomateriaalit käyttäytyvät ei vain staattisen, mutta myös dynaamisen kuormituksen aikana, on erittäin tärkeää.

Työn tavoitteena oli tutkia erilaisten polymeeripohjaisten biomateriaalien käyttäytymistä staattisesti ja dynaamisesti kuormittamalla ja myös kahdessa eri ympäristössä, kuivassa laboratorio ympäristössä sekä fysiologisesti simuloidussa olosuhteessa, joka muodostui vesipitoisesta ja 37 °C asteisesta ympäristöstä. Jännitys-myötymä käyttäytymistä sekä staattista ja dynaamista jännitys relaksaatio- ja virumiskäyttäytymistä tarkasteltiin muun muassa.

Työssä saatiin selville, että ihmiskehossa käytettävien biomateriaalien luotettavien mekaanisten tulosten aikaansaamiseksi testit pitäisi suorittaa 37° C asteessa, ainakin vesiliuoksessa. Veden ja lämpimän ympäristön lisääminen testeihin saa testatut materiaalit käyttäytymään elastisemmin ja joustavammin. Vaikka staattisia testejä voidaan käyttää perusmekaanisten ominaisuuksien määrittämiseen, kattavampaa tietoa saa myös dynaamisesti kuormittavalla näytteitä. Polymeerien viskoelastisuuden vuoksi mekaanisten testien suunnittelu on tärkeää, sillä eri parametrit, kuten testinopeudet, voivat antaa eri tuloksia.

PREFACE

This study was performed in the Biomaterials and Tissue Engineering group in the Department of Electronics and Communication Engineering in the Tampere University of Technology.

First, I would like to express my gratitude to Professor Minna Kellomäki and Ph.D. Kaarlo Paakinaho for offering me this great opportunity and giving me help and guidance during my thesis. I would also like to thank M.Sc. Laura Johansson and M.Sc. Inari Lyyra for providing me with materials for this study. I am also deeply grateful to Raimo Peurakoski for his help with the bone samples and M.Sc. Janne Koivisto for his assistance regarding the mechanical testing manual. I would also like to thank all my colleagues at the Department of Electronics and Communication Engineering for their assistance and for providing a nice working place. For their continuous help in the laboratory, I would like to thank Heikki Liejumäki and Suvi Heinämäki. Finally, I would like to thank my family and friends for their support.

Tampere, 22.11.2016

Sanna Karjalainen

TABLE OF CONTENTS

ABBREVIATIONS

°C	Celsius degree
ε	Strain
σ	Stress
DSC	Differential scanning calorimetry
E	Modulus
GPa	Gigapascal
Hz	Hertz
PEG	Polyethylene glycol
PLA	Polylactide
PLCL	Poly(L-lactide-co-ε-caprolactone)
MCP	Metacarpophalangeal joint
MPa	Megapascal
T_g	Glass transition temperature
TCP	Tricalcium phosphate
TGA	Thermogravimetric analysis

1. INTRODUCTION

In its basic form mechanical testing incorporates a testing apparatus in an ambient laboratory environment in order to determine the mechanical behavior of materials under investigation. The mechanical behavior of materials refers to the responses a mechanical stimulus such as tensile or compressive force causes to the materials. The force can be delivered with an increasing amount of load resulting in deformation and possible facture of the specimen or the load can be delivered dynamically with a specific amount of load for predetermined number of cycles or until failure occurs due to fatigue of the specimen. [1,2]

Determining mechanical properties is important for designing high quality end products that work as intended and have the properties that ensure that the mechanical forces acting on the product during its lifetime can be withstand. For new materials the mechanical properties need to be determined, whereas for familiar materials the mechanical properties need to be confirmed. [1] Mechanical tests concerning medical implants and the biomaterials they are made of are especially important due to the extreme conditions inside the human body and the different tissues they are replacing. For example, materials replacing bone has to have different mechanical properties compared to materials that can be used in cardiovascular implants or in plastic surgery to replace soft tissues. It is important to know the mechanical properties of the implant as well as the tissue the implant is replacing and further in contact with upon implantation, be it hard or soft tissue. For example, the mechanical properties of bone have been widely studied, because the bones in the human body have to withstand a lot of different forces during a lifetime and any possible bone implants have to be able to do the same. One example of the problems associated with bone implants is stress shielding, which can cause bone resorption, implant loosening and finally failure of the implant since the implant as a stiffer material takes most of the loads the body usually experiences and shields the neighboring bone from the normal stresses that usually help to keep the bone strong and healthy. Thus, determining and comparing the elastic modulus of tissues and the replacing biomaterials is one of the first things to do when designing implants. [3-5]

The purpose of this thesis was to learn the use of a novel mechanical testing device and utilizing it in order to perform both static and dynamic tests in ambient laboratory environment as well as in simulated physiological condition with aqueous and 37 °C environment. Polymer based biomaterials, as scaffold constructs and as materials, were chosen to be tested along with biological material representation of cancellous bone of a pig tested dry. Part of the thesis was to also produce a simple manual for the mechanical testing device (Instron Electropuls E1000).

2. STATIC AND DYNAMIC MECHANICAL TESTING

Fundamental mechanical properties can be ascertained from a mechanical test by subjecting a specimen to a steadily increasing load until necessary properties can be determined or failure of the specimen occurs. However, when more complex mechanical behavior, such as fatigue, needs to be determined, subjecting a specimen to multiple cycles of loading and unloading is used instead. These loading conditions can be characterized as static (also referred as quasi-static) and dynamic, respectively. [6,7]

Where static mechanical testing imposes a load on a specimen using a fixed slow speed and is usually not time-dependent, dynamic mechanical testing is time-dependent and imposes the load or strain on to the specimen periodically or cyclically, using the same modes of loading (e.g. tensile) as in the static tests. The periodic or cyclic loading uses typically a waveform such as sinusoidal, with the speed rate determined by frequency. [1,7]

Another way to distinguish between static or more specifically quasi-static and dynamic testing is by the strain rate or the velocity of the test. Quasi-static tests generally use strain rates of 10^{-2}-10^{-3} s^{-1} or constant velocity without acceleration whereas dynamic tests generally use higher strain rates, for example dynamic tension and compressive tests can use rates from 10^{-1} to 10^{2} s^{-1} or accelerating velocity. [7]

Static mechanical testing done to obtain basic mechanical properties is the most common and traditional method of testing but dynamic mechanical testing is especially important in the biomedical field, because the loads acting on the body are seldom static but dynamic. For example, the strain rates for slow walking and more active movement can be 10^{-4} s^{-1} and 10^{-3} s^{-1}, respectively but walking and running are repetitive actions and can subject the body to cyclic mechanical loading and fatigue. Dynamic tests can use loading frequencies ranging from 10^{-2} to 10^{2} Hz, but tests on biomaterials and biomedical devices use approximately 1 Hz frequency, since it is similar to a walking motion and the beating of a heart (1.2 Hz). Using larger frequencies can also subject a polymeric biomaterial to intrinsic heating and thus change the mechanical behavior. [1,2,8-10]

2.1 Stress-Strain

Mechanical testing is performed to determine the mechanical behavior of materials by applying an external force. The structural mechanical properties of tested samples can be determined from the relationship between the load and the displacement caused by the applied force, however, the basic material properties of the tested samples can be obtained by analyzing the stress-strain curves, making stress and strain important concepts of mechanical testing. Stress can be described as the force acting on the material surface when it is being loaded and strain as the response (deformation) to that stress. [2]

There are two different ways to refer to stress and strain, by engineering stress and engineering strain or by true stress and true strain. Engineering stress is the direct load (F) applied to a specimen divided by its original cross-sectional area (A_0) (Figure 1), whereas true stress takes into account the cross-sectional area (A_i) of the specimen where the deformation occurs due to the load. Engineering and true stresses and strains are used interchangeably during elastic deformation, but true stress and strain are usually used during plastic deformation, when the specimen changes shape more significantly. [1]

Engineering stress can be thus expressed as

$$\sigma = \frac{F}{A_0} \tag{1}$$

and true stress as

$$\sigma_T = \frac{F}{A_i} \tag{2}$$

Engineering strain describes the change in the specimen length (Δl) compared to the original length (l_0), whereas true strain can be described as the natural logarithm of the current length divided by the original length. [1]

In other words, engineering strain is

$$\varepsilon = \frac{l_i - l_0}{l_0} = \frac{\Delta l}{l_0} \tag{3}$$

and true strain is

$$\varepsilon_T = ln\frac{l_i}{l_0} \tag{4}$$

Engineering stress/strain are more often used since determining true stress/strain require the right equipment in order to define the changing values of area and length of samples during testing [1,7].

The acting loads are measured as Newtons (N) and the affected areas as mm^2, thus the dimensions for the stresses above are N/mm^2 or in other words megapascals MPa, whereas the strains are dimensionless or mm/mm. However, common way to refer to strain is also by using percentages. [11]

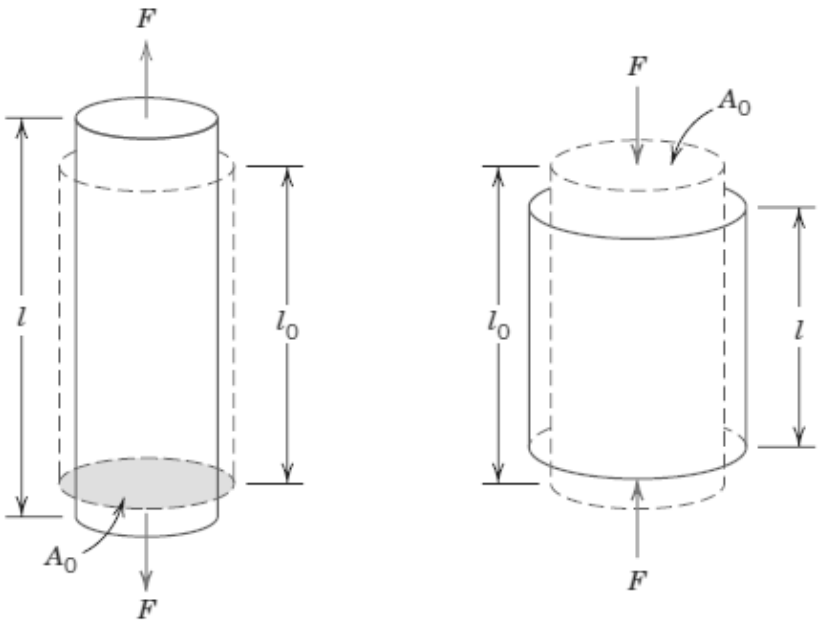

Figure 1. *Schematic illustration on applied load affecting the specimen length [1]*

The stresses and strains mentioned above are applicable for tensile and compressive loading modes. The distinction between tensile and compressive modes is usually indicated by using either positive sign for tensile and negative sign for compressive since during tensile load the change in specimen length is positive and in compression the change is negative. In tensile and compressive stress, the acting load is normal to the cross-sectional area making them uniaxial. Mechanical testing can be done using different kinds of loading modes depending on the specimen material, the service conditions of the specimen and what kind of property information is being investigated. The four main loading modes are tension, compression, shear (torsion) and bending. In this thesis only tensile and compressive loads are considered. [1,2,11]

Using tension as the main load mode in mechanical testing is one of the most common ways to evaluate materials, because of the many mechanical properties it exposes. In the basic form of a tension test, a specimen is gripped from both ends of the specimen and pulled upwards with increasing amount of load, resulting in elongation and usually

fracture of the specimen. The amount of load causing the deformation of the sample and the elongation of the specimen are measured and displayed as a stress-strain curve. [1] Figure 2 shows typical curves for polymeric, metallic and ceramic materials. [8]

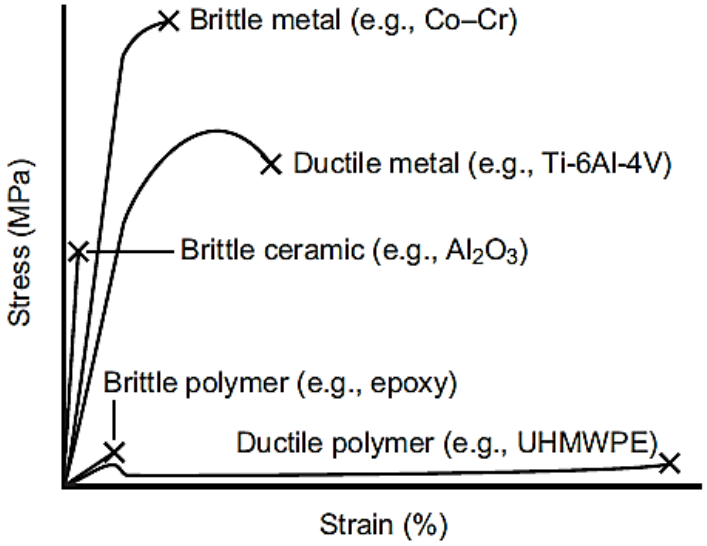

Figure 2. *Tensile stress-strain curves for different materials [8]*

The first linear part of the tensile stress-strain curve is the elastic region where the deformation is elastic and nonpermanent. The relationship between stress and strain is proportional and is known as Hooke's law

$$\sigma = E\varepsilon \qquad (5)$$

The constant E is called (Young's) modulus or modulus of elasticity and represents the stiffness of a material or resistance to the deformation. In some cases, for example for some polymers, the elastic region is not linear, so tangent or secant modulus is used instead and calculated as shown in Figure 3. For metals and ceramics, the values of modulus of elasticity are comparable but for polymers they tend to be lower. If the material is isotropic then the modulus of elasticity is the same in every direction, but if the material is anisotropic, the value of E can vary. [1] For example, the elastic modulus of human long bone parallel to the bone axis can be measured as 17.4 GPa, but 11.7 GPa when in perpendicular to the bone axis. [12] In addition, during testing the temperature, the environment, the test speed, as well as the properties of the samples such as density and porosity, can change the value of elastic modulus for the same material. [7,13,14]

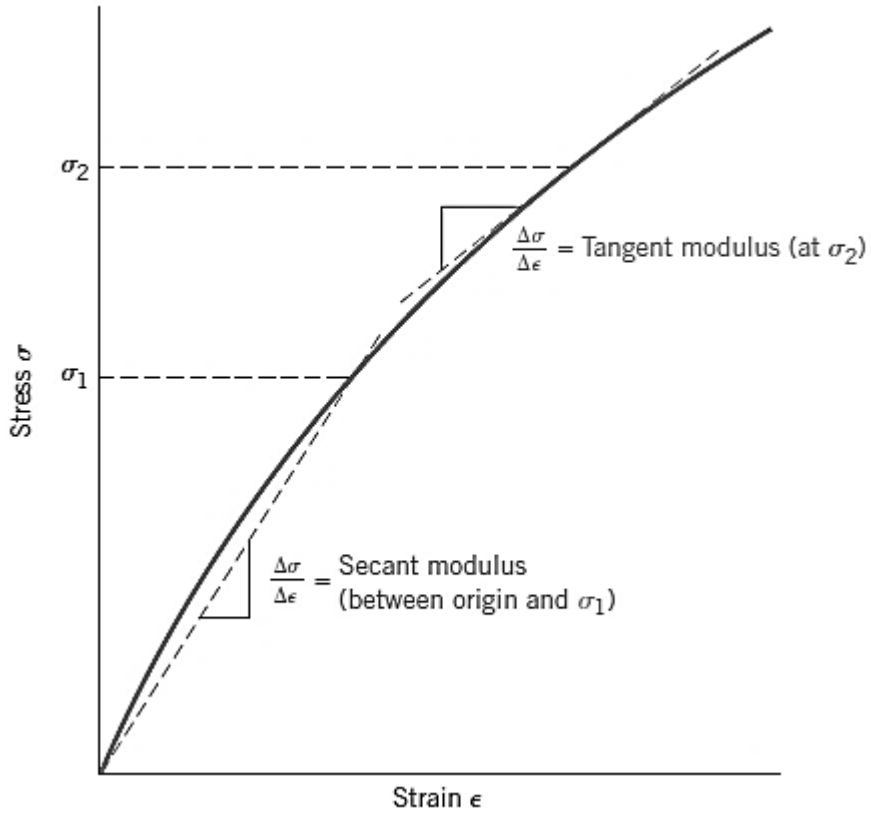

Figure 3. *Representation of a nonlinear elastic region[1]*

Usually it is assumed that the elastic deformation is independent of time, meaning that instantaneous elastic strain caused by stress, stays constant over the period of loading and when the stress is released, the strain returns to zero. However, for polymers it is typical that the elastic deformation is time-dependent, the elastic deformation continues after load is applied and the recovery of strain is not instantaneous, but need certain amount of time. This behavior is known as anelasticity in case of metals and ceramics, but viscoelasticity when concerning polymers since the significance is greater. [1]

After elastic region in the stress-strain curve, deformation is no longer reversible, but permanent. The change from elastic region to plastic region is termed yielding and the stress at the point of yielding is known as yield strength σ_y. The transition from elastic region to plastic region is not always easy to establish due to gradual transition and thus to determine the yield strength from the stress-strain curve, parallel line to the initial linear elastic portion is used. The line is constructed so that it is offset with certain amount of strain, most often 0.002 (0.2%) and the yield strength is the point where the line and curve intersects and is known as (0.2 % -) offset yield strength. [8,15,16] If the elastic portion of the stress-strain curve is nonlinear, the yield strength is determined by using stress that produces some amount of strain. Some materials can experience two yield points, first initial maximum followed by a lower stress. This is typical behavior for linear polymers (Figure 4) and the maximum stress is used as the yield strength. [15]

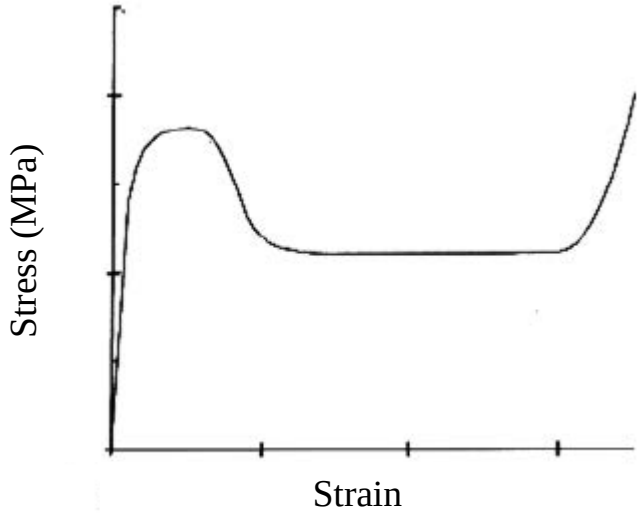

Figure 4. *Schematic illustration of maximum and minimum yield points in the stress-strain curve of linear polymer. Adapted from [15]*

Some brittle ceramics may experience fracture before yielding and thus do not have a yield strength, only tensile strength, the next important mechanical property found in the tensile stress-strain curve. [2]

Tensile strength or ultimate strength is located at the highest point of the curve. For ductile materials ultimate strength corresponds to the start of necking, which ultimately leads to a fracture at a level of stress known as fracture strength. However, for brittle materials, the ultimate strength is the stress where fracture occurs and either ultimate or fracture strength can be used. [1,15]

Brittle materials compared to ductile materials have undergone little or no plastic deformation before fracture occurs. The degree of plastic deformation sustained at fracture is known as ductility and can be described as percent elongation

$$\%EL = \left(\frac{l_f - l_0}{l_0}\right) \times 100 \qquad (6)$$

where l_0 represent the initial specimen length and l_f the length at fracture or as percent area fraction:

$$\%RA = \left(\frac{A_f - A_0}{A_0}\right) \times 100 \qquad (7)$$

where A_0 represents the initial cross-sectional area and A_f , the area of the fracture. [1,2,8]

The stress-strain curve can be also used to determine the modulus of resilience (U_r) and modulus of toughness (U_t). Resilience represents the ability of a material to absorb energy during elastic deformation and then recover said energy when unloaded, whereas toughness represents the ability to absorb energy up to fracture. [1,7]

In contrast to tensile test, in the basic concept of a compressive test a specimen is subjected to a load by squeezing it between two flat surfaces or platens. There are multiple reasons why compressive tests are done to materials instead of the usually easier tensile tests. The most common reasons are that the material needs to withstand compressive loads in service, the workability of the material is under investigation, the material is brittle or porous or the behavior of the material under larger strains is preferred. Also smaller specimens can be used. [1,7,17] Compression tests have two limiting problems that can cause varying distributions of stress and strain and thus cause difficulties in interpretation of the results. Buckling is a result of compressive loads on too long and slender specimens and barreling or bulging of the specimen is caused by friction between the ends of the specimen and the loading surfaces. Buckling can be avoided by using specimens with low height-to-diameter ratio and barreling by lubrication. [17]

The resulting stress-strain curve from a compressive test is similar to the one resulting from a tensile test however, the values for mechanical properties from compressive test tend to be larger [10,18]. For example, tensile tests of cortical bone resulted reportedly in tensile strength of 92-188 MPa and elastic modulus of 7.1-28.2 GPa, whereas compressive tests resulted in compressive strength of 133-295 MPa and elastic modulus of 14.7-34.3 GPa. [10,18] Figure 5 shows a compressive stress-strain curve of cancellous bone. Three distinct regions can be seen. First is the linear elastic region showing elastic behavior at low stresses, then plastic region and finally fracture region also known as densification where stress increases sharply. [10] In case of some foams and porous structures, the middle region exhibits plateauing, in other words there is no increase in stress while the deformation continues, since the pores are collapsing due to the compressive forces. When all the pores have collapsed, the stress increases, because the material becomes denser and thus stiffer. [10,19]

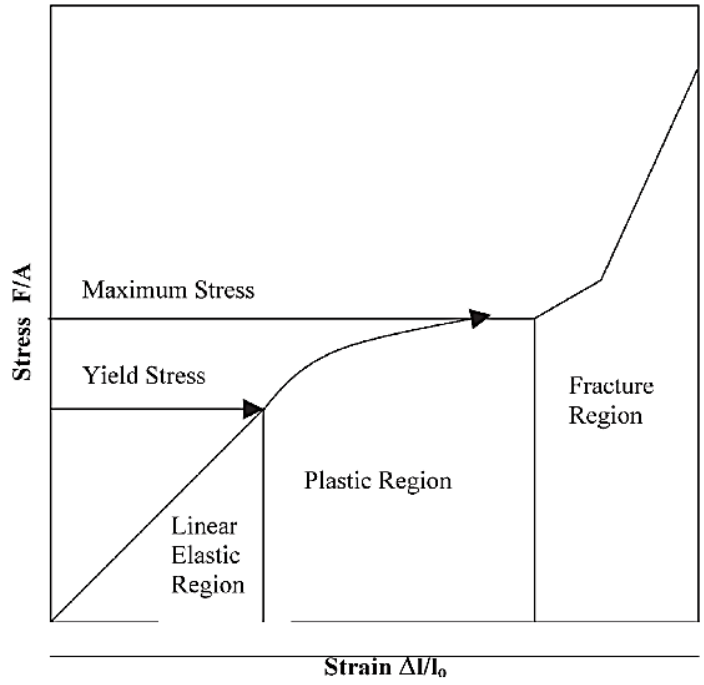

Figure 5. *Typical compressive stress-strain curve for cancellous bone [10]*

Since elastic and plastic deformation behaviors are similar in compression and in tension, the elastic modulus and yield strength can be determined from the compressive stress-strain curve the same way as from tensile stress-strain curve, even though the values might differ [20].

2.2 Viscoelasticity

Viscoelasticity is a combination of elastic and viscous behavior. Under static load elastically behaving material deforms instantaneously and recovers fully once the load is removed. Viscous material however, experiences delayed deformation, which is permanent. As a result, under a load viscoelastic material experiences immediate elastic strain but is followed by time-dependent strain. Many materials associated with biomedical application are viscoelastic in nature, especially biological tissues in body temperature and polymers particularly near or above the glass transition temperature. Additionally, some metals and ceramics can behave viscoelastically in elevated temperatures. Under quasi-static conditions, creep and stress relaxation deformations are typical for viscoelastic materials but cannot be ascertained from the stress-strain curves and need experiments especially for them. [1,6-8,21,22]

The viscoelastic behavior of materials can be predicted by constitutive mathematical models, in which purely elastic elements are represented by springs ($\sigma=E\varepsilon$,) and purely viscous elements as dashpots ($\sigma=\eta\dot{\varepsilon}$, where η is the viscosity coefficient and $\dot{\varepsilon}$ the strain rate). Because of the complexity of viscoelastic materials, in the mathematical models both elements are present. In Maxwell model the elastic and viscous elements are

connected in series, while in Kelvin/Voigt model the elements are connected in parallel. Both of these models present some issues regarding creep and stress relaxation predictions, so standard linear solid model can be used instead, where one spring element is parallel with the elements of Maxwell model.[7,16,22-25] Without going into details, the elements, models and mathematical equations are presented in Figure 6.

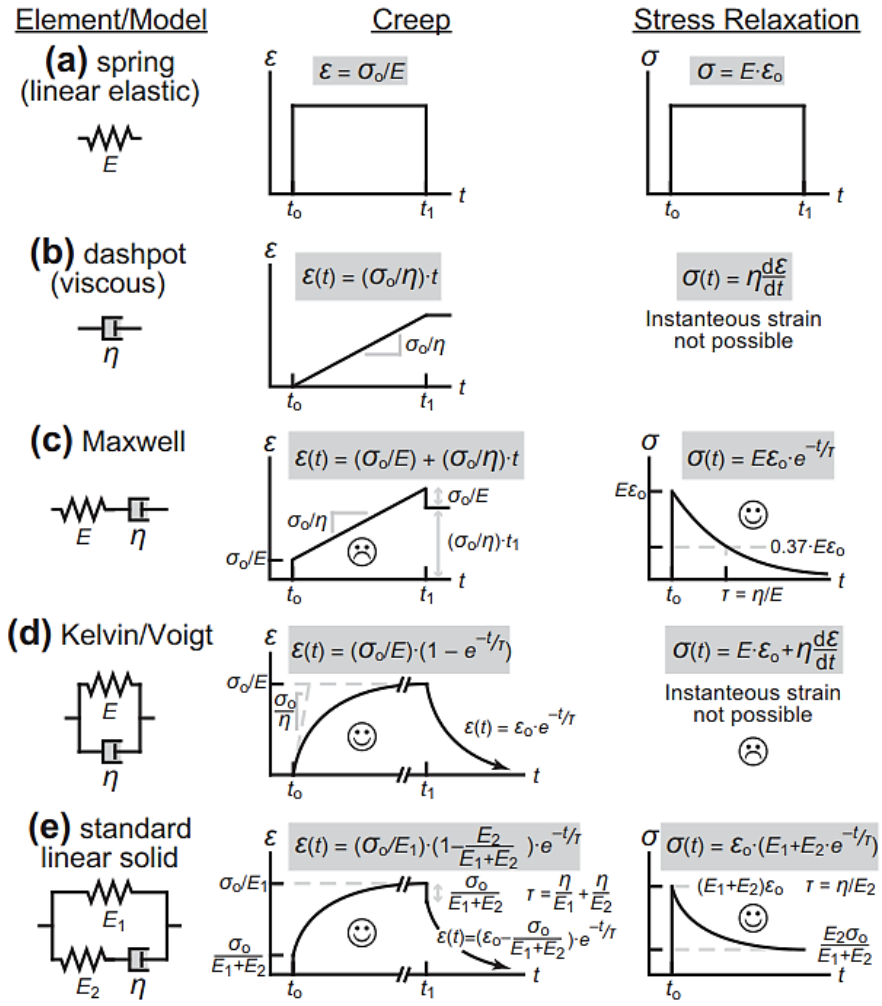

Figure 6. *The constitutive mathematical models for viscoelastic materials [7]*

The basic concepts of creep and stress relaxation are explained in the following sections.

2.2.1 Creep

Creep can be defined as permanent and time-dependent deformation under constant stress even below yield stresses and sometimes at an elevated temperature. Creep is experienced by many materials, especially by polymers even at room temperatures but also by metals and ceramics at higher temperatures. Typical creep tests are conducted usually by constant tensile stress but ceramics often experience creep at elevated temperatures when exposed to compressive stresses, so high temperature compressive

creep tests are typical for ceramics. The stress is kept constant and strain is measured as a function of time (Figure 7). [1,2,6,26,27]

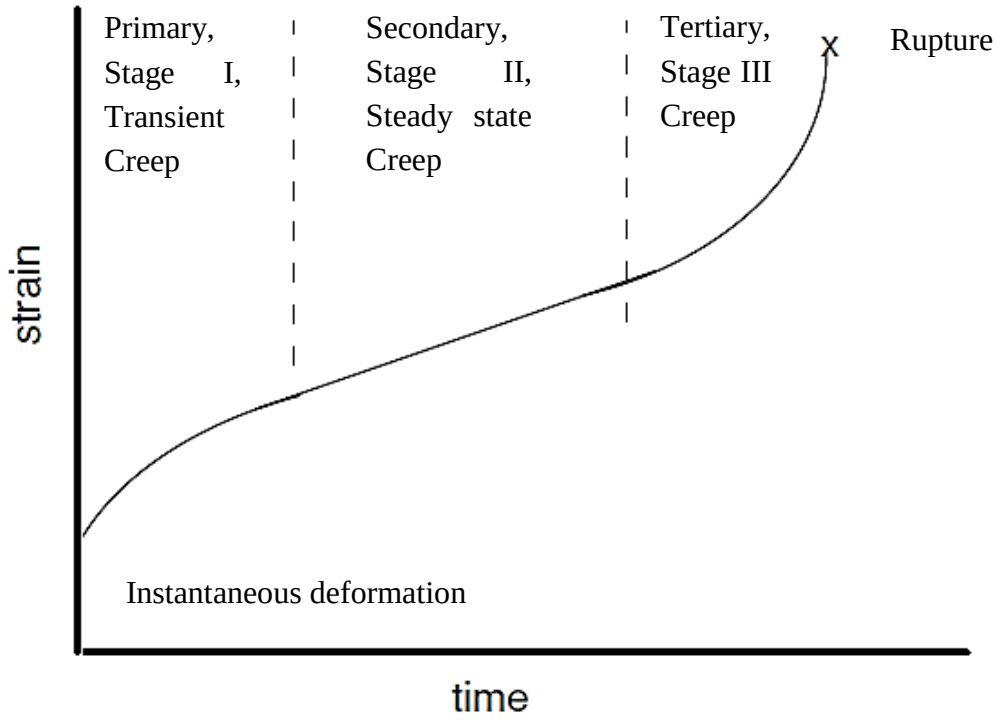

Figure 7. *Typical creep curve. Adapted from [1,2,26]*

Three stages can be recognized from creep behavior. After the instantaneous deformation due to ramping to the wanted stress value, stage I of primary or transient creep occur showing decreasing creep rate, followed by stage II of secondary or steady-state creep where the creep rate is constant. The final stage III is tertiary creep with increasing creep rate ending in rupture.[1,2,7] In some cases the test can be ended before transition to stage III can occur. Figure 8 represents a common creep behavior of a viscoelastic material that experiences strain recovery after the constant load has been removed.[21]

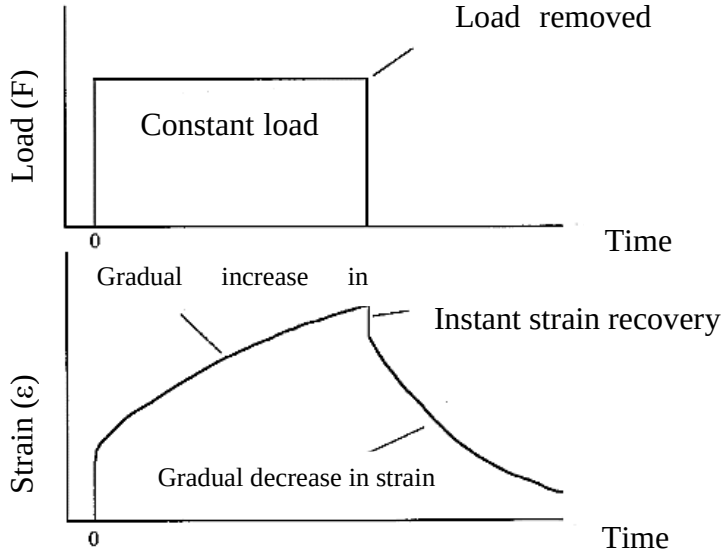

Figure 8. *Creep behavior of a viscoelastic material [21]*

Creep is heavily influenced by temperature and stress values. In some instances, it is possible that at low temperatures and stresses, only stages I and II occur and at high enough temperatures and stresses, the transition from stage I to stage III can occur so rapidly that stage II is not seen in the creep curve. Also many materials have a minimum temperature below where creep does not occur but show increased creep rate at elevated temperatures. Materials capable of plastic deformation do not have a minimum stress level where creep does not occur but increase in stresses result in increased creep rates in all stages. [6]

Determining creep behavior dynamically is also possible. Cyclic creep test can be conducted by subjecting the sample to oscillating stress for a specific number of cycles and then determining the amount of creep from the elongations at the start and end of the test. [28]

2.2.2 Stress Relaxation

Where creep experiments rely on constant stress, stress relaxation experiments use constant strain. The specimen is deformed rapidly until predetermined strain level and kept constant for predetermined amount of time. The stress needed to keep the strain constant is measured as a function of time. Typically, the stress experiences a rapid decline at the beginning and then plateauing towards the end. Unlike long creep experiments, stress relaxation tests do not end up in failure. The decrease of the stress is typical for viscoelastic materials due to processes of molecular relaxations within the materials. [1,6] Figure 9 represents a typical stress relaxation curve of a viscoelastic material [21]. Determining the stress relaxation behavior of biomaterials is important in applications where deformation is kept constant, for example, when filling defect

cavities or when the biomaterial is related to tissues like ligaments and tendons that experience stress relaxations. [8,20,29]

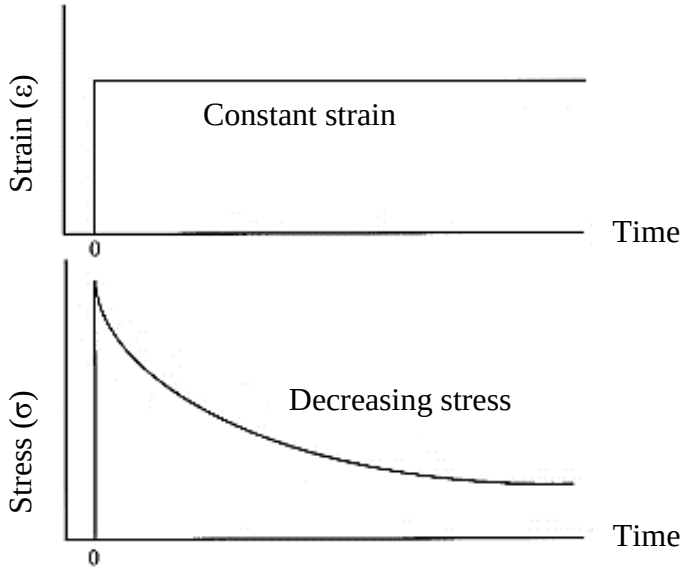

Figure 9. *Typical stress relaxation of a viscoelastic material. Adapted from [21]*

As with creep, stress relaxation behavior can be determined cyclically by subjecting the sample to oscillating elongation and observing the decrease in stress at the end of the test compared to the beginning [28].

2.2.3 Hysteresis

Hysteresis curves are obtained by cyclically loading a sample and producing loading and unloading curves. The size and shape of the curves depend on the material being tested. During deformation by external force, elastic material stores all of the energy applied and has the same loading and unloading curves in a stress-strain graph, but viscoelastic material dissipates some of the energy during deformation, resulting in separate loading and unloading curves in the stress-strain graph. The area between the curves is known as hysteresis or energy dissipation and can be determined by subtracting the area underneath the unloading curve from the area underneath the loading curve.[7,21,25,30]

2.3 Fatigue

Fatigue of a material occurs when it is subjected to repeated actions of stress or strain. When materials are exposed to dynamic and changing stresses long enough, fatigue failure can result at stress levels lower than the tensile or yield strength determined from a static test. [26] Fatigue failure is typical for metals and polymers but not for ceramics, since they rarely experience plastic deformation [31]. Fatigue as a phenomenon is

important in biomedical applications, because the human body is constantly in motion both voluntary and involuntary, and both hard tissues and soft tissues are subjected to different repeated and cyclic stresses. [6]

Fatigue can be divided in to three stages; crack nucleation, crack growth and fatigue fracture. The initiation of cracks result from inhomogeneous stress levels at microscopic levels, due to defects or other structural irregularities. Then those cracks grow to a critical size due to the exposure to cyclic stresses and finally fracture occurs when the area without cracks is not capable of sustaining the maximum stresses imposed during a loading cycle. [7,31]

The parameters for fatigue tests include waveform, frequency, mode of loading, levels for cyclic stress or cyclic strain, and test duration. Sinusoidal waveform is the most commonly used in fatigue tests and the frequencies can vary depending on the application it is used for, the test duration and the specimen material. For example, tests done with simulated body movement can use frequencies comparable to walking, or if the duration of the test is too long higher frequencies can be used to speed up the test, however some polymers can suffer from overheating and melting if too high frequencies are used. Fatigue tests are usually conducted using tension-compression as the mode of loading but tension-tension, bending and torsional loading modes can also be used. During tension-compression loading cycle, the stress alternates between maximum tensile stress (σ_{max}) and minimum compressive stress (σ_{min}) (Figure 10). The mean stress can be defined as

$$\sigma_m = \frac{\sigma_{max}+\sigma_{min}}{2} \quad (8)$$

and the amplitude as

$$\sigma_a = \frac{\sigma_{max}-\sigma_{min}}{2} \quad (9)$$

The range of stress amplitude is

$$\Delta\sigma = \sigma_{max} - \sigma_{min} \quad (10)$$

The ratio between the maximum and minimum stress amplitude is

$$R = \frac{\sigma_{max}}{\sigma_{min}} \quad (11)$$

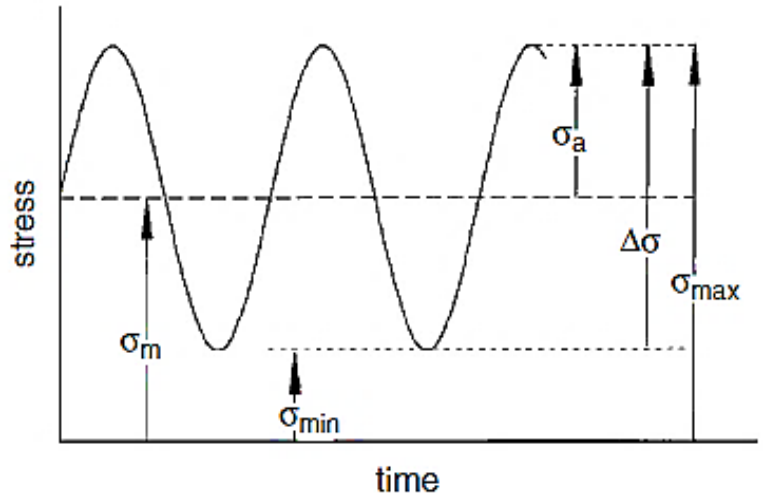

Figure 10. *Schematic illustration of tension-compression cyclic loading [31]*

When the tensile and compressive stresses are equal, the stress cycle is reversed and R=-1, but for tension-tension fatigue the mean stress is greater than zero and 0<R<1. [7,26,31] Tension-tension fatigue is usually used on specimens that have viscoelasticity, because tension-compression can cause buckling after number of cycles.[8]

The common fatigue test subjects a specimen to cycles of maximum stress that is usually about two thirds of the tensile strength obtained from a static test. The number of cycles until failure is counted and then the test is repeated on other specimens using lower values of maximum stress. The results are typically reported as S-N curves, where S represents the stress amplitude and N the number of cycles to failure. Figure 11 shows a basic representation of an S-N curve. [26,31]

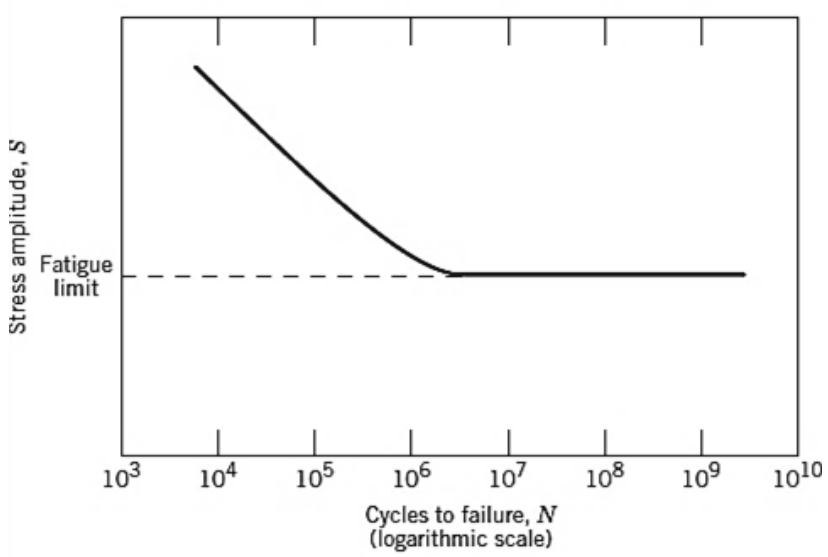

Figure 11. *Typical S-N curve demonstrating the fatigue limit [26]*

The compiled data are plotted as the stress amplitude versus the logarithm of the number of cycles until failure. The number of load cycles to failure at a specific stress level represents the fatigue life and can be increased by decreasing the applied stress per cycle or decreased by increasing the applied stress per cycle. The fatigue limit or endurance limit, as shown in Figure 11, is stress amplitude below where failure will never occur. In other words, essentially infinite number of cycles with stresses below the limit could occur without causing failure. [7,26] However, not all materials experience this limit and the S-N curve continues to slope down decreasing the stress amplitude for failure even at large number of cycles (Figure 12). Alternatively, fatigue strength is then used to depict the stress corresponding to a specific number of cycles, for example 10^7. [7,26,31]

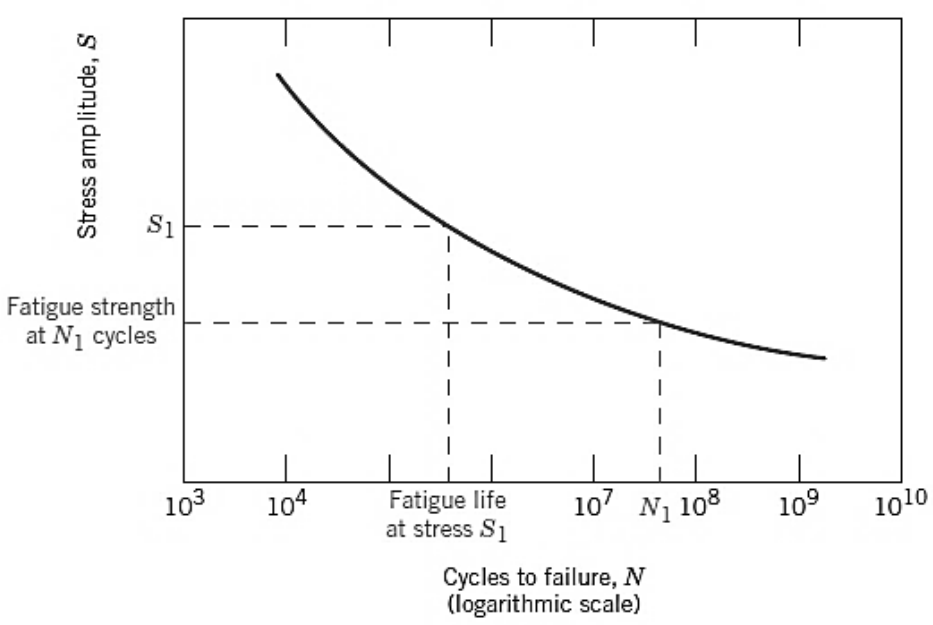

Figure 12. *Schematic illustration demonstrating fatigue life at specific stress level and fatigue strength at specific number of cycles [26]*

Fatigue failure can be divided into two types. Low-cycle fatigue is caused by loading cycles with stress levels even higher than yield strength causing both elastic and plastic strain each cycle and ultimately resulting in relatively short fatigue life. This kind of fatigue can occur at cycles less than 10^4 to 10^5. High-cycle fatigue on the other hand is caused by loading cycles with lower stress levels causing only elastic strain and resulting in higher fatigue lives than the 10^4 to 10^5 cycles of low-cycle fatigue. [26]

3. TESTING CONSIDERATIONS

For a mechanical test to be successful, careful test design is important. Conditions of the test should reflect the service environment of the product or material under investigation or what kind of information is required and thus take into account the right parameters such as loading mode and its amount and duration, as well as the environment in which the test takes place, in order to produce relevant test results. Consistency and reproducibility are also important things to consider, so different standards concerning mechanical testing should be taken into account. Possible loading modes depending on the specimen materials are tensile, compression, shear and bending and the duration of the test can be as quick as a second or as long as a year. Usually the mechanical testing is done in ambient laboratory condition, most often specified in different standards, meaning room temperature with specific humidity, as dry as possible. However, testing for example, the mechanical behavior of biological tissues may need the environment or the tissue itself to be wet using for example water or phosphate buffered saline in higher temperatures. [1,7,9]

Different specifications on the specimens can be considered. The geometry of a specimen as well as how many specimens should be used in mechanical testing depends on the type of test and material. Different standards can be used to determine the proper specimen specifications. The typical specimen used in tensile tests is the dogbone specimen consisting of a reduced gauge section in the center where the deformation is confined and with larger shoulders to make clamping of the specimen easier (Figure 13). [1,2] The dogbone specimen can have either circular or rectangular cross-section. Different sizes of the dogbone specimen can be used, but the gauge length should always be larger, usually at least four times than the diameter or width of the dogbone. [1] However, the size of the dogbone mold as well as the amount of material on hand can affect the size of the sam

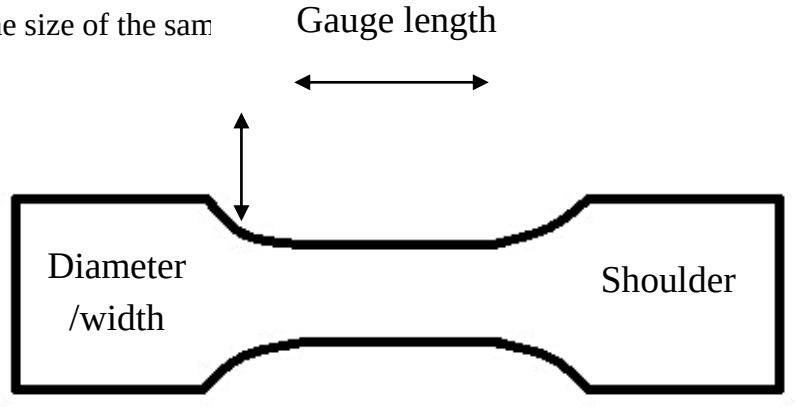

Figure 13. *Typical tensile specimen*

Compression specimens can be smaller than tensile specimens without the reduced gauge section and in the shape of rectangular or circular (Figure 14). It is usually required that the ratio between the height and the diameter of the specimen is low, preferable at least 1:2 to reduce buckling of the specimen during testing. [13,17,32] But again the amount of material can affect the size.

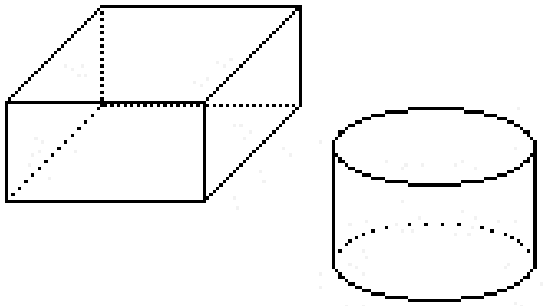

Figure 14*. Examples of compression specimens*

The number of test specimens required in mechanical tests can vary a lot. Fundamental properties from quasi-static tests can be tested with only five test pieces but if the material is anisotropic, tests need to be done on specimens that take in account the different directions resulting in different values. [1,9] Generally speaking large number of test specimens can increase the accuracy of test results, but also increase the costs [9].

There are a lot of different mechanical testing machines on the market today. One of the most common ones is the universal mechanical testing apparatus, which enables the use of different modes of loading. The apparatus usually consists of a fixed frame containing a load cell for measuring the applied load, an actuator or a crosshead that is used to apply the load, a controller to set testing variables and parameters as well as acquire data, and test fixtures like grips or platens for the specimens. [7] Figure 15 is one representation of a mechanical testing machine.

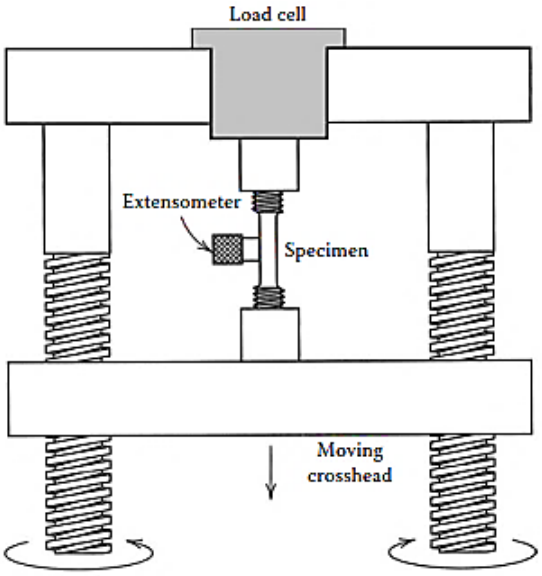

Figure 15. *Basic illustration of a screw-driven mechanical testing apparatus [33]*

There are four different test frames to drive the crosshead; electromechanical (screw), hydraulic, pneumatic and moving magnet. Electromechanical actuator is normally used in quasi-static tests, because it is not capable of operating in frequencies as needed for more dynamic tests. The other three are used instead. [7,9] The load cell is used to measure the magnitude of the applied load and can be specified for example for only tension, compression or both. Linear variable displacement transducer (LVDT) or an encoder can be used to measure the actuator displacement during testing. However, extensometers can be used to measure the precise elongation or deformation of the specimen usually by direct contact with the specimen. The purpose of grips is to clamp the specimen and transfer the load from the actuator on to the specimen. Clamping can be achieved by a screw, either hydraulic or pneumatic piston, wedge or scissors. For a compression test, flat plates are used to transfer the compressive load on to the specimen located between the plates. If tests are done in environment other than ambient laboratory, temperature-controlled fluid baths, ovens or other environmental chambers need to be able to be fitted around the mechanical test sample. [7]

4. APPLICATIONS

In this section, the application of mechanical testing and mechanical behavior to few selected anatomical constructs and sites as well as scaffolds are considered.

4.1 Biomechanics

In order to create a biomaterial construct intended to replace and otherwise come into contact with tissues in the human body, it is important to have some kind of knowledge of the properties of the host and the surrounding tissue, so that the construct behaves mechanically similarly as long as necessary. If the biomaterial construct is a permanent fixture, it needs to have enough long-term mechanical stability based on the surrounding tissue and the location while biodegradable construct needs the necessary mechanical properties until new tissue is formed and the mechanical stability is transferred to the new tissue as the biomaterial construct deteriorates. [8,34]

4.1.1 Bone

The mechanical properties of bone, a complex composite structure providing support, protection and movement, depend on the hierarchical level being studied. The human body is comprised of over 200 whole bones, the upper most level of the hierarchy. The next level consists of two anatomically distinguished bone types, cortical (compact) and cancellous (trabecular) bone, which leads to the next level of individual osteons comprising cortical bone and individual trabeculae comprising cancellous bone. Further decrease in structure size leads to the final levels, the different laminations of cortical and cancellous bones made out of collagen fibers consisting of collagen molecules and crystals. [10,35-37]

Bone as a hard connective tissue is a composite structure comprising of both organic and inorganic materials. Organic matrix being about 25 to 35% of dry weight and inorganic matrix between 60 to 70%. The majority of the organic matrix is comprised of type I collagen fibrils, whereas the inorganic mineral substance consists of calcium phosphate hydroxyapatite. When comparing the mechanical properties of collagen fibrils and calcium phosphates, collagen is strong, flexible and viscoelastic when subjected to tensile or bending stresses, but calcium phosphates in the crystal form are hard and thus capable of withstanding compression, but may shatter when subjected to bending and abrupt impacts. Together the collagens prevent the inorganic matrix from

brittle fracturing, while the hydroxyapatite prevents the yielding of the organic matrix. [38-41]

Cortical and cancellous bones comprise the macrostructure of the bone tissue and while they have similar compositions, though differently formed, macroscopically they have dissimilar densities due to different porosities and thus have different mechanical properties. Cortical bone is much denser than cancellous bone, the porosity ranging from 5 to 30 % compared to the 30 to 90 % porosity of cancellous bone. [41,42] While cortical bone exhibits a higher slope in a stress-strain curve compared to cancellous bone (Figure 16) meaning that the elastic modulus is higher in case of cortical bone, the cancellous bone is more flexible and can withstand considerably more strains before failure. [35,41]

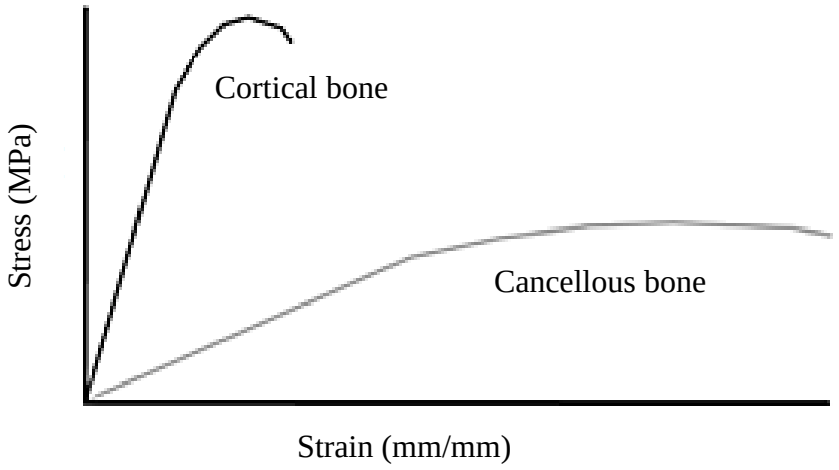

Figure 16. *Stress-strain behavior of cortical and cancellous bones. Adapted from [35]*

The elastic modulus of cancellous bone can vary between 0.1 and 1.5 GPa and cortical bone between 7 and 30 GPa. The compression strength of cancellous bone on the other hand ranges from 1.9 to 50 MPa while for cortical bone the values range from 130 to 240 MPa [3,43].

Both bone types behave mechanically anisotropically meaning that the mechanical properties of cortical and cancellous bone are greater in the longitudinal direction compared to transverse loading direction, because the collagen fibrils are oriented longitudinally. In addition, the values of strength and modulus also vary depending on the loading mode. Compressive test results in greater strength and modulus compared to tensile testing. Other factors affecting the mechanical properties of the bone types are the age, health and to some degree the sex of the subjects, from which whole bone the samples have been taken, as well as the region, because in addition to anisotropy, bones behave mechanically heterogeneously. In general, the variations in mechanical properties are greater in cancellous bone than in cortical bone. [10,44,45]

Bone as a whole consists of both cortical and cancellous bone and additionally of soft materials like blood vessels, nerve fibers and bone marrow and depending on the location they can be classified as long bones, short bones or flat bones [10]. Determining mechanical properties of whole bones is much more complex than those of cortical and cancellous bones. The mechanical behavior of whole bones compared to bones as tissue is more structural than material based, concentrating more on understanding behavior under physiological and traumatic conditions that can lead to fractures for instance. Understanding the different forces and loading conditions that different whole bones come in contact with, is important in order to produce mechanical tests in a laboratory setting. [46] For example, during standing both tensile and compression forces are subjected to the femur [38].

4.1.2 Articular Cartilage

Cartilage can be classified into fibrous, elastic and hyaline. Of the three, hyaline as articular cartilage is located at the ends of bones in many freely moving joints and is essential for the normal joint movement by transferring loads on the joint surface, absorbing shocks and helping in wear resistance and smooth movement of the joint [47]. The thickness of the articular cartilage depends on different joints and the location inside the joint. The thickest it is at the ends of tibia and femur, approximately 2 to 4 mm [41]. Many orthopedic problems are associated with the abnormal loss of articular cartilage, which usually should be able to last wear up to eighty years. The abnormal wear of articular cartilage is painful and common problem usually solved with replacement implant, however much work has been done in trying to find alternative solutions from tissue engineering point of view. [47]

Articular cartilage has a heterogeneous and anisotropic structure, hard and calcified near the bone with collagen fibers oriented perpendicular to the bone surface, but rather soft and wet at the joint surface with collagen fibers oriented parallel (Figure 17). In some aspects cartilage is quite simple material as it contains no blood vessels or nerves, does not have a lymphatic system and has only small amounts of cells. On the other hand, articular cartilage is viscoelastic and biphasic in nature containing a solid phase of mostly type II collagen fibrils in a porous mesh with glycoproteins and chondrocytes, and interstitial fluid phase consisting mostly of water, but also electrolytes. [37,41,48]

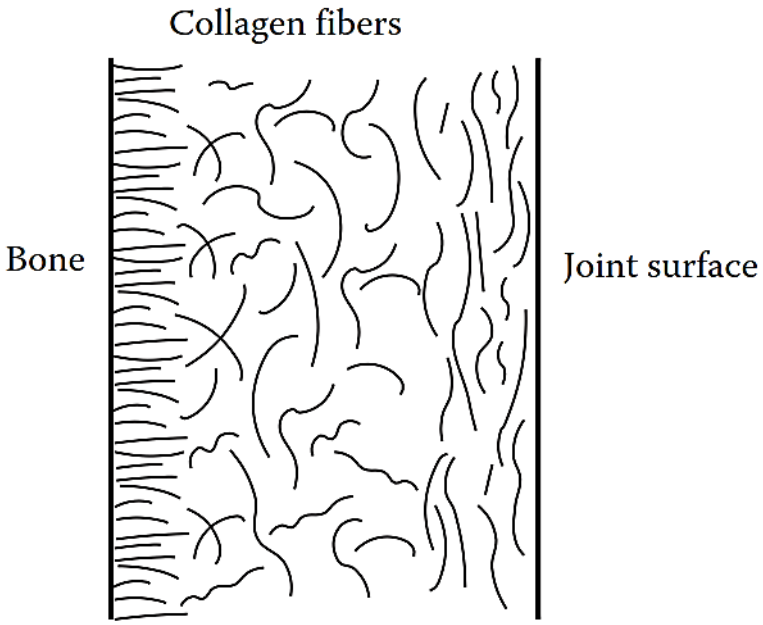

Figure 17. *Collagen fiber orientation in cartilage [37]*

Normal joint movements cause articular cartilage to come in contact with complex tensile, compressive and shear loads. The ability to withstand tensile loads comes from the collagen fibrils, whereas the negatively charged proteoglycans resist compressive forces and together the collagen fibrils and proteoglycans as a solid matrix resist the shear forces. The compressive forces subjected to articular cartilage can be many times body weight during which the interstitial water flows through the porous structure of the cartilage and becomes pressurized giving support. [47] Reportedly, the pressure on the interstitial fluid during walking can range between 5 and 6 MPa [49,50].

The stress-strain behavior of articular cartilage can be determined by tensile and compression tests. Figure 18 represents a tensile stress-strain graph of articular cartilage displaying a curve typical for biological tissues containing collagen. At the start of the curve is a toe region, where collagen fibers are relaxed and mixed up, but when the deformation continues further, the collagen fibrils start to stretch and become more aligned resulting in the linear part of the stress-strain curve. The final part of the curve is ultimately the failure, when maximum amount of deformation has occurred. [51] Due to the collagen fibers, articular cartilage is anisotropic and the tensile modulus can vary between 1 and over 30 MPa depending on how the fibers are aligned as well as the joint itself, the location inside the joint and the depth of the location [45,51].

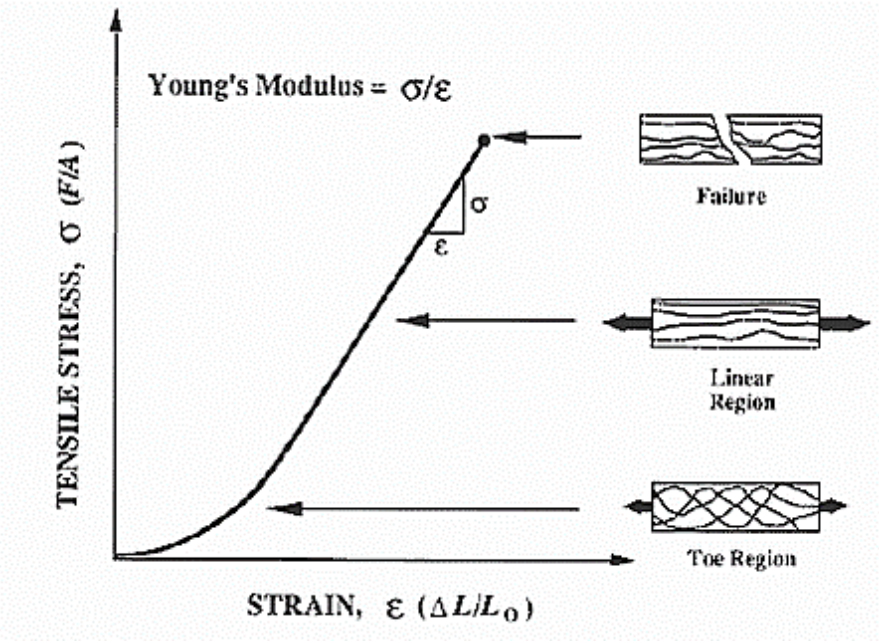

Figure 18. *Tensile stress-strain curve for articular cartilage [52]*

While in a tensile test, the articular cartilage is machined into thin strips, compression tests can be done to either cylindrical cartilage explants, without underlying bone (unconfined or confined), with bone (confined) or *in situ* by indentation method. The compressive stress-strain behavior of cartilage is however, highly dependent on the speed rate used in testing. During slow deformation, there is no flow resistance and water can seep out of the tissue without providing any resistance to the deformation but during fast deformation, the collagen matrix hinders the fluid flow and thus the tissue behaves more stiffly.[51] As with tensile modulus, the compressive modulus is also dependent on the location of the tested cartilage and the depth [53].

In addition to determining elastic modulus of cartilage using a steady rate deformation test, creep or sometimes stress relaxation tests are conducted instead to get the aggregate modulus due to the viscoelastic nature of articular cartilage. In fact, the aggregate modulus is more commonly used and describes the stiffness when the flow of water has equilibrated, the higher the value, the stiffer the cartilage. The aggregate modulus of articular cartilage ranges reportedly from 0.4 to 0.9 MPa [51,52,54].

4.1.3 Tendons and Ligaments

Both tendons and ligaments are formed by parallel collagen fibers to produce soft yet inelastic fibrous tissue between bone and muscle to transfer muscle forces or between two bones in order to stabilize joints. The mechanical behavior of tendons and ligaments under tension is highly influenced by the collagen fibers and for ligaments they tend to be of smaller diameter compared to tendons. Figure 19 is a tensile stress-strain curve of tendons and ligaments, showing the initial toe region, with crimped

fibers, followed by the linear region where more and more fibers start to stretch from their crimped positions, before seemingly yielding and failure of the fibers occur. [37,41,47]

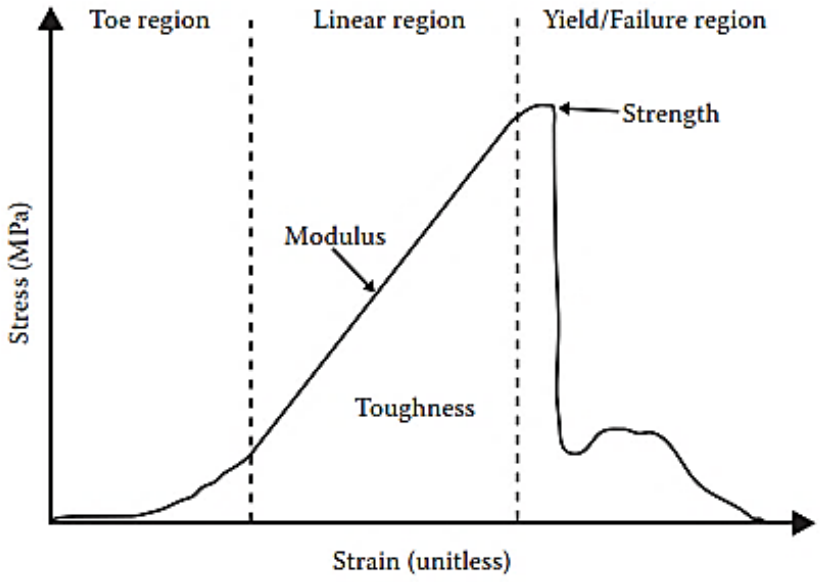

Figure 19. *Schematic representation of stress-strain behavior of tendons and ligaments [25]*

The mechanical properties of the tissues depend highly on the location of the tissue and age, as well as the testing speed and environment. [52,55] The reported elastic modulus values of human ligaments can range from 5 to 430 MPa [28] while for tendons they are between 1200 and 1800 MPa [56]. For example, in case of ligaments, the safe physiological range in the stress-strain curve is between 0 and 3 % strain or between 0 and 40 MPa stress, from toe region to slightly in the elastic region. Any further deformation can lead to injury due to overuse and end up in rupture of the ligament. [41]

As biological tissues both tendons and ligaments are viscoelastic and experience time-dependent behavior. Creep and stress relaxation tests are commonly done both statically and dynamically in vitro since during physiological activities, tendons and ligaments experience both creep and stress relaxation. During walking for instance, cyclic stress relaxation occurs when the tissues are subjected to near constant strains dynamically leading to softening of the tissues, whereas creep, caused by stretching exercises for instance, can lead to the elongation of the tissues due to creep. [29,41,57]

In addition to creep and stress relaxation behavior, as viscoelastic materials tendons and ligaments experience hysteresis phenomena and the loading and unloading of the tissues result in energy dissipation that diminishes from cycle to cycle. Because the mechanical behavior is different from cycle to cycle, tests on tendons and ligaments are often performed by first subjecting the samples to preconditioning cycles of loading in order

to get as uniform loading history as possible. [25,58-60] Preconditioning and then waiting before testing to eliminate loading history, has also been used when testing [61].

4.1.4 Joints

Joints or articulations are connections between the bones in the human body. Joints can differ both structurally and functionally, depending on whether the bones are connected by cartilage, fibrous connective tissue or if the connecting area is filled with fluid or whether the movement between the bones is hindered, somewhat moveable or entirely moveable. In this section the mechanical behavior of three joints at different locations are considered. Since joints can be rather complex structures, determining the basic stress-strain characteristics is rather difficult, so the focus lies on other mechanical aspects affecting the loads.

4.1.4.1 Finger

The fingers contain three different bones (distal, middle and proximal phalanxes), with distal interphalangeal joint (DIP) between the distal and middle phalanxes, proximal interphalangeal joint (PIP) between the proximal and middle phalanxes as well as metacarpophalangeal joint (MCP) between the proximal phalanx and the head of metacarpal (Figure 20). These joints are capable of flexion and extension although the MCP is also capable of abduction and adduction.[62]

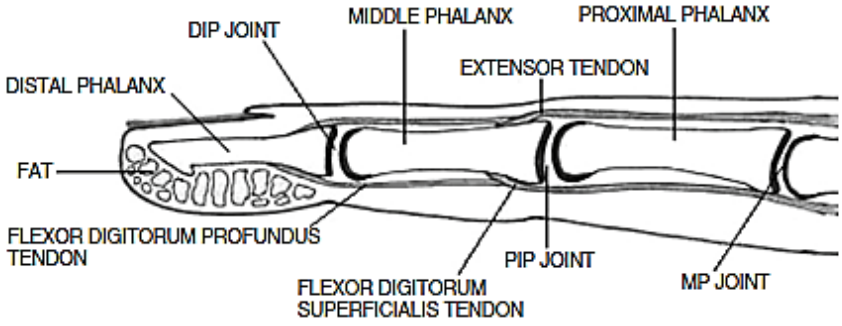

Figure 20. *The anatomy of the finger [62]*

The mechanical behavior of the joints is difficult to predict since both compression and shear forces act in the joints during everyday life and different aspects can influence the forces acting on the joints. Gripping and pinching motions use different amounts of forces and thus can cause different amounts of joint contact forces on the fingers as well as between the three finger joints. The difficulty lies in determining the joint contact forces reliably, since the actual contact forces are difficult to measure, thus mathematical models are used instead. For example, one model suggests that when applying a gripping function of 80N force it would lead to maximum internal contact forces of 279N, 437N and 387N for the DIP, PIP and MCP joints respectively [63]

while 66 N tip pinch strength would lead to 179N, 331N and 299N maximum internal joint contact forces for DIP, PIP and MCP respectively. The amount of joint contact forces gripping and pinching motions can cause in the joints depend on the age and sex, as well as the health of the joints, among other things. [64] For example, rheumatoid arthritis, an inflammatory disease that leads to the destruction of joints, can cause the maximum forces of gripping and pinching motions to drop by a third [63]. Reportedly, the maximum pinching forces for normal women and men have been 49N and 74N. [65] To treat diseases affecting the finger joints, different options have been developed. Prostheses in the MCP joints are most common, including the Swanson implant and knitted joint scaffold spacer. While the Swanson implant is a permanent fixture and requires such mechanical properties, the knitted joint scaffolds is intended to be used as a temporary porous spacer to facilitate the growth of natural fibrous tissue. [66-68]

4.1.4.2 Hip

The hip joint is located between the head of the femur and the acetabulum of the hip bone and bears a significant amount of the human weight thus requiring a lot of strength and stability during physiological activities such as walking and running, even just standing on one leg can cause reportedly only slightly less loading on the joint compared to walking [69]. The hip joint is capable of flexion and extension, internal and external rotation as well as abduction and adduction. [70] The forces acting on the hip joint depend on the physical activity, the duration and the bodyweight. [9,71] For example, normal walking speed can cause forces of 3 to 3.5 times bodyweight (BW) depending on the age of the walker. Also during walking different stages of the walking cycle can cause different loads on the hip. [71,72]

Because of the dynamic movement in the hip joint, wear and tear (osteoarthritis) are very common problems in the hip joint. Total hip replacement is a popular way to treat severe arthritis as well as difficult fractures, common among elderly. In the hip replacement the head of the femur and the acetabulum are removed and replaced with permanent implant thus, knowing the different forces, as well as the frictions and wears the implant materials are subjected to is important. Reportedly, average forces acting on the hip joint, acquired from hip replacement patients, can vary from 2.4 times BW to 3 times BW. [69,71]

4.1.4.3 Knee

The knee joint is the largest joint of the human body, consisting of two joints inside an articular capsule, the tibiofemoral and patellofemoral joints. As with the hip joint, the forces acting on the knee depend on the type of activity as well as the bodyweight. The forces acting on the knee are complex and the most severe but two different ways exist for determining them. Mathematical calculations of forces acting on the knee can take in

to account the joint contact forces, muscle forces, and ligament forces but the values can vary a lot depending on publications, for example during walking the contact forces can differ from 2 to even 6.7 or 7.1 times BW and result in cartilage deformation of 3%. [50,73-76] To avoid the uncertainties mathematical calculations can result in, *in vivo* measurements of knee joint forces can be done by inserting an implant that can measure the three contact forces (tibiofemoral, muscle and soft tissue structure) and their moments. In contrast, the forces measured *in vivo* tend to be less than the mathematical calculations [74,75].

As with hip joint, knee joint can also suffer from osteoarthritis and can prohibit the activities needed daily. While exercise has been suggested as a way to treat the limitations a patient with osteoarthritis might experience [77], total knee replacement is a way to treat patients with arthritis and other joint affecting diseases. Because of the intricate nature of the knee, the structure, as well as the different repeated loads during daily activities, designing the artificial knee joint is difficult. [50]

4.2 Scaffolds

The materials used as biodegradable scaffolds are usually based on natural polymers, synthetic polymers, ceramics or their composites. Careful design of scaffolds includes determining the mechanical properties of the materials as well as the construct itself. Depending on the anatomical site of the scaffold implantation, as well as the duration of healing, the scaffold should have the mechanical properties to handle the implantation process and the environmental loadings during healing and tissue regrowth. While the importance of good mechanical properties mimicking the host tissue is significant, porous structure, that might diminish the mechanical properties, is also necessary for tissue growth, so careful scaffold design requires balancing mechanical properties with porosity. [34]

Polylactides and lactic copolymers are among the most used scaffold materials due to their versatile properties including, but not limited to, biodegradability and processability. Lactic acid having two possible stereoisomers, L- and D-isomers, of which L-lactic acid is a natural by-product of the metabolic system, can be polymerized into high molecular weight polymer chains and hydrolytically degraded when in the human body. While a homopolymer poly(L-lactide) (PLLA) produced from pure L-lactide, is semicrystalline, hard and brittle, copolymerizing it with the D-lactide results in decrease of crystallinity, as well as brittleness. Further copolymerization with ε-caprolactone can increase the elastic properties and produce overall good mechanical strength. For example, the tensile modulus of PLLA fibers can range between 6.5 and 16 GPa, while copolymerization with caprolactone can decrease the modulus to range between 5.6 and 8.2 GPa, depending on the ratio of the polymers. [78-81] One way to produce a porous scaffold structure using polylactides is to utilize fibers in the forms of braids, non-woven structures and knits like the joint scaffold for MCP joint. [67,82-86]

Making ceramic scaffolds for hard tissue regeneration, i.e. bone, with β-tricalcium phosphate is common due to the high mechanical stiffness, osteoconductivity and similarity to the inorganic phase of bone. However, as a ceramic, β-TCP is also very brittle and hard lacking any ductility and thus difficult to shape. Elastic modulus measurements of β-TCP crystals have reached values of 120 GPa. By combining the TCP with polymers, such as polylactides and their copolymers, the osteoconductivity of the ceramic is joined with the biodegradability and processability of the polymers even though some of the mechanical properties are decreased. [34,79,87-89] For example PLA rods without TCP content had elastic modulus of 21 GPa that increased the more TCP was added. Addition of 50% TCP increased the modulus by almost the same amount. [90]

In addition, to basic mechanical testing of scaffolds in order to determine the mechanical behavior, mechanical loading has also been used in order to study the degradation behavior of scaffolds as well as the behavior of cells seeded in scaffolds, while the scaffold is under static or dynamic loading [91-93]. It has been proved that tissue regrowth requires mechanical stimulation. For example, without the right amount of physiological stress, bone mass can diminish. [94]

5. MATERIALS

This section of the thesis describes the materials used in the practical work.

The mechanical tests conducted in physiologically simulated conditions were done with a temperature controlled fluid bath (Instron Temperature controlled fluid recirculator) using tap water and 37 °C. The samples were kept prior to testing in a buffer solution in a shaking incubator (Multitron AJ 118 g, Infors, Bottmingen, Switzerland) in 37 °C with a shaking speed of 100 RPM. The buffer solution used was (Sörensen) phosphate buffer solution prepared according to ISO 15814 Implants for surgery – Copolymers and blends based on Polylactide – in vitro degradation testing. The amounts of reagents and the final pH of the solutions can be seen in Table 1 below. The pHs were measured using calibrated Mettler Toledo SevenMulti MP 225 pH-meter (Mettler-Toledo International Inc., Greifensee, Switzerland).

Table 1. *The amounts of reagents and pH of buffer solutions*

Na_2HPO_4 (g)	15.483	15.483	7.741
KH_2PO_4 (g)	3.32	3.307	1.65
pH	7.49	7.48	7.46

5.1 Porous Scaffolds

Two porous scaffolds (Figure 21) based on the same copolymer were studied. The first set of samples tested were composite scaffolds made of poly(lactide-co-ε-caprolactone) 70/30 with 50 wt% β-tricalcium phosphate with the TCP granule size ranging from 100 to 300 µm. The second set of scaffold samples was made from the same PLCL without the ceramic content. Both scaffold materials were gamma sterilized prior to testing with minimum dose of 25 kGy. Both scaffold types were mechanically tested dry and after two and fourteen days in buffer solution with two to six parallel samples.

Figure 21. *The porous scaffolds*

5.2 Dogbones

The same materials tested in porous scaffold forms were also tested as dogbone shaped with 10 mm gauge length. Samples were tested dry and in simulated physiological condition after 2 days in vitro. Two to six parallel samples were used depending on the tests. The materials were sterilized prior to testing using gamma sterilization with minimum dose of 25 kGy.

5.3 Joint scaffolds

Three knitted scaffold structures also known as joint scaffolds were studied. First tested was a scaffold made of polylactide (96L/4D) blended with 15 wt-% polyethylene glycol and the other two similar but significantly smaller structures made of PLA 96/4 (Figure 22).

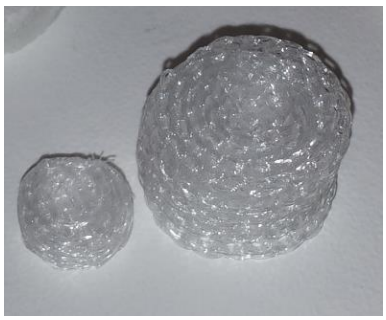

Figure 22. *Two different sized joint scaffolds*

The PLA blended with PEG scaffolds were non-sterilized, with diameters of approximately 13 mm and heights of 10 mm. Three time points were used; 0 dry, 2 days in vitro and 14 days in vitro. Three to six parallel samples were used in the mechanical tests.

The two PLA 96/4 scaffolds were both gamma sterilized and intended only as investigational devices. Three samples of scaffolds sized Ø8x3.5mm (Bionx Implants Ltd. Code S21, ɣ-sterilized 10/2000) were tested dry, whereas scaffolds of size

Ø8x3.6mm (Linvatec Biomaterials Ltd. Ref JS0836, code S64, sterile 06/2008) were mechanically tested dry and in simulated physiological condition after two days in buffer solution using four and three parallel samples. When needed the smaller joint scaffolds are referred to as PLA 96/4 (Bionx) and PLA 96/4 (Linvatec).

5.4 Fibers

Three different medical grade fibers of two materials were tested. Multifilament and monofilament PLA 96/4 and monofilament PLA 96/4 with 10% TCP were tested dry and in simulated physiological conditions after two days in buffer solution. Six or alternatively three parallel samples were tested mechanically.

5.5 Cancellous Bone

Cancellous bone taken from the distal femur of a pig was mechanically tested in dry ambient conditions. Samples from both medial and lateral were used. Figure 23 demonstrates the locations of the taken samples.

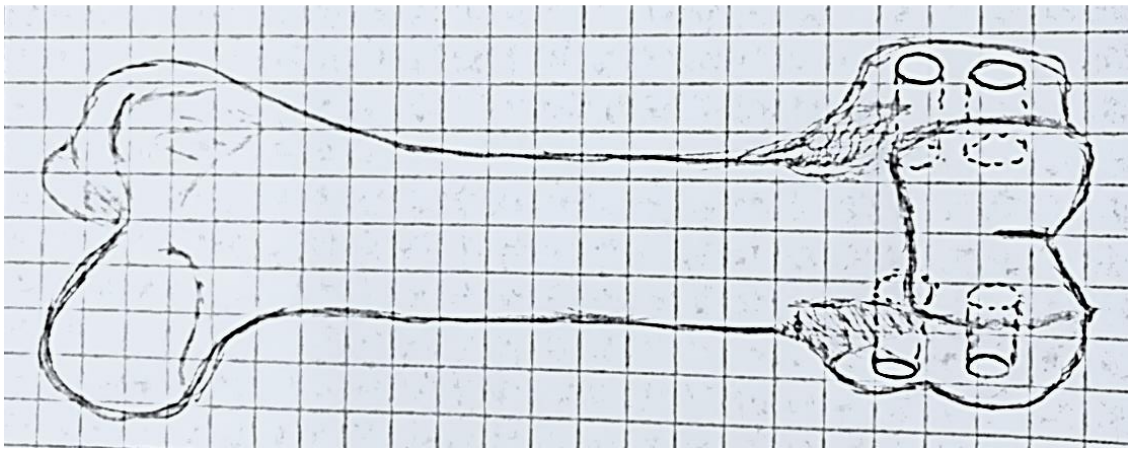

Figure 23. *Drawn illustration of the pig femur and the locations where the samples were obtained*

Three to seven parallel bone samples were ultimately obtained and tested mechanically.

6. METHODS

In this section the used methods in the practical work are described starting from the sample preparations, followed by the mechanical tests and finishing with the additional tests. Table 2 summarizes those characterization methods.

Table 2. *Summary of the characterization methods*

	Mechanical tests								Additional tests		
	Modulus	**Stress-strain behavior**	**Static stress relaxation**	**Dynamic stress relaxation**	**Compressibility**	**Static creep**	**Dynamic creep**	**Hysteresis**	**Water absorption**	**DSC**	**TGA**
PLCL-TCP50 porous scaffold	x	x	x	x				x	x	x	x
PLCL porous scaffold	x	x	x	x				x	x	x	
PLCL-TCP50 dogbone	x	x		x				x	x	x	x
PLCL dogbone	x	x		x				x	x	x	
PLA+PEG15 joint scaffold	x	x			x	x	x	x	x	x	
PLA 96/4 joint scaffold (Linvatec)	x	x			x		x	x	x	x	
PLA 96/4 joint scaffold (Bionx)	x	x			x					x	
PLA 96/4 4-filament	x	x		x				x			
PLA 96/4 monofilament	x	x		x				x			
PLA 96/4 + TCP10 monofilament	x	x		x				x			
Cancellous bone	x	x		x				x			x

6.1 Sample Preparation

PLCL-TCP50 and PLCL rods processed with supercritical CO_2 to produce porous structure, were cut into cylindrical scaffold samples with Vernier caliber and scalpel to as close to 7.5 mm height as possible, and using custom made punch and a hammer to punch as close to 15mm diameter as possible. Because the samples were made by hand, the heights and diameters had broad tolerances. The diameters and heights were

measured prior to testing and averages of three measurements were used. For PLCL-TCP50 samples the average diameter and average height were 14.9 ± 0.2 mm and 7.6 ± 0.2 mm and for PLCL samples 15.0 ± 0.2 mm and 7.3 ± 0.5 mm. Table 3 summarizes the measured parameters of all the samples used in this thesis as well as the original amount of samples. The compressive mechanical tests of the porous scaffolds were done using three time points; 0 dry, 2 days in vitro and 14 days in vitro with six parallel samples in case of the composite samples and two and three parallel samples in case of polymer samples.

Table 3. *Measured parameters of all the samples*

	Height/gauge length (mm)	Diameter (mm)	Width (mm)	Thickness (mm)	Samples
PLCL-TCP50 porous scaffold	7.6 ± 0.2	14.9 ± 0.2	-	-	36
PLCL porous scaffold	7.3 ± 0.5	15.0 ± 0.2	-	-	15
PLCL-TCP50 dogbone	10	-	5.2 ± 0.05	0.9 ± 0.02	33
PLCL dogbone	10	-	4.9 ± 0.1	1.0 ± 0.06	36
PLA+PEG15 joint scaffold	9.6 ± 0.2	13.2 ± 0.3	-	-	54
PLA 96/4 joint scaffold (Linvatec)	3.5 ± 0.1	7.7 ± 0.1	-	-	14
PLA 96/4 joint scaffold (Bionx)	4.0 ± 0.3	7.7 ± 0.05	-	-	3
PLA 96/4 4-filament	20	0.41 ± 0.06	-	-	18
PLA 96/4 monofilament	20	0.096 ± 0.02	-	-	18
PLA 96/4 + TCP10 monofilament	20	0.085 ± 0.01	-	-	18
Cancellous bone	5.4 ± 1.2	10.0 ± 0.2	-	-	14

In order to make the dogbone shaped samples, PLCL-TCP50 and PLCL rods were cut into smaller pieces and compressed into sheets with NIKE Hydraulics (Type ZB110, NIKE Hydraulics Ab, Eskilstuna Sweden) compression molding apparatus. The pieces were put between two thin metallic sheets individually and placed between the compression platens and warmed until 85 °C in case of the composite and alternatively 80 °C in case of the polymer, at which point the compression plates were pressed

together with 20 MPa pressure for few minutes, after which the heat was switched off and the cooling on and the plates were let to cool until approximately 40 °C. The PLCL-TCP50 or PLCL sheet between the metallic sheets was then taken out of the compression and put into the freezer (-26 °C) until the material could be removed from the sheets. Dogbone shaped samples were then punched from the sheets using a mold (Figure 24) with 10 mm gauge length and 40 mm overall length. The thickness and width of the samples were measured prior to testing and for PLCL-TCP50 dogbone they were 0.9 ± 0.02 mm and 5.2 ± 0.05 mm and for PLCL dogbone they were 1.0 ± 0.06 mm and 4.9 ± 0.1mm.

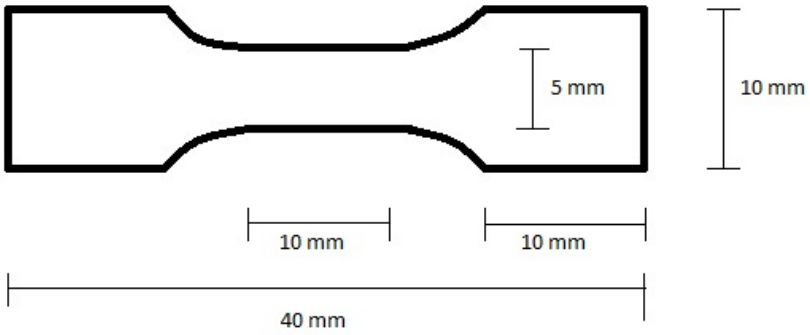

Figure 24. *Presentation of the used dogbone mold*

As mentioned before, the joint scaffolds were priorly made, so only the diameters and heights were measured before performing tests. For PLA+PEG15 the diameter was 13.2 ± 0.3 mm and height 9.6 ± 0.2 mm, for PLA 96/4 (Linvatec) the diameter was 7.7 ± 0.1 mm and height 3.5 ± 0.1 mm and for PLA 96/4 (Bionx) the values were 7.7 ± 0.05 mm and 4.0 ± 0.3 mm.

The fiber samples were made by cutting approximately 30mm length pieces from the provided yarns. The diameters of the samples tested dry were first measured and then taped to a paper mold giving the samples a gauge length of 20 mm. In contrast, the samples tested in simulated physiological conditions were placed in test tubes filled with buffer solution and the diameters were measured after two days prior to testing and then taped to plastic molds resulting in the same 20 mm gauge length. The diameters of each filament were measured individually from three different locations. In case of the multifilament samples, each filament diameters were added together to get the overall diameter of the 4-filament samples. The diameters were 0.41 ± 0.06 mm for the PLA 96/4 multifilament and 0.096 ± 0.02 mm and 0.085 ± 0.01 for the PLA 96/4 and PLA + TCP10 monofilaments, respectively.

With the aim of making the cancellous bone samples, two frozen pig legs were melted overnight, after which the femurs were separated from the tibias and cleaned as close to bone as possible using a surgical blade. The cancellous bone samples were taken from the distal femurs from both medial and lateral sides. The samples were obtained by band

sawing the femurs and then drilling the samples with diameters of approximately 15.5 mm and heights of approximately 10mm with vertical boring machine. The samples were then decreased in size by punching to approximately 10 mm diameter. The original height was then cut in half with a surgical blade. The diameters and heights were measured prior to testing and the average values were 10.0 ± 0.2 mm and 5.4 ± 1.2 mm. The samples were then put into a freezer until testing in order to retain the original water content. Prior to testing the samples were taken out of the freezer and let thaw. Before testing the bone samples were kept in buffer solution in order to keep the samples sufficiently moist.

6.2 Mechanical Tests

All the static and dynamic mechanical tests were performed unconfined with Instron Electropuls E1000 (High Wycombe, UK) testing device equipped with 250 N and 2 kN load cells. Dry tensile tests were conducted using upper and lower grips provided by Instron however, in tensile tests simulating physiological conditions, custom made lower grip was used with the upper grip from Instron. Additionally, all the compression tests were made using a lower platen procured from Instron and custom made upper platen with a diameter of 18 mm coupled with other parts needed for the compressor provided by Instron.

6.2.1 Modulus and Stress-Strain Behavior

The elastic moduli and stress-strain characteristics of the different materials were determined by applying either compressive or tensile load quasi-statically until predetermined amount of strain or load, depending on the sample being tested, was reached.

In order to determine the moduli of the porous scaffolds (Figure 27) and cancellous bone samples, they were tested by compressing 1mm/min until 20% strain was reached. The used crosshead speed was adapted from the standard SFS-EN ISO 604 Plastics. Determination of compressive properties.

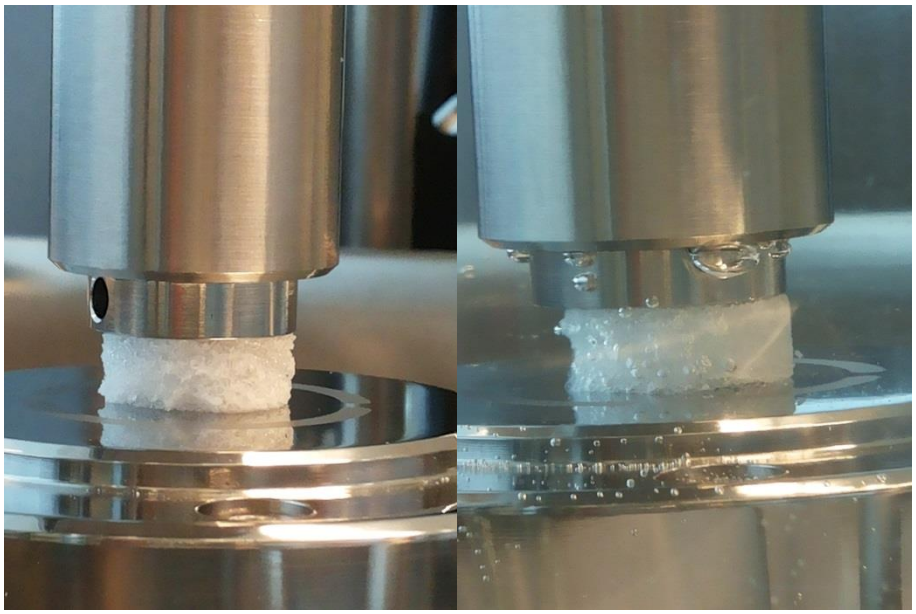

Figure 25. *Compression test of the PLCL-TCP50 scaffolds*

The moduli of the joint scaffolds were determined from samples compressing 2 mm/min until 500N. The moduli were determined from between 0 and 20 % strain from the stress-strain curve. The used crosshead speed was chosen according to previous thesis studying joint scaffolds [95].

Tensile load was applied to the dogbone samples in order to determine the moduli. Samples were first strained to 2 mm/min (adapted from standard SFS-EN ISO 527-1 Plastics. Determination of tensile properties. Part 1: General Principles) until 300 % strain was reached (Figure 25). Additionally, for comparison, 10 mm/min until 300 % strain and 120 mm/min until 100 % strain were also tested. In order to determine whether dynamic loading in the elastic region had any effect on the moduli, samples were also strained to 150% strain 2mm/min after dynamic loading (1 Hz, between 0 and 1% strain). All the moduli were determined from the seemingly linear part of first 1 % strain.

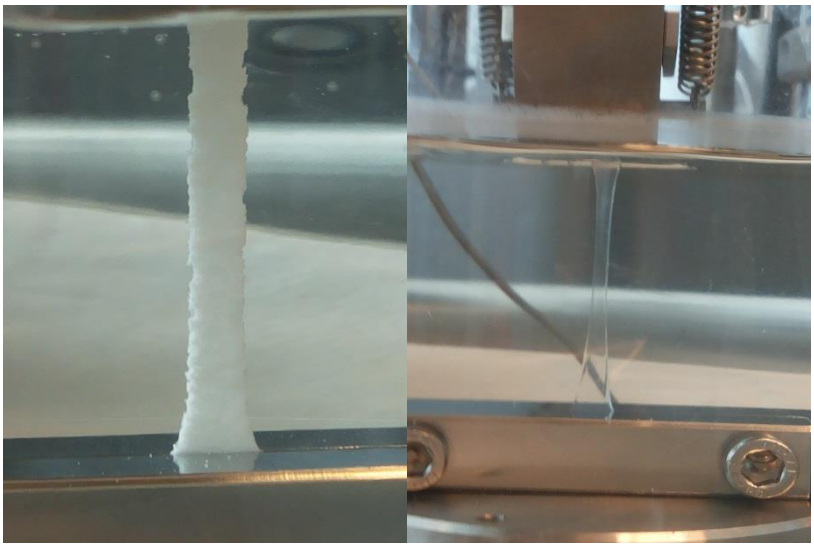

Figure 26. *Tensile testing of the dogbones*

The moduli of the fibers were determined by straining the samples 20 mm/min until the fibers broke. The chosen crosshead speed was adapted from standards SFS-EN 13895 Textiles. Monofilaments. Determination of tensile properties and SFS-EN ISO 5079 Textiles. Fibers. Determination of breaking force and elongation at break. The tangent moduli of the fibers were determined from the linear part of the stress-strain curve. Additionally, the stress and load at yielding as well as stress, load and strain at break were determined. Table 4 summarizes all the standards and sources used in determining the testing parameters for stress-strain behavior tests.

Table 4. *The used standards and sources in determination of stress-strain behavior*

	SFS-EN ISO 604 [a]	SFS-EN ISO 527-1 [b]	SFS-EN 13895 [c]	SFS-EN ISO 5079 [d]	Previous thesis [e]
PLCL-TCP50 porous scaffold	x				
PLCL porous scaffold	x				
PLCL-TCP50 dogbone		x			
PLCL dogbone		x			
PLA+PEG15 joint scaffold					x
PLA 96/4 joint scaffold (Linvatec)					x
PLA 96/4 joint scaffold (Bionx)					x
PLA 96/4 4-filament			x	x	
PLA 96/4 monofilament			x	x	
PLA 96/4 + TCP10 monofilament			x	x	
Cancellous bone	x				

[a] Plastics. Determination of tensile properties. Part 1: General principles

[b] Plastics. Determination of tensile properties

[c] Textiles. Monofilaments. Determination of tensile properties

[d] Textiles. Fibers. Determination of breaking force and elongation at break

[e] Mutanen, M. Studies of bioreconstructive small-joint prostheses (2004)

In general, the graphs of stress-strain behavior were formed by creating average curves of the parallel samples of the different studied specimens. The moduli of the different samples were determined by fitting a trendline in the linear part of the stress-strain curves resulting in tangent moduli. The trendline was usually fitted somewhere in the range of 0 to 20 % strain. For compression tests the first 5 % strain were ignored due to usually occurring toe region (machine settling, surface unevenness). The moduli of each parallel sample were determined, after which the averages and standard deviations were calculated. Materials with only two parallel samples show the difference between the average and the maximum and minimum values instead of standard deviation.

6.2.2 Compressibility

The compressibility of the different joint scaffolds was tested by compressing to 500 N with the crosshead speed of 2 mm/min (Figure 26) and the amounts of compression in terms of strain and displacement were observed from 80 N, 220 N and 440 N. These values were used in a previous thesis to represent the forces a rheumatoid arthritis

patient, a healthy woman and a healthy man, respectively, can experience in the MCP joint. [95] Physiologically speaking, in addition to compression, the MCP joint also experiences shear forces, but due to simplification of the test method, only flat compression was used in the test.

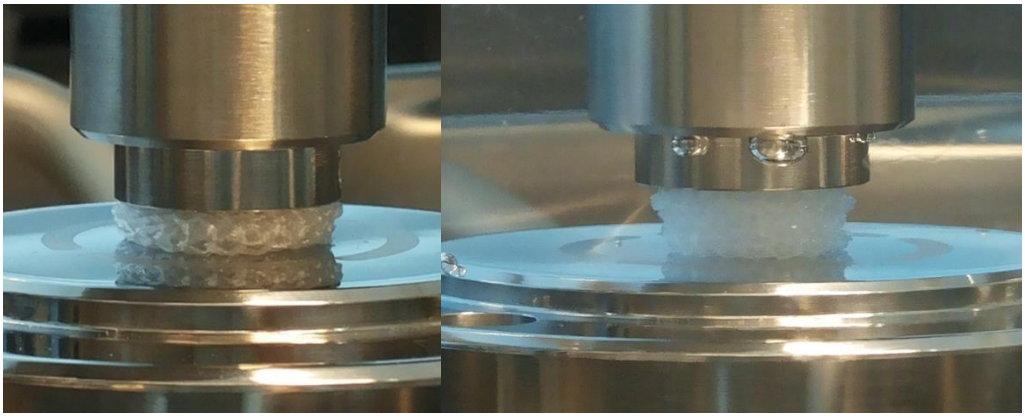

Figure 27. *Dry and physiologically simulated compressions of PLA + PEG15 joint scaffold*

6.2.3 Stress Relaxation

Stress relaxation tests were only conducted to the porous scaffolds. The tests were done to the same samples used to determine the moduli. After the compression to 20 % strain, the samples were decompressed using the same 1 mm/min crosshead speed until the actuator reached its original placement. The viscoelastic samples were left to recover for one minute so that they could recover as much as possible of their original height. The samples were then compressed back to 20 % strain in two seconds and held in that position for 1000 seconds (a little less than 17 minutes). The decrease in stress was observed.

6.2.4 Creep

The creep properties in a smaller scale than usual creep tests were done to the PLA blended with PEG scaffolds by compressing to 50 N in two seconds followed by holding that compression for 1000 seconds. The increase in compressive strain was observed against increasing time.

6.2.5 Dynamic Loading

The different samples were tested dynamically by either compression or tensile using either strain or load amplitudes with sinusoidal waveform, a simplification of a dynamic movement. The load/stress or strain/displacement from the first and last cycles were

observed as well as the percentage change between the cycles. Table 5 summarizes the parameters used in the dynamic tests.

Table 5. *Parameters of the dynamic tests*

	Frequency (Hz)	Pre-strain (%)	Amplitude	Cycles
PLCL-TCP50 porous scaffold	0.5	5	10 %	500
PLCL porous scaffold	0.5	5	10 %	500
PLCL-TCP50 dogbone	1	-	0.50 %	1000
	1	99.5	0.50 %	1000
PLCL dogbone	1	-	0.50 %	1000
	1	99.5	0.50 %	1000
PLA+PEG15 joint scaffold	1	-	25 N	1000
PLA 96/4 joint scaffold (Linvatec)	1	-	25 N	1000
PLA 96/4 joint scaffold (Bionx)	-	-	-	-
PLA 96/4 4-filament	1	-	1 %	1000
PLA 96/4 monofilament	1	-	1 %	1000
PLA 96/4 + TCP10 monofilament	1	-	1 %	1000
Cancellous bone	0.5	-	5 %	500
	1	-	5 %	1000

Also stress-strain hysteresis curves from the dynamic tests were done. These curves or loops are a way to observe both sample and testing machine behavior as well as evaluate the energy dissipation during the cycles. For clarity, in the hysteresis graphs, only loops from the first, the 50^{th} and the last (either 500^{th} or 1000^{th}) cycles are presented. The first cycles differ from the other cycles, because in order to get sinusoidal waveform, the test required a ramp to the value used as amplitude.

From the porous scaffolds the composite scaffolds were tested first by imposing dynamic compression onto the samples. The first sample was intended to be first compressed to 10 % strain in 5 seconds, followed by 1000 cycles of sinusoidal waveform with 10% strain amplitude and 1 Hz frequency. However, the test was ended at 70 cycles, because it was determined that the 1 Hz test speed was too fast and the scaffold being tested did not have enough time to recover to its initial height and instead started to ‘hop’ too much due to the fast speed. Thus the test speed was changed to 0.5 Hz and also the cycle amount was reduced to 500 in order to keep the 1000 s test duration. The first test sample was therefore tested again with the new parameters. After

the test had ended it was determined that there was still too much empty space between the sample and the compressor platen when the actuator was at zero strain, subsequently for the next five samples, the test parameters were changed to include pre-strain of 5% by first compressing to 15% strain followed by 500 cycles of sinewave with 0.5Hz test speed and 10% strain amplitude. The polymer porous scaffolds were then tested using the same test method.

The dogbone samples were dynamically tested in two ways. First by dynamic tension essentially in the elastic region of a stress-strain curve; the samples were first strained to 0.5 % in 1 second followed by 1000 cycles of sinusoidal waveform with 1 Hz test speed and 0.5 % strain amplitude. Additionally, for comparison, samples were also tested dynamically past the elastic region by first straining to 100 % strain in 5 seconds, equal to 120 mm/min, followed by 1000 cycles of sinusoidal waveform with 1 Hz test speed and 0.5 % strain amplitude.

The dynamic compression behavior of the joint scaffolds was tested by compressing to first 25 N load in five seconds, followed by 1000 cycles of sinusoidal waveform with 1 Hz frequency and 25 N load amplitude.

The fibers were tested dynamically in the elastic region by first straining to 1 % strain in one second followed by 1000 cycles of sinusoidal waveform with 1 Hz frequency and 1 % strain amplitude.

The cancellous bone samples were also tested by dynamic compression. The samples were first compressed to 5 % strain in 5 seconds followed by either 500 cycles of sinusoidal waveform with 0.5 Hz frequency, or alternatively 1000 cycles of sinusoidal waveform with 1 Hz frequency. Both methods used 5 % strain amplitude.

6.3 Additional Tests

6.3.1 Water Absorption

The amounts of water the porous scaffolds, dogbones and the joint scaffolds absorbed during *in vitro* was observed. Samples were taken out of the incubator, the surfaces were tapped with paper and the wet masses were weighed prior to testing. After tests, samples were put to dry under fume hood until dry enough to be put in vacuum chamber (WTB Binder 78532 Tuttlingen, Germany). After vacuum dry, the samples were weighed. Water absorption was then calculated by dividing the difference between the wet sample weight and the dry sample weight with the dry sample weight.

6.3.2 Thermal Analysis

Thermal analysis included the differential scanning calorimetry and thermogravimetric analysis of the mechanically tested samples. The DSC samples were prepared by cutting 5-10 mg of the mechanically tested samples and placing the pieces inside the DSC sample vessel, between a pan and a lid, which was then compressed closed. The TGA samples were made by cutting 20-30mg sized pieces of the original samples.

The DSC samples were then placed in DSC testing machine (Q1000, TA Instruments, New Castle, Delaware, USA). The samples were tested by first heating from 0 to 200 °C using a heating rate of 20 °C/min, the samples were then cooled to 0 °C with 50 °C/min cooling rate and then reheated to 200°C with the same heating rate of 20 °C/min. The porous scaffolds and dogbones were also tested by using a different starting temperature of -40 °C. From the resulting curves the melting temperatures (first heating) and glass transition temperatures (second heating) were determined.

The TGA tests were done to the porous scaffolds and dogbones that had TCP. Tests were completed using a TGA testing machine (Q500 TA Instruments, New Castle, Delaware, USA) to determine the TCP content of the composite material samples. The samples were heated to 700 °C using a heating rate of 20 °C/min followed by 1-minute isothermal hold. The amount of TCP was observed. In addition, TGA tests were performed to the cancellous bone in order to determine the amount of inorganic or mineral component in the bone. The samples were heated to 800 °C with the same heating rate.

7. RESULTS AND DISCUSSION

In this section the results and discussions are presented. In order to produce clear and readable graphs, the error bars have been left out of graphs containing more than one curve.

7.1 Porous Scaffolds

The porous scaffolds were mechanically tested in dry and in physiologically simulated conditions. The samples tested in physiologically simulated conditions were kept prior to testing either two or fourteen days in buffer solution and Figure 28 represents the average water absorption of the scaffolds during their time in vitro. While the water absorption of two weeks in vitro is slightly greater than the water absorption of two days in vitro for both materials, the biggest overall difference is between the materials. The PLCL scaffold structures absorbed more than twice the amount of water than the scaffolds with the ceramic content, suggesting that the pure polymer scaffolds were more porous, absorbing more water inside the structure. The water absorption values for both materials were also very high, considering the amount of time the samples were *in vitro* as well as the values presented in a previous study on the same materials [96]. Granting the scaffold sizes were much larger in this thesis as well as the degree of porosity, meaning that more water remained inside the pores increasing the weight even though the scaffolds were tapped with paper.

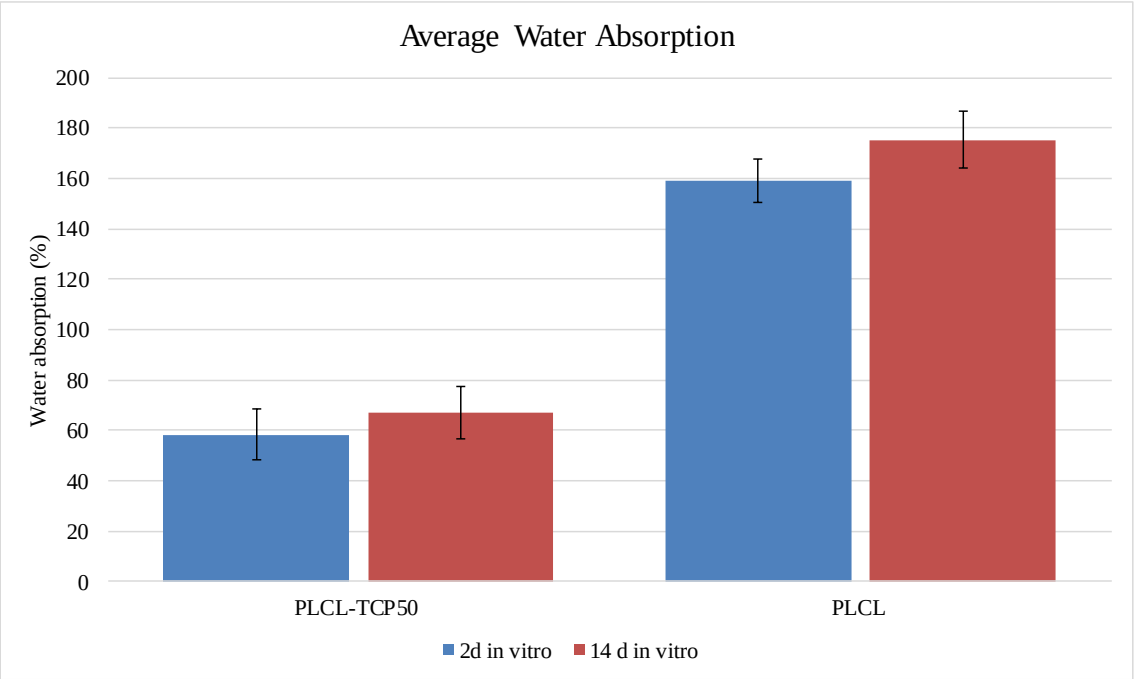

Figure 28. *The average water absorption of the porous scaffolds (PLCL-TCP50 2d in vitro n=10, 14d in vitro n=11 and PLCL n=5)*

The TGA tests on the PLCL-TCP50 scaffolds showed that while most samples did contain approximately 50% TCP (between 48% and 52%), there were samples in all test points that contained significantly less. Of the 0 dry samples four had TCP between 14 and 24%, of the 2d in vitro samples two had TCP between 14 and 21%, and of the 14d in vitro samples one had 14% TCP content. The samples having the lesser amount of TCP had lower values in the mechanical tests, so the samples were left out of the results for the mechanical tests. The average TCP content of the 0 dry samples was 50.0 ± 0.01% (n=8), while the content was for 2d in vitro samples 50.1 ± 0.01% (n=10) and 14d in vitro samples 50.2 ± 0.01% (n=11).

The DSC results showing the crystallinity of the porous scaffolds are presented in Figure 29. Overall the PLCL showed significantly more crystallization than the PLCL-TCP50. The pure polymer scaffold presented slight crystallinity even in the 0 dry samples whereas the polymer-ceramic composite did not. The average crystallinity of the 0 dry PLCL scaffolds was 6.7 ± 0.2 J/g. After *in vitro* the average crystallinity of PLCL increased to 21.0 ± 1.5 J/g and 23.6 ± 0.1 J/g for two days and two weeks in vitro, respectively. The PLCL-TCP50 scaffolds started to show crystallinity after two days in vitro, resulting in the average crystallinity of 9.0 ± 3.1 J/g for 2d in vitro samples and 8.9 ± 0.4 J/g for 14d in vitro samples. The crystallinity shows in the DSC heating curves as shallow drop opposed to peaks accustomed to e.g. PLA, meaning that the crystals were small and needed only little energy in wide temperature range (from 40 to 120°C) in order to be melted. The glass transition temperature was approximately 22°C for both materials for all test points.

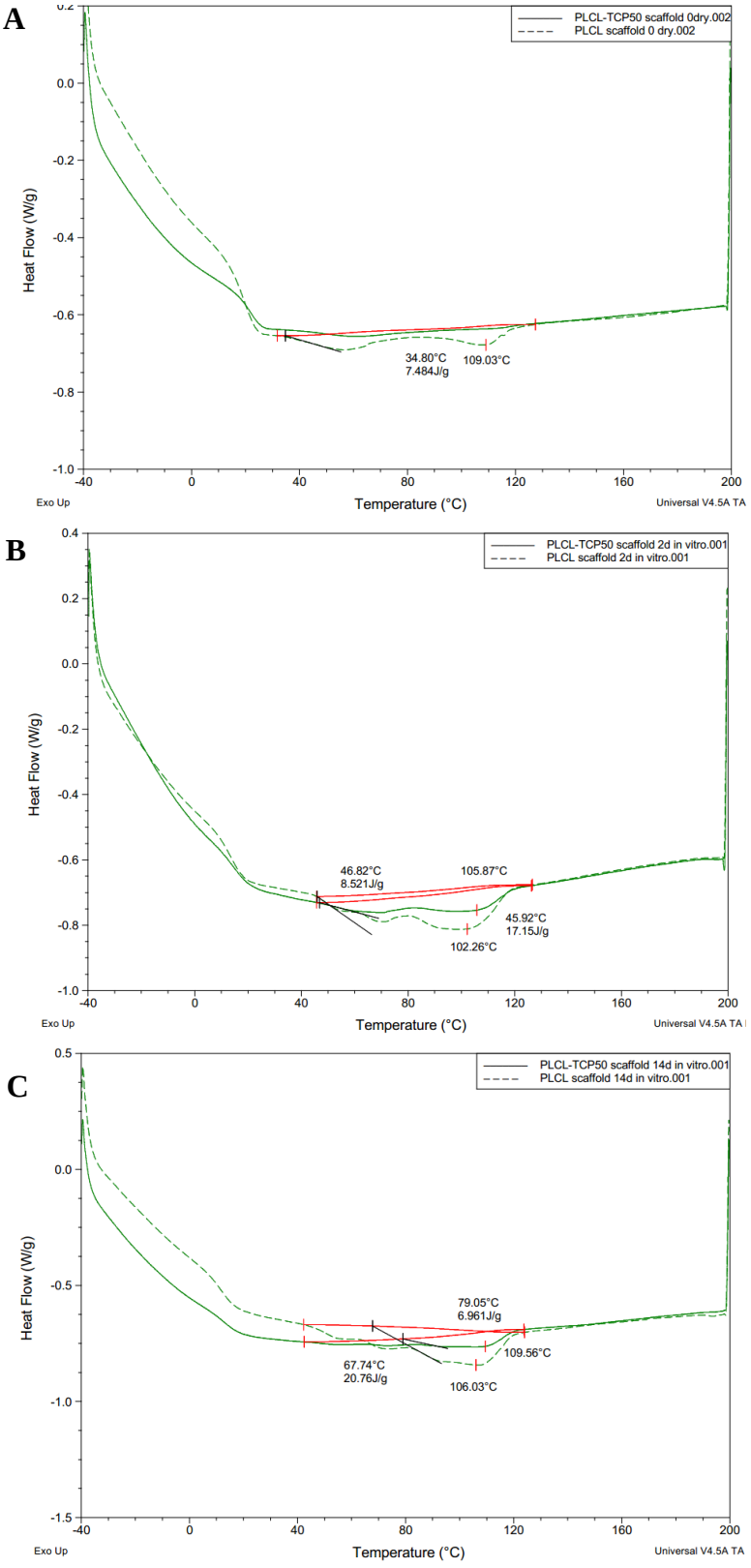

Figure 29. *DSC curves for porous scaffolds (n=1) A. 0 dry B. 2d in vitro and C. 14d in vitro*

The mechanical testing of the porous scaffolds was started by compressing to 20 % strain using the 1mm/min testing speed, which equals to approximately 0.002 s^{-1} strain

rate, close to values bone experiences during physiological activities such as walking [10]. Figure 30 represents the average stress-strain curves that were obtained.

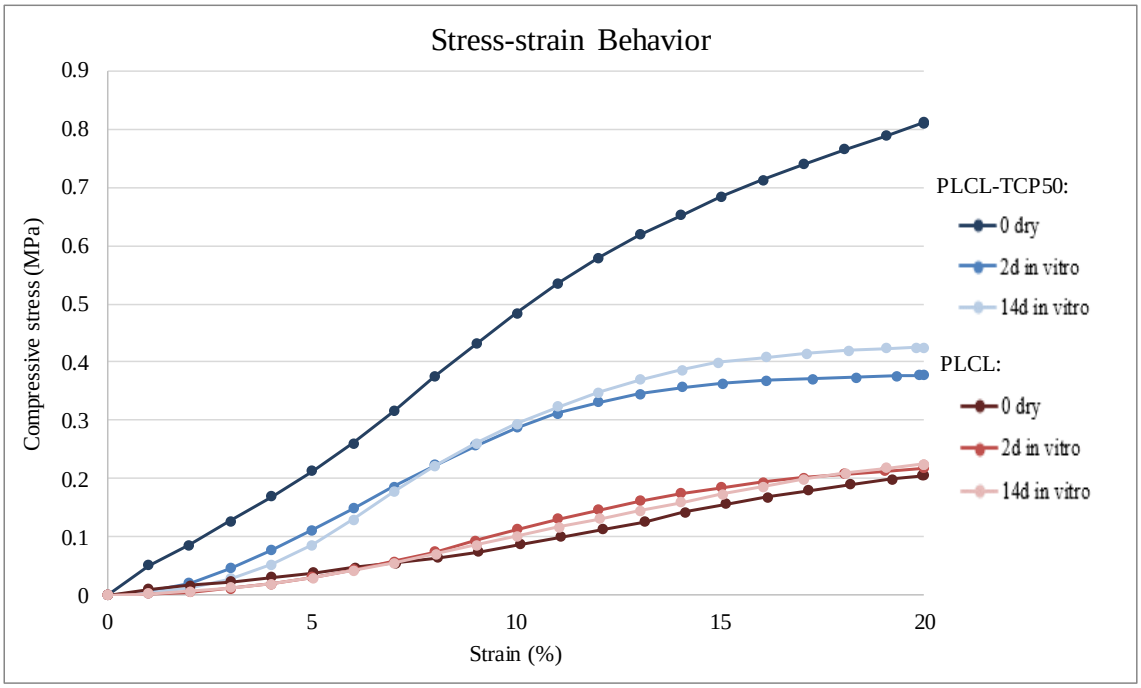

Figure 30. *The Stress-strain behavior of the porous scaffolds (PLCL-TCP50 n=4/5/6, PLCL n=3). The standard deviations of stress ranged from 0 to ± 0.32, from 0 to ± 0.047 and from 0 to ± 0.048 in case of PLCL-TCP50 0 dry, 2d and 14d in vitro, respectively. The same values for PLCL were 0 to ± 0.022, 0 to ± 0.022 and 0 to ± 0.082*

Of the two materials, the stress-strain behavior of PLCL-TCP50 differed between dry and wet tests the most. On average the dry samples required more force in order to be compressed and the stress can be seen increasing steadily as the compression continued and no discernable toe region can be seen at the start of the curve. Also, the stress-plateau region is not as clear as with other curves. Instead, the softer and more pliable samples due to wet and warmer environment, had stress-strain curves much lower in the graphs and required less force to be compressed compared to dry. There is not much difference between the samples tested after either two days or two weeks in the buffer solution. Both curves exhibit a toe region before stress starts to steadily increase until about 14% when the stress needed to compress the samples start to plateau.

Compared to the ceramic-composite scaffold, the dry and physiologically simulated stress-strain curves of the PLCL scaffolds are much more similar with each other, with slight hints that the physiologically simulated samples were tougher. However, due to the lack of ceramic content, the forces and therefore the stresses needed for the compressions were much smaller compared to the PLCL-TCP50 scaffolds. Although not seen in the graph, similarly to the composite scaffolds, the 0 dry PLCL did not exhibit clear toe region but the physiologically simulated scaffolds did. The shapes of

the curves did not plateau towards the end, instead increased, though slower than the 0 dry PLCL-TCP50.

Due to the fact that the scaffolds were only compressed to 20 % of their height, no ultimate rupture could be detected nor likely to have been seen at all had the compressions continued, thus the compressive strength of the scaffolds could be observed from selected strain value. Observing the average stress-strain curves, at 10 % strain the average compressive strength of dry PLCL-TCP50 was more or less 0.5 MPa while the strengths of the physiologically simulated samples were approximately 0.3 MPa. For the PLCL samples the average compressive strength was around 0.1 MPa for all testing conditions. Compared to the compressive strengths bones experience daily, the values were significantly lower [3,43,94] indicating that the scaffolds could be more suitable for bone applications not requiring high strengths. However, since the tests were performed as unconfined, it is possible that the scaffolds could have behaved more stiffly had they been confined into a defect like structure, since the confinement would have hindered the flow of both air and liquid out of the porous structure.

Figure 31 shows the calculated average moduli of the porous scaffolds, determined from the linear portion of the stress-strain curves between 5 and 15 % strain.

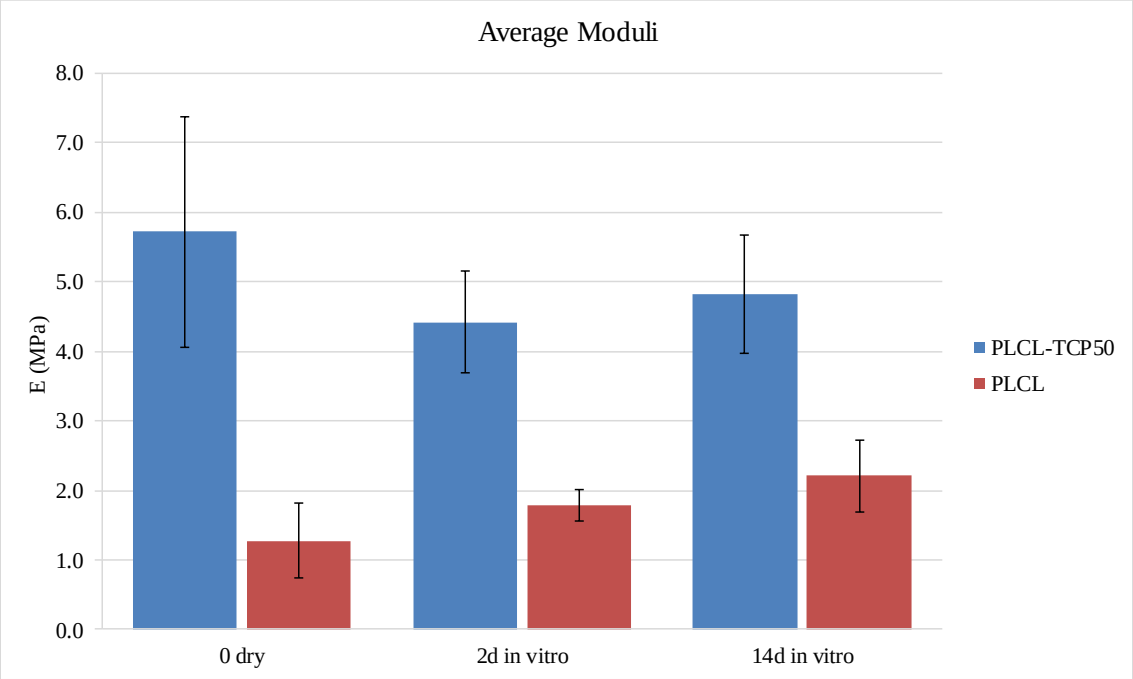

Figure 31. *The average moduli of the porous scaffolds (PLCL-TCP50 n=4/5/6, PLCL n=3). The error bars show the standard deviations*

Of the porous scaffolds, the largest average modulus originated from the PLCL-TCP50 samples tested dry (5.7 ± 1.7 MPa) and the smallest from the PLCL samples in the same testing condition (1.3 ± 0.5 MPa). Interestingly, the modulus values increased the longer the samples were kept in buffer solution, in other words the average moduli acquired

from tests after two days in buffer solution (4.4 ± 0.7 MPa for PLCL-TCP50 and 1.8 ± 0.2 MPa for PLCL) were lower than the average moduli from tests after fourteen days in buffer solution (4.8 ± 0.9 MPa and 2.2 ± 0.5 MPa), also the PLCL physiologically simulated samples had larger moduli than the dry. The modulus is generally dependent on the testing temperature as well as the aqueous environment, so by increasing the testing temperature as well as introducing water, the average moduli of the 0 dry PLCL samples should have been higher as was the average modulus of dry PLCL-TCP50. [7] The DSC results showed significant crystallization of the PLCL samples that might explain the increase in moduli of the PLCL scaffolds. The DSC curves indicated that both materials had glass transition temperatures close to 22 °C when tested dry, meaning that the PLCL samples should have been acting slightly stiffer tested in ambient laboratory conditions compared to the 37 °C way above T_g, since introducing water into the scaffolds more than likely caused the T_g to lower even further in case of the physiologically simulated scaffolds during testing. [97] Crystallization of the 14d in vitro PLCL-TCP50 samples might also explain the slight increase in stiffness compared to the 2d in vitro samples.

Monitoring the stress relaxation behavior of scaffolds is one way to determine viscoelastic mechanical behavior, since most biological tissues as viscoelastic materials, as well as implant materials in certain situations might experience it. [7,8]Small-scale stress relaxation test was conducted on to the porous scaffolds. The initial load and stress needed to compress the scaffolds to 20% strain was compared to the load and stress after keeping the compressions for 1000 seconds. The graphs in Figure 32 represent the average stress relaxation curves for PLCL-TCP50 and PLCL scaffolds, respectively.

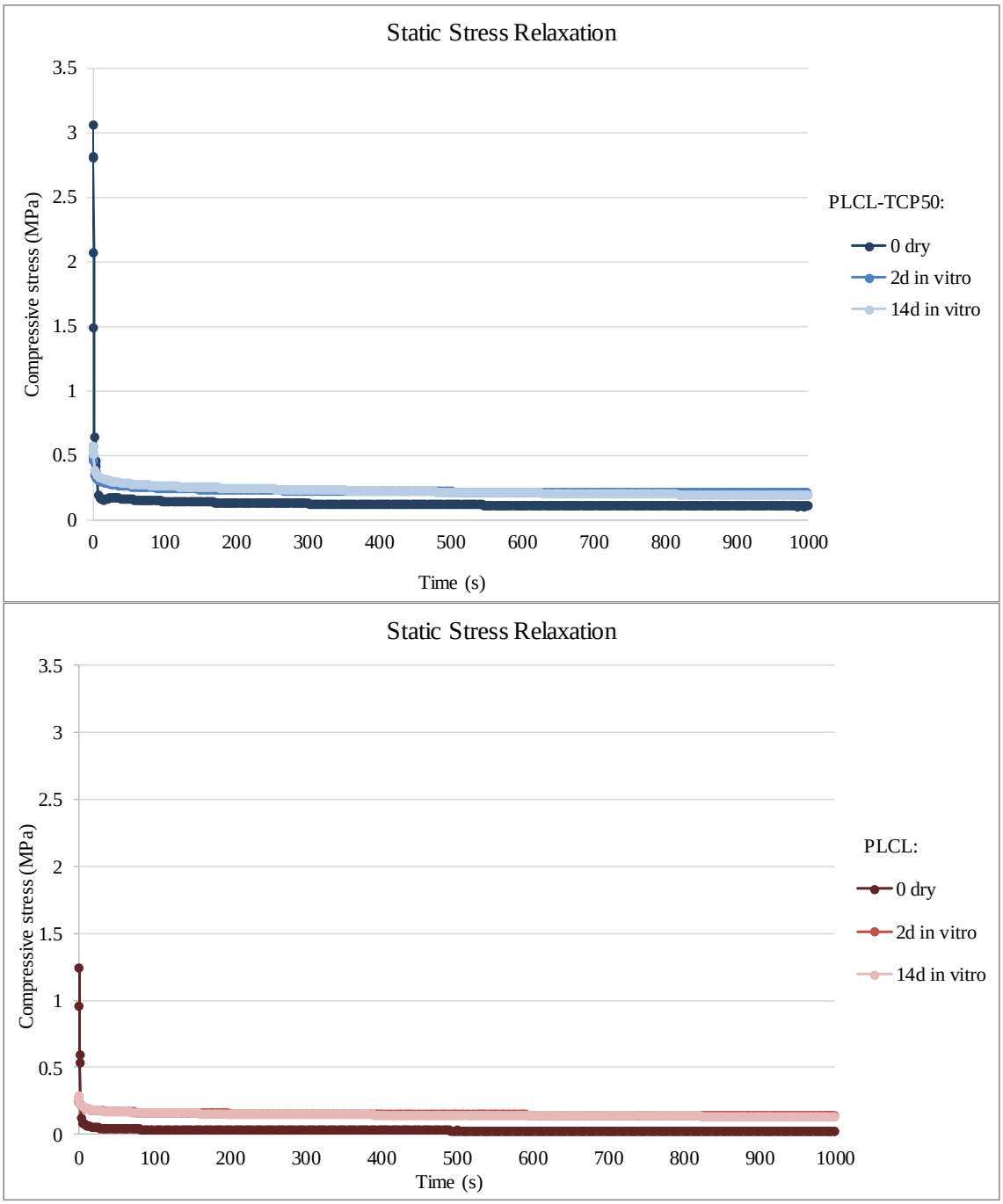

Figure 32. *The average stress relaxation curves of A. PLCL-TCP50 (n=4/5/6) and B. PLCL (n=3) scaffolds. The standard deviations of stress ranged between ± 1.1 and ± 0.02, ± 0.071 and ± 0.024, and between ± 0.062 and ±0.025 in case of PLCL-TCP50 0 dry, 2d and 14d in vitro, respectively. The same values for PLCL were ± 0.19 and ± 0.003, ± 0.028 and ± 0.011, as well as ± 0.04 and ± 0.011*

The relaxation curves show that the initial stress at the beginning of the test, is larger compared to the end. Also the decrease in compressive stress, is not slow, instead in all testing conditions the decline of the curves and ultimate plateauing occurred very quickly. In case of PLCL-TCP50 dry scaffolds, the equilibrium occurred after 7 seconds, while physiologically simulated scaffolds experienced the equilibrium after 2

seconds. PLCL scaffolds in physiologically simulated conditions behaved similarly with the PLCL-TCP50 counterparts, however in dry conditions the plateauing occurred earlier, after 5 second hold.

The two scaffolds had also in common that while the initial stresses of scaffolds tested dry were much larger compared to the scaffolds tested under physiologically simulated conditions, the wet tested samples retained more stress during holding, the dry samples relaxed almost to zero. It is possible that that during the in vitro time, the polymer chains have gravitated towards more energetically stabile state, which lead to a more perfect state energetically and thus had a big effect on the stresses during compression [97,98], however more tests should be conducted to confirm this theory. Other explanation might be that the crystallization during the in vitro resulted in reduced amount of amorphous parts and thus less elastic behavior and helped retain more stress. Overall, the stresses needed to compress the scaffolds were larger with PLCL-TCP50 scaffolds due to the ceramic content.

In Figure 33A the average load values at initial compression and after 1000 seconds are presented. While stress values are more material based, the load values represent the structural side of the scaffolds. The B graph on the other, hand shows the percentage change between those two compressions, in other words the percentage relaxation, calculated using the following equation:

$$Relaxation\ (\%) = \frac{initial\ compression - compression\ after\ 1000s}{initial\ compression} \times 100\% \qquad (11)$$

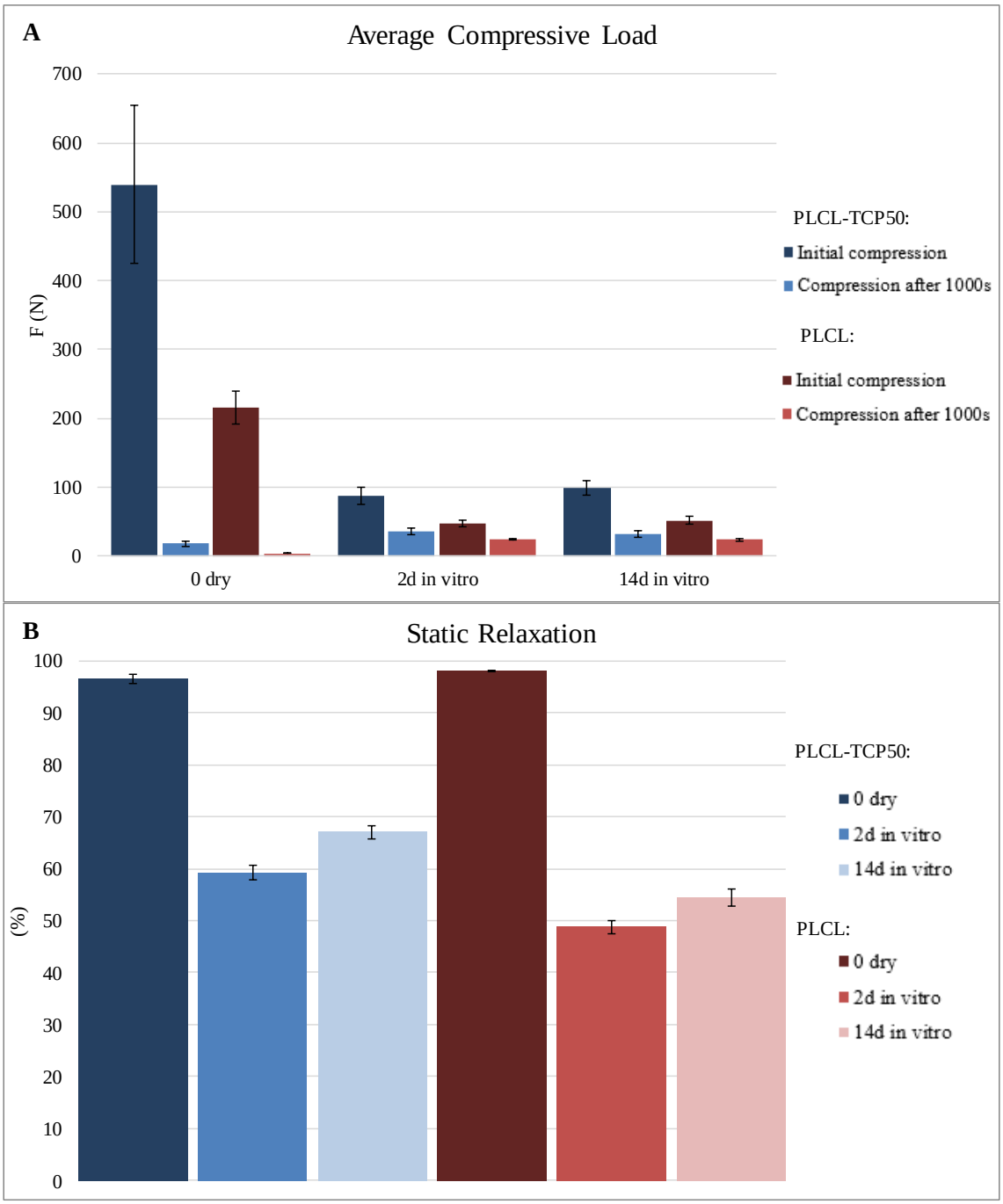

Figure 33. *A. The average load values of the porous scaffolds at initial compression and after 1000 seconds B. The average percentage relaxation between the compressions (PLCL-TCP50 n=4/5/6, PLCL n=3)*

Graph A demonstrates the huge effect of the addition of ceramic on the loads needed to compress scaffolds. In all scenarios PLCL-TCP50 required 50 % as much force in order to be compressed to the wanted strain. From graph A it is easy to assume that the biggest relaxation occurred to dry PLCL-TCP50, however, from graph B it can be observed that actually dry PLCL had a slightly bigger relaxation. In case of PLCL-TCP50 the change was 96.5 ± 0.9 % and for PLCL 98.2 ± 0.2 %. In case of the physiologically simulated scaffolds, the percentage relaxation was 59.2 ± 1.4 % and

67.0 ± 1.3 % for PLCL-TCP50 2d and 14 in vitro time points, respectively, while for PLCL the values were 48.7 ± 1.2 % and 54.4 ± 1.7 %. The percentage change increased the longer the samples were kept in the buffer solution, because the initial stress and load at the beginning were larger with 14d in vitro samples while after 1000 s the values were practically the same.

Overall, the relaxation of the porous scaffolds occurred significantly fast compared to for example cortical bone that start to experience the equilibrium of stress after 60 000 seconds. [99] Since the test duration was quite short at 1000 s and the observed stress in megapascals, it is unknown whether further observable relaxation could have occurred had the test continued. Also bigger initial compression could have caused different kind of a curve.

In contrast to static relaxation test, by dynamically loading the porous samples, the dynamic relaxation behavior was also observed. While a scaffold for example as a defect filler experiences static relaxation, dynamic loading can also occur during daily activities. The porous scaffolds were dynamically loaded between 5 and 25 % compressive strain. The decrease in stress was observed from the first cycle to the last and the resulting compressive stress-cycles curves are presented in Figure 34. The 500 cycle amount is equal to 1000 second test duration comparable to the static test.

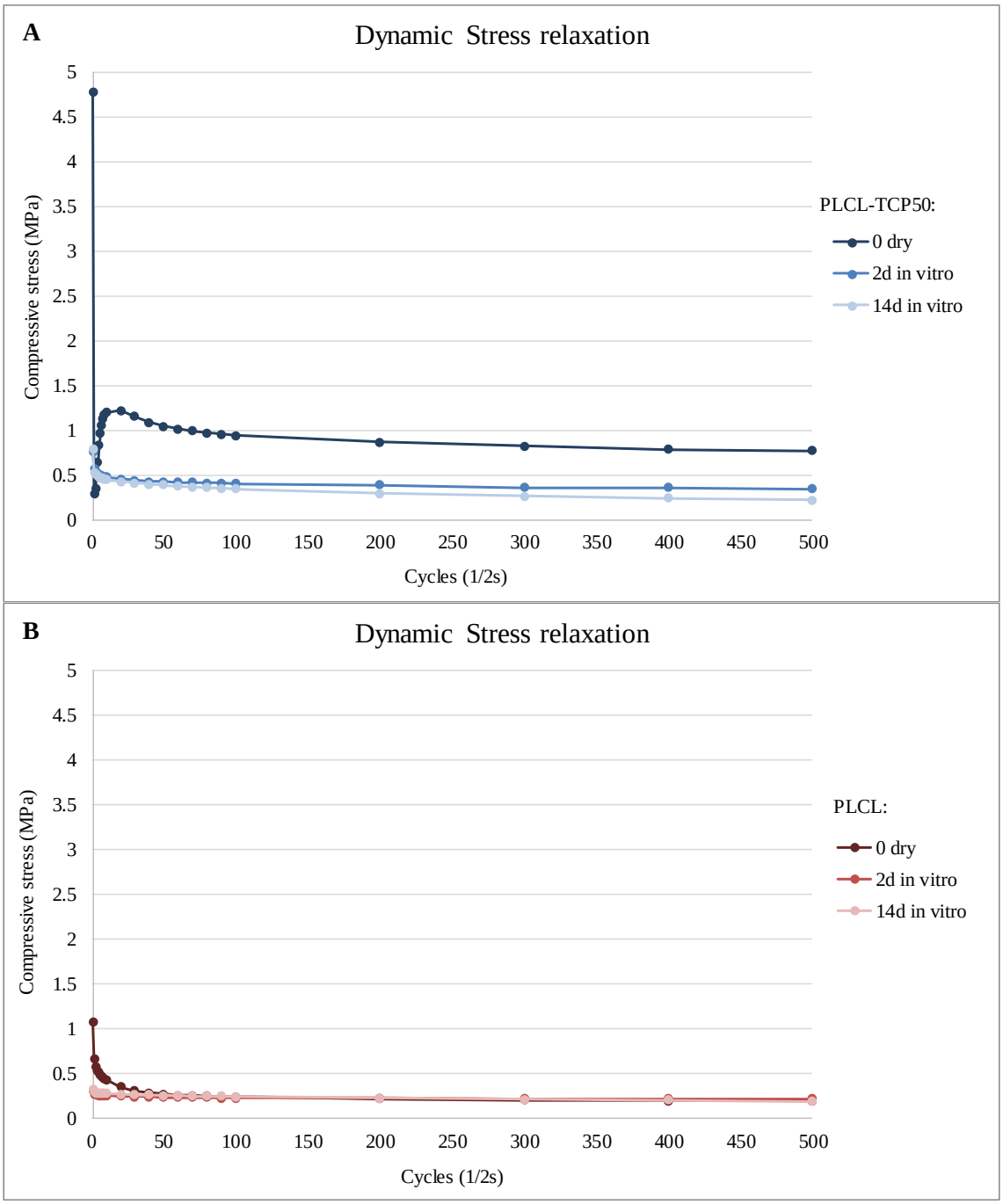

Figure 34. *The average dynamic stress relaxation of porous scaffolds. A. PLCL-TCP50 (n=4/5) B. PLCL (n=2). The standard deviations of stress ranged from ± 0.64 to ± 0.13, from ± 0.16 to ± 0.056, and from ±0.16 to ±0.041 in case of PLCL-TCP50 0 dry, 2d and 14d in vitro, respectively. For PLCL the values represent the maximum and minimum of the two samples and ranged from ± 0.039 to 0, from ± 0.037 to 0.028 and from ±0.0055 to 0.014*

The dynamic relaxation behavior of the porous scaffolds is mostly similar with the static relaxation test, at first the needed stress to deliver the wanted amount of deformation is larger compared to what is needed in the end of the test. Also the curves seem to plateau toward the end, or at least slow down their decrease, the physiologically simulated

scaffolds faster than the dry ones. Also the acting forces are seemingly much higher with PLCL-TCP50 scaffolds than with the PLCL scaffolds.

While the PLCL curves are very alike after 100 cycles, with slight differing towards the end, clear difference can be seen between the PLCL-TCP50 dry and physiologically simulated scaffolds. The 2d in vitro and 14d in vitro curves were practically the same until the 100^{th} cycle at which point they started to diverge while the dry PLCL-TCP50 curve was very different at the start compared to the other curves. Instead of the quick decrease of stress, that ultimately slowed down towards the end, the needed compressive stress diminished dramatically to a value significantly different from the end. Up to the tenth cycle the compressive stress increased again, followed by a small plateauing until the 20^{th} cycle before finally the ultimate slow lessening of the stress occurred. This behavior was consistent to every 0 dry parallel sample, meaning that the behavior was likely due to the combined effect of the machine settling and the stiffness of the scaffolds. The initial maximum compressive load caused the compressive deformation of the scaffolds and because the scaffolds did not act as elastically as the scaffolds tested in physiologically simulated conditions, the scaffolds did not recover their initial height, making them slightly stiffer and resulting in the increase in compressive stress. Further dynamic loading caused the scaffolds to remain in the compressed state and only slight compression was needed for the test resulting in the ultimate decrease of the compressive stress.

In Figure 35 the compressive load values of the scaffolds at the start of the cycles and at the end are presented, as well as the average percentage relaxation between the two cycles.

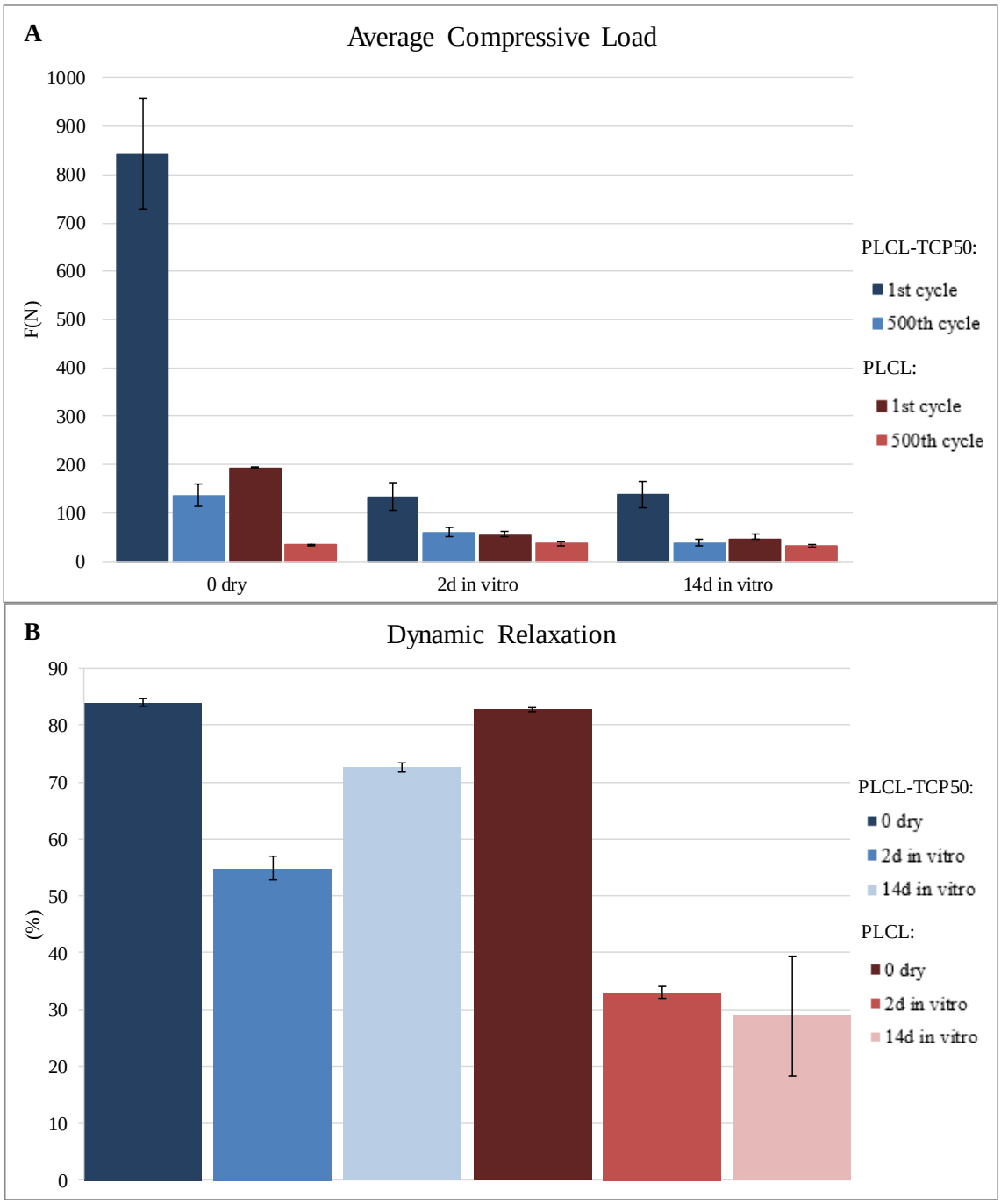

Figure 35. *A. The average load values at first and last cycle. B. The average percentage relaxation between the cycles (PLCL-TCP50 n=4/5 and PLCL n=2). Error bars show the standard deviation for PLCL-TCP50 samples and maximum and minimum of the two samples for PLCL*

Graph A demonstrates clearly the significant difference in compressive forces when comparing the column of the first cycle of dry PLCL-TCP50 to every other column. On the other hand, it also demonstrates how similarly the PLCL-TCP50 2d and 14d in vitro scaffold behave in the first cycle and differ by almost half in the last, while practically the only differing bar with the PLCL scaffolds is the 0 dry first cycle, the

physiologically simulated in the first cycle and all the bars in the last cycle being very similar with each other.

Graph B shows that while it is easy to assume that the dry PLCL-TCP50 would relax the most between the cycles and while it is true when looking at the amounts, the percentage change is actually very similar to that of dry PLCL (84.0 ± 0.6 % and 82.7 ± 0.4%, respectively) The difference between the dry and physiologically simulated scaffolds was more obvious with the PLCL scaffolds, while the difference between 2d and 14d in vitro scaffolds was more obvious with the PLCL-TCP50 scaffolds.

Compared to the static relaxation test, overall the porous scaffolds experienced less stress relaxation during the 1000 second test duration when dynamically loaded, the only exception being PLCL-TCP50 tested after 14 days in buffer solution.

In addition to the relaxation tests, viscoelastic behavior can also be observed from hysteresis curves. From the same dynamic results, the stress-strain hysteresis graphs for PLCL-TCP50 and PLCL, respectively can be seen in Figure 36.

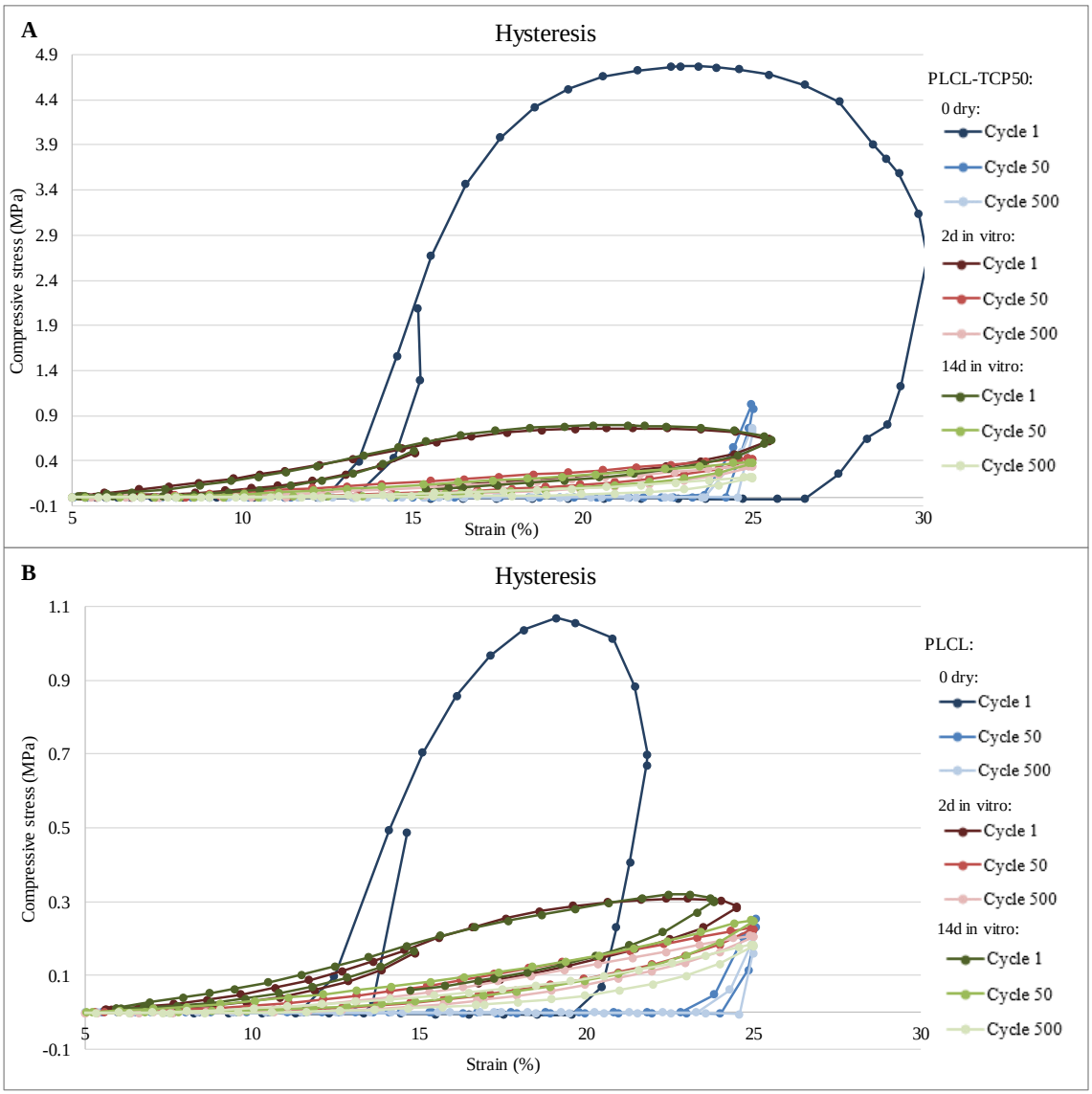

Figure 36. *The stress-strain hysteresis of A. PLCL-TCP50 (n=4/5) and B. PLCL scaffolds (n=2)*

If the curves had behaved as expected, the loops would have been at 5% minimum strain and 25% maximum strain, however in Figure 30 it can be clearly seen that it is not the case. While in case of PLCL-TCP50 the maximum strain is actually in all test conditions in the first cycle more than 25 %, way more in case of 0 dry, the PLCL actually had less than 25 %, once again more significantly in case of 0 dry. In other words, the testing machine either compressed too much or not enough in the first cycle, however by cycle 50, in all cases, the right amount of compression had been applied.

For both materials, the first cycle tested dry had the largest area inside the loop, meaning that there is large amount of energy dissipation during the first cycle, and because the area underneath the loop is quite small, only little energy is returned. This results in the behavior of the 50th and 500th cycles, only small loops can be seen in the graphs. The compression of the first cycle caused the dry samples to deform and only

small recovery happened before another compression cycle occurred. The physiologically simulated samples on the other hand, had quite similar loops between first, 50th and the 500th cycles. While the first cycle was slightly bigger, the area underneath however, seemed to be in the same size category, meaning that after the first cycle most of the original scaffold shape was recovered. Towards the end of the cycles, however, the stress at maximum strain dropped and less energy was needed for the compression and some of the deformation did not have enough time to recover.

7.2 Dogbones

The dogbones were tested mechanically dry and after two days in buffer solution. While of the porous scaffolds, the PLCL had the biggest water absorption, the opposite was true with the dogbones. As seen in Figure 37, The PLCL-TCP50 absorbed almost two times the water compared to the PLCL. In addition, because the dogbones where solid materials, the water absorption was significantly less compared to the porous scaffolds.

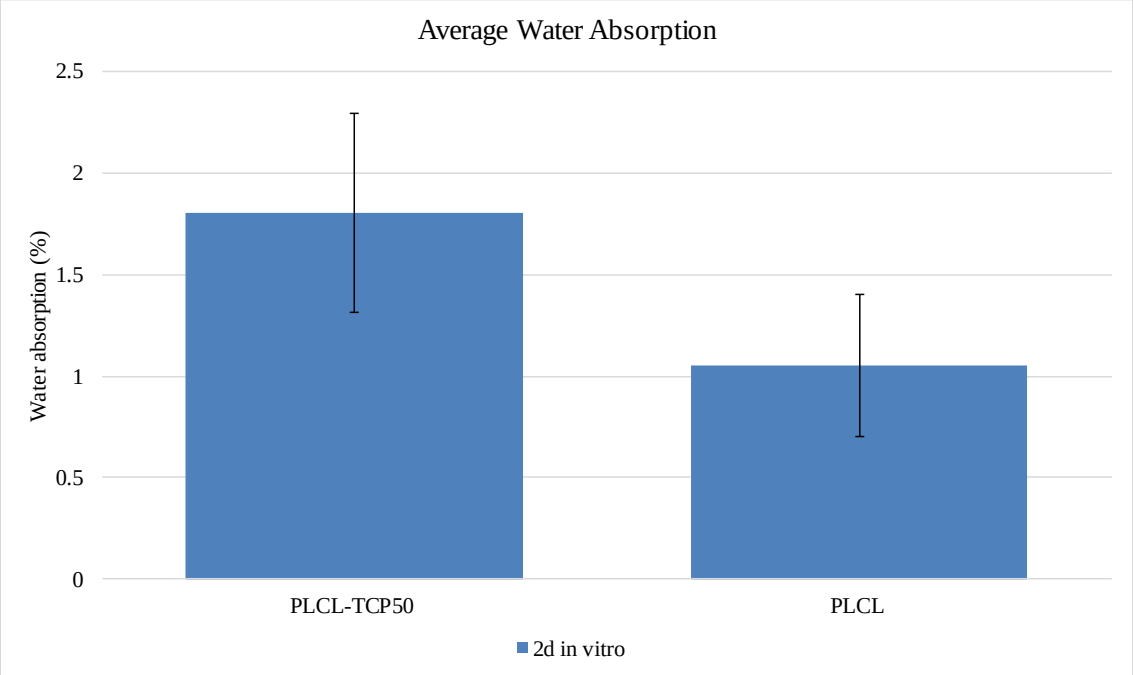

Figure 37. *The average water absorption of dogbones (PLCL-TCP50 n=17 and PLCL n=18)*

The TGA tests on the PLCL-TCP50 dogbones revealed that the amount of TCP was slightly greater than expected. Overall, the amounts ranged between 53 and 65 % (58.5 ± 0.04 % n=12) but, because none of the tested samples had less than 30 % TCP like the scaffolds, no samples were disregarded from the results of mechanical tests.

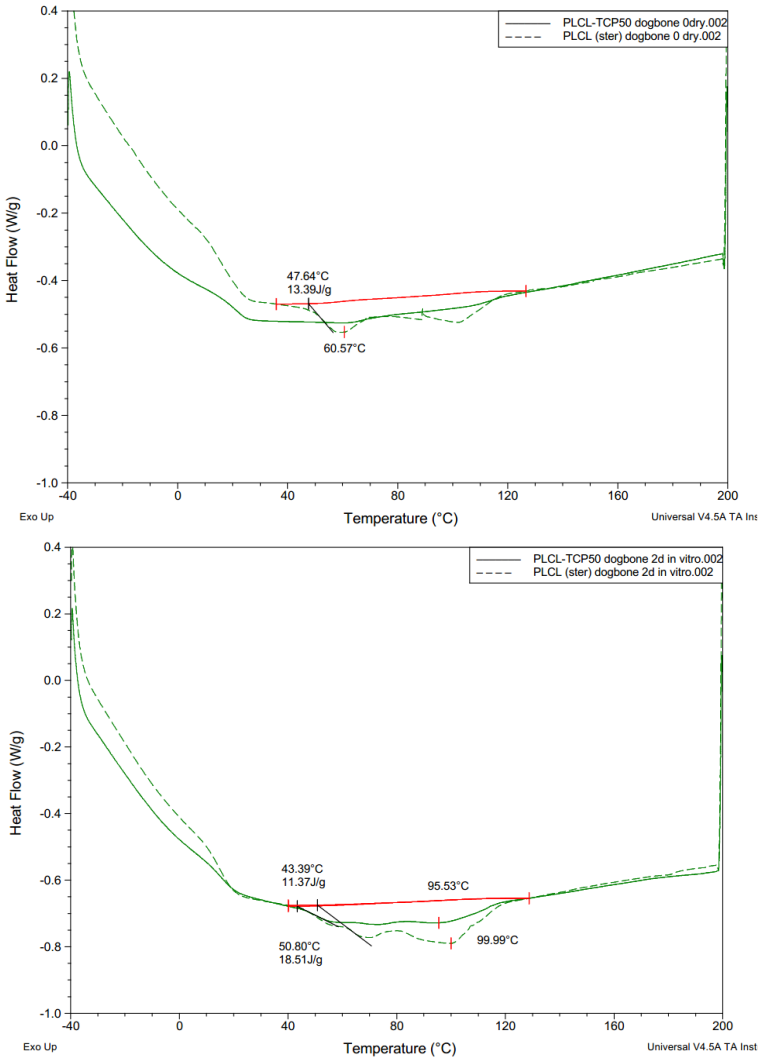

Figure 38. *The DSC results of the dogbones*

Figure 38 represents the crystallinity of the dogbone samples obtained from DSC results. Similarly, to the scaffolds, while PLCL exhibits crystallinity both without being in buffer solution and after two days in buffer solution, the PLCL-TCP50 only shows crystallinity after being in buffer solution for two days. The crystallinity of PLCL was 8.7 ± 3.1 J/g and 18.8 ± 0.1 J/g for 0 dry and 2d in vitro samples, respectively and for 2d in vitro PLCL-TCP50 the crystallinity was 8.3 ± 2.8 J/g.

The stress-strain behavior of the dogbones were tested in different ways. In Figures 39A and 40C the samples were pulled to 300 % strain using two different testing speeds and in graphs 39B and 40D samples were strained to 100% using very fast speed and after dynamically loading the samples first in the elastic region of the stress-strain curve.

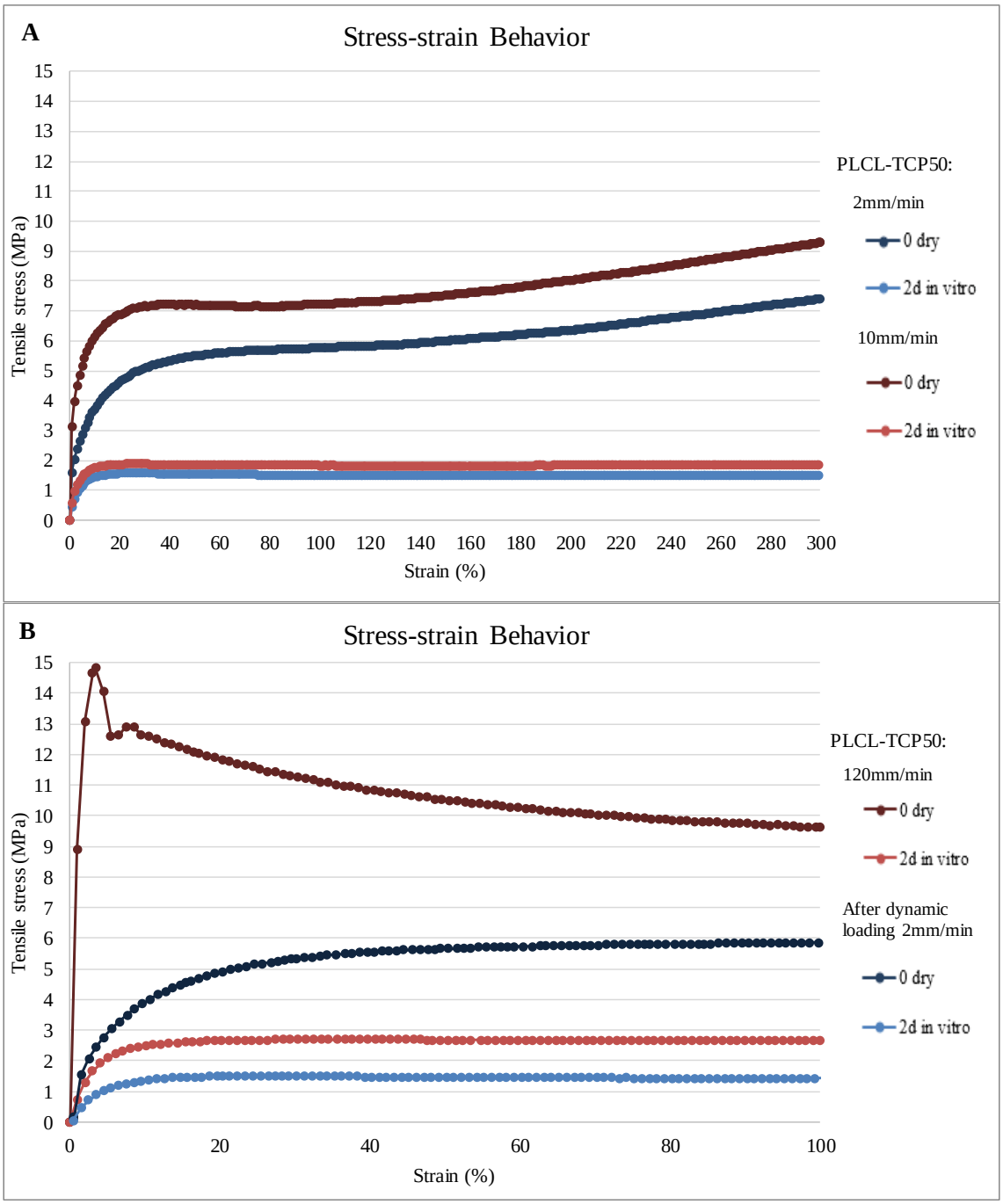

Figure 39. *The stress-strain behavior of PLCL-TCP50 dogbones. A. Straining to 300% 2mm/min (n=6, deviation of stress between 0 and ± 0.74 for dry and between 0 and ± 0.17 for 2d in vitro) and 10mm/min (n=2, error of stress between 0 and ± 0.65 for dry and between 0 and ± 0.33 for 2d) B. Straining to 100% 120mm/min (n=3, deviation of stress between 0 and ± 2.0 for dry and between 0 and ± 0.26 for 2d) and 2mm/min after dynamic loading (n=5/6, deviation of stress between ±0.10 and ± 0.37 for dry and between ± 0.070 and ± 0.18 for 2d)*

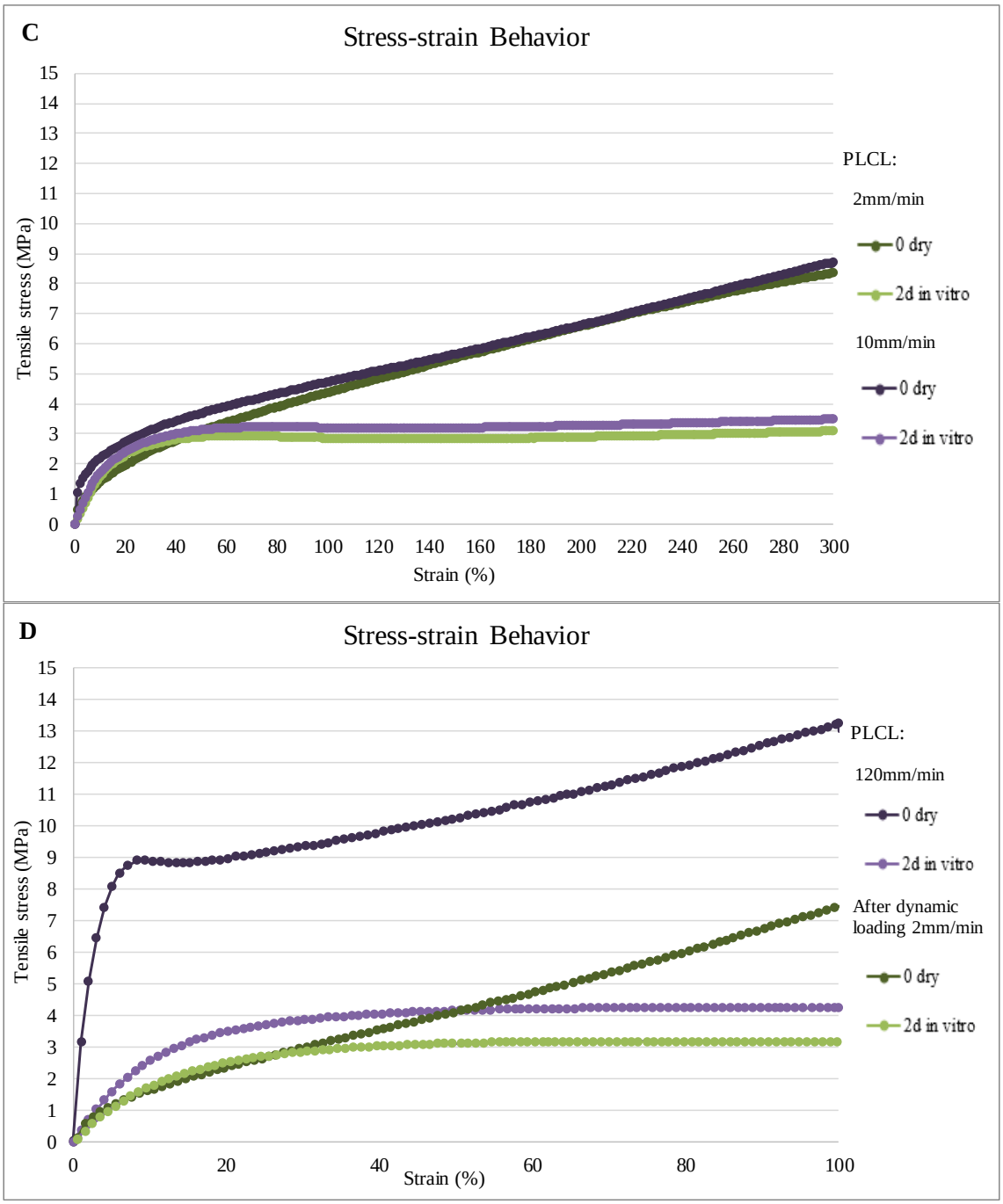

Figure 40. *The stress-strain behavior of PLCL dogbones. C. Straining to 300% 2mm/min (n=4, deviation of stress between 0 and ± 1.5 for dry and between 0 and ± 0.39 for 2d) and 10mm/min (n=3/2, deviation of stress between 0 and ± 2.0 for dry and error of stress between 0 and ± 0.24 for 2d) and D. Straining to 100% 120mm/min (n=3, deviation of stress between 0 and ± 4.3 for dry and between 0 and ± 0.37 for 2d) and 2mm/min after dynamic loading (n=6, deviation of stress between ± 0.44 and ± 6.8 for dry and between ± 0.025 and ± 0.55 for 2d)*

The mechanical behavior of polymers is significantly affected by the testing environment and the speed of testing [20,23] . In almost all of the cases, the dry testing of the samples resulted in strain hardening of the materials. After initial elastic region and yielding of the material, the stress started to steadily rise until the end of the test.

Only exception of the dry samples was PLCL-TCP50 with 120 mm/min testing speed. Instead of strain hardening, after yielding the stress needed to stretch the dogbones started to drop first dramatically then steadily, indicating that the brittle behavior of the TCP came in to affect. If the tests had been continued, it is highly possible that the PLCL-TCP50 samples might have broken at some point. Otherwise all the test samples stayed relatively intact during testing, although the PLCL-TCP50 samples did show some crazing at the edges of the gauge section without leading to a break. After the tests and after samples were taken out of the grips, all the samples recovered their shape, the wet samples faster than the dry ones.

As for the samples tested in water in 37°C, after yielding, in all cases, the stress needed to continue pulling the samples stayed virtually the same i.e. plateaued. The yield point can be observed from the graphs to be affected by both the testing speed and the condition, as well as which material is under observation. PLCL in dry condition and with the slowest testing speed seemed to have no yielding, instead the stress increased steadily after 1 % strain. However, increasing test speed and warmer testing conditions exhibit clear yielding. Overall, yielding occurred earlier with PLCL-TCP50 samples compared to PLCL samples showing yielding.

The increase of testing speed from 2 mm/min to 10 mm/min had more of an impact with the 0 dry PLCL-TCP50 samples. Comparison of the A and B graphs show that for PLCL the curves are very similar with each other, both 0 dry and 2d in vitro, while PLCL-TCP50 exhibits different 0 dry curves and similar 2d in vitro curves. Further increase in testing speed to 120 mm/min showed more of an impact with both of the materials in dry condition while 2d in vitro only resulted in slightly different curves compared to the slower testing speeds.

If the increase in testing speed had overall more impact with the 0 dry PLCL-TCP50 samples, the prior dynamic loading had more of an impact with the 0 dry PLCL. While observing the two graphs of PLCL it can be noticed that the priorly dynamically loaded samples experienced more strain hardening resulting in a more dramatically rising curve.

Overall, it can also be observed that while PLCL-TCP50 showed higher initial stiffness, because of the TCP particles, generally in the end PLCL required more stress to be strained than PLCL-TCP50. The difference in the initial stiffness behavior can also be seen in Figure 41 showing the different modulus values from the different stress-strain curves.

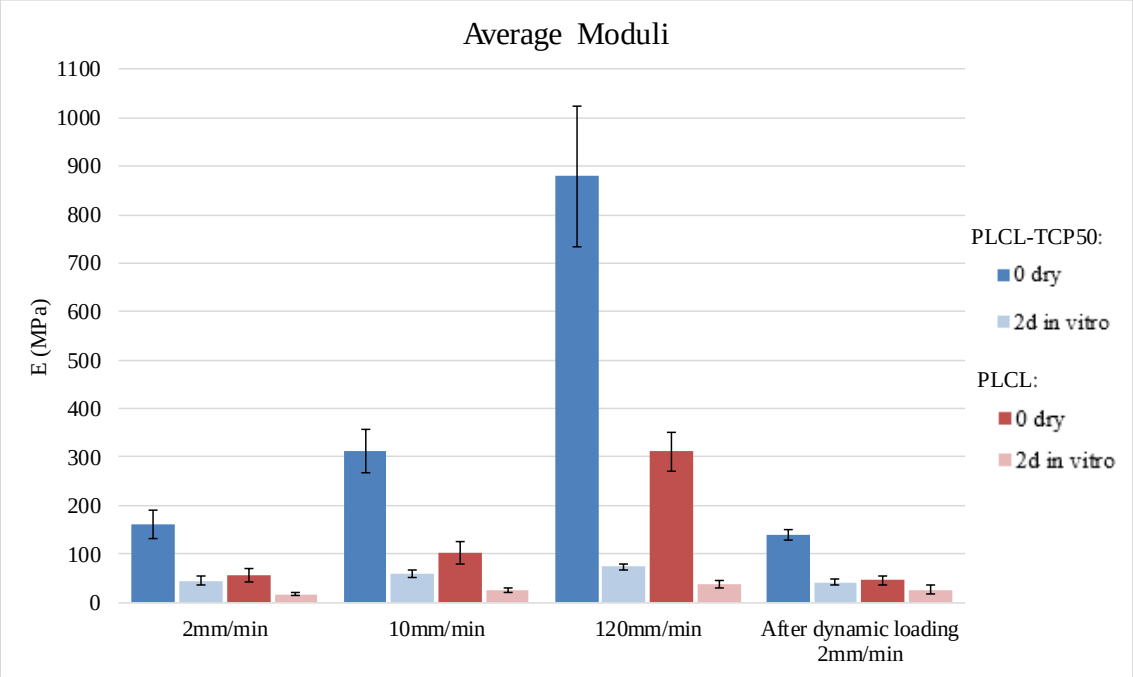

Figure 41. *The average moduli of the dogbone materials (2 mm/min n=6, 10 mm/min PLCL-TCP50 n=2 and PLCL n=3, 120 mm/min n=3, After dynamic loading PLCL-TCP50 n=5/6 and PLCL=6)*

Generally, the highest average moduli were from tests in dry conditions and PLCL-TCP50. As expected the PLCL-TCP50 strained to 100 % with the fastest testing speed had the highest average modulus of 880.1 ± 145.1 MPa. The equivalent PLCL average modulus of 311.4 ± 39.7 MPa on the other hand is very similar to the average modulus 312.1 ± 44.7 MPa of PLCL-TCP50 tested with 10 mm/min testing speed. Compared to the modulus values gotten from tests in dry conditions the average moduli from tests simulating physiological conditions were significantly lower and the lowest average modulus of 17.1 ± 2.3 MPa was obtained from PLCL samples tested 2 mm/min without the prior dynamic loading.

When comparing the moduli of the methods using 2 mm/min test speed, in most cases the average moduli was less if prior dynamic loading was inflicted, suggesting that dynamic loading caused softening of the materials, however, in the case of PLCL tested after two days in buffer solution, the modulus was actually somewhat higher after dynamic loading, indicating that the samples had stiffened after dynamic loading.

Overall, dry environment tests resulted in higher moduli compared to tests in physiologically simulated environment and increasing the testing speed resulted in significantly higher modulus for both materials when tested dry, however the combination of increased temperature and aqueous environment only caused the modulus to rise slightly when the test speed was increased. Obviously designing the test method is important, because in dry conditions determining one modulus value might not be enough, in simulated physiological conditions it might be.

The dogbones were also dynamically tested in tensile mode in two different ways, first in the essentially elastic region, determined from a stress-strain curve and secondly by first straining quickly to 100 %, past the yield point. The decrease in stress was observed and the subsequent curves can be seen in Figure 42.

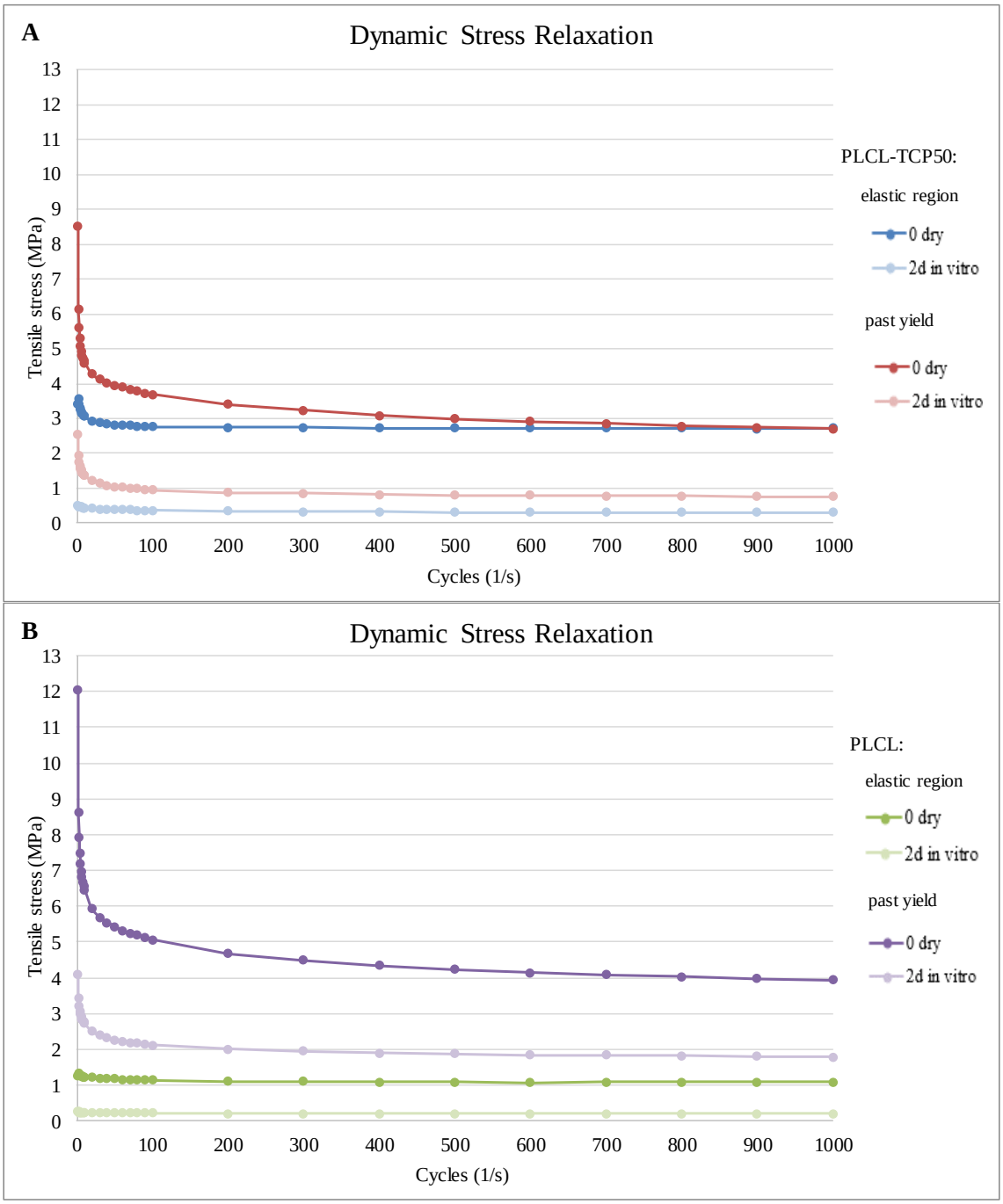

Figure 42. *The dynamic stress relaxation curves of the dogbones. A. PLCL-TCP50 elastic region (n=5, standard deviation ranges between ± 0.53 and ± 0.40 for 0 dry and between ± 0.072 and ± 0.037 for 2d in vitro) and past yield (n=3, deviation ranges between ± 0.59 and ± 0.17 for 0 dry and between ± 0.23 and ± 0.086 for 2d) and B. PLCL elastic region (n=4/6, deviation ranges between ± 0.29 and ± 0.22 for 0 dry and between ± 0.10 and ± 0.066 for 2d) and past yield (n=3 deviation ranges between ± 4.1 and ± 1.7 for 0 dry and between ± 0.15 and ± 0.076 for 2d)*

While the 0 dry samples loaded dynamically past the yield point exhibit highest tensile forces, the physiologically simulated samples loaded in the elastic region show the least. Also, while those 0 dry samples have curves that decrease fast in the beginning and slowdown in the end, the elastic region 2d in vitro curves seem to be quite linear, meaning that there seems to be no difference between the start and the end of the curves. For the most part, the curves seem to depict the scenario were in the elastic region, the PLCL-TCP50 was much tougher whereas, past yield point the PLCL material required more forces to deform and thus behaved more toughly.

In Figure 43, the average load values at the first and the last cycles have been compiled as well as the average percentage relaxation between the two cycles.

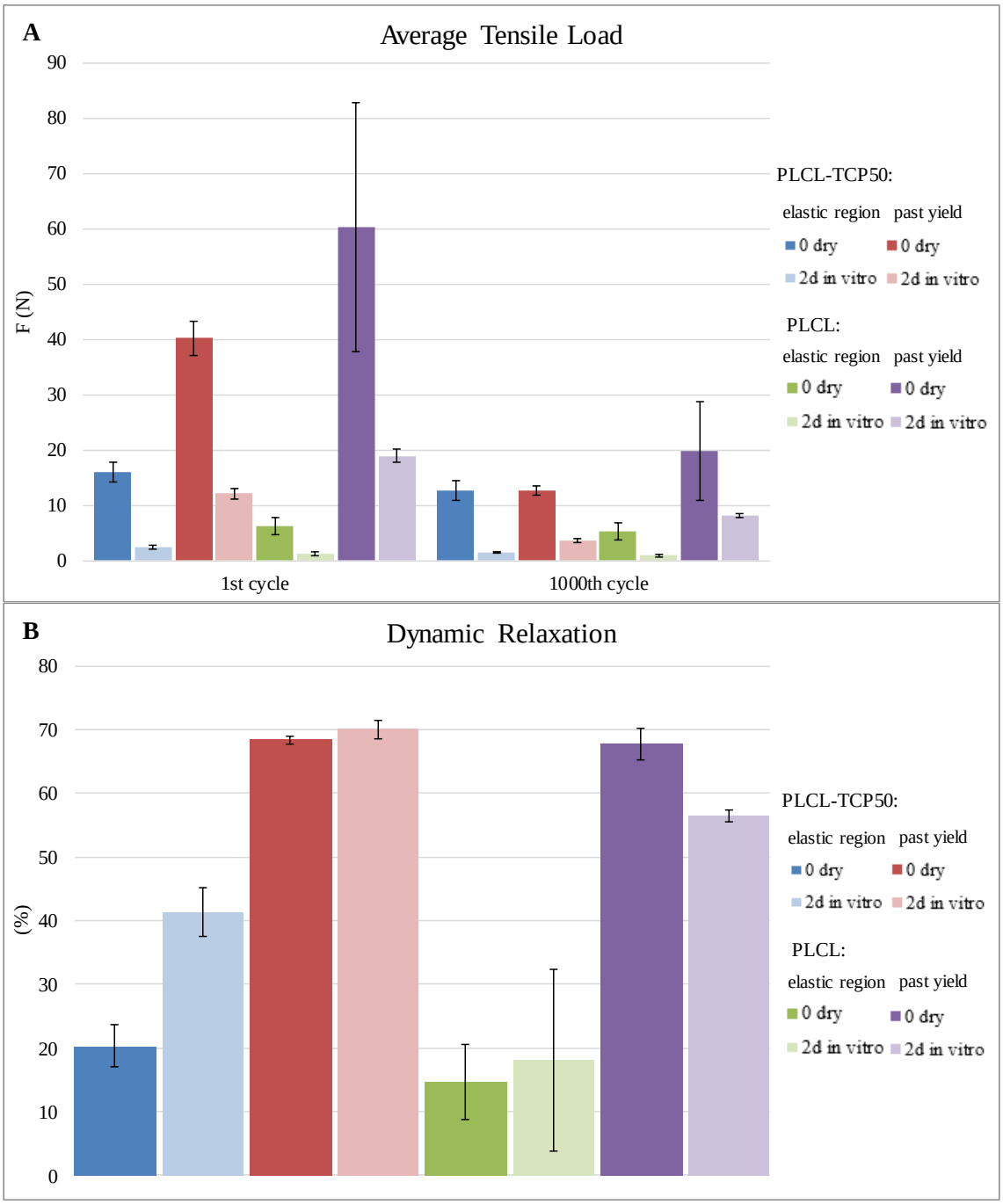

Figure 43. *A. The average load of the dogbones at the first and last cycles and B. The average percentage change between the cycles (PLCL-TCP50 elastic region n=5, past yield n=3 and PLCL elastic region n=4/6, past yield n=3)*

Graph A confirms that the forces of drily tested samples were much higher compared to the physiologically simulated samples, especially the samples tested past yield. Overall, the percentage relaxation between the first and the last cycle is highest with the PLCL-TCP50 dogbones, however the difference is extremely small between the PLCL-TCP50 and PLCL 0 dry past yield. Also, while the PLCL-TCP50 dogbones had the most difference in the relaxation values between 0 dry and 2d in vitro tested in the elastic region, the opposite was true with the PLCL dogbones. Furthermore, while in all the

other cases, the most stress relaxation occurred in the samples tested in physiologically simulated conditions, PLCL past yield experienced the most in dry condition.

Stress-strain hysteresis curves, also obtained from the two different dynamic loadings resulting in two very different hysteresis graphs, are presented in Figures 44 and 45 for PLCL-TCP50 and PLCL, respectively. The first hysteresis graph was a product from dynamic loading in the elastic region, more specifically between 0 and 1 % strain and the second graph past yield, between 99.5 and 100.5 %.

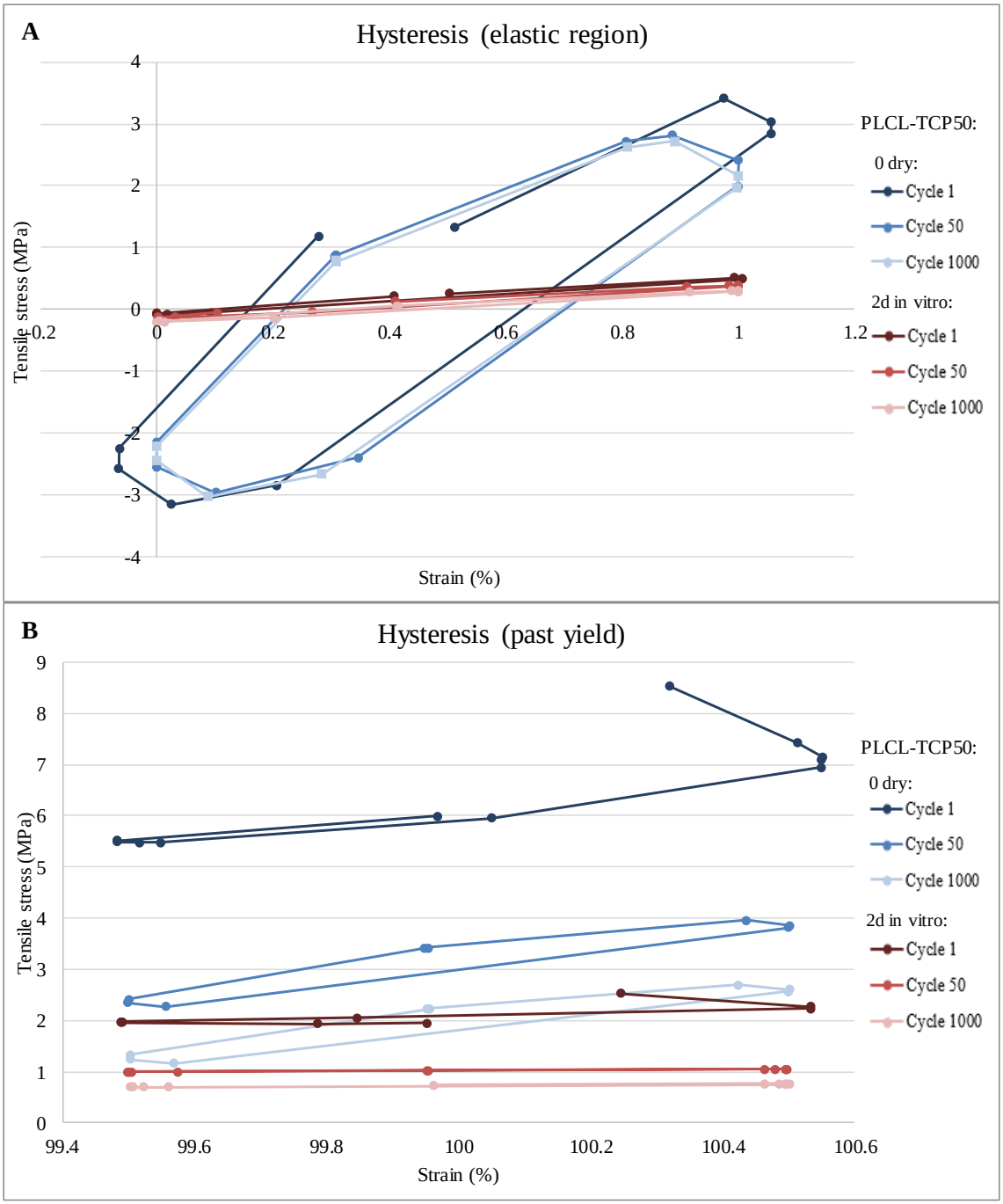

Figure 44. *The stress-strain hysteresis graphs of PLCL-TCP50 dogbone A. in the elastic region (n=5) and B. past yield (n=3)*

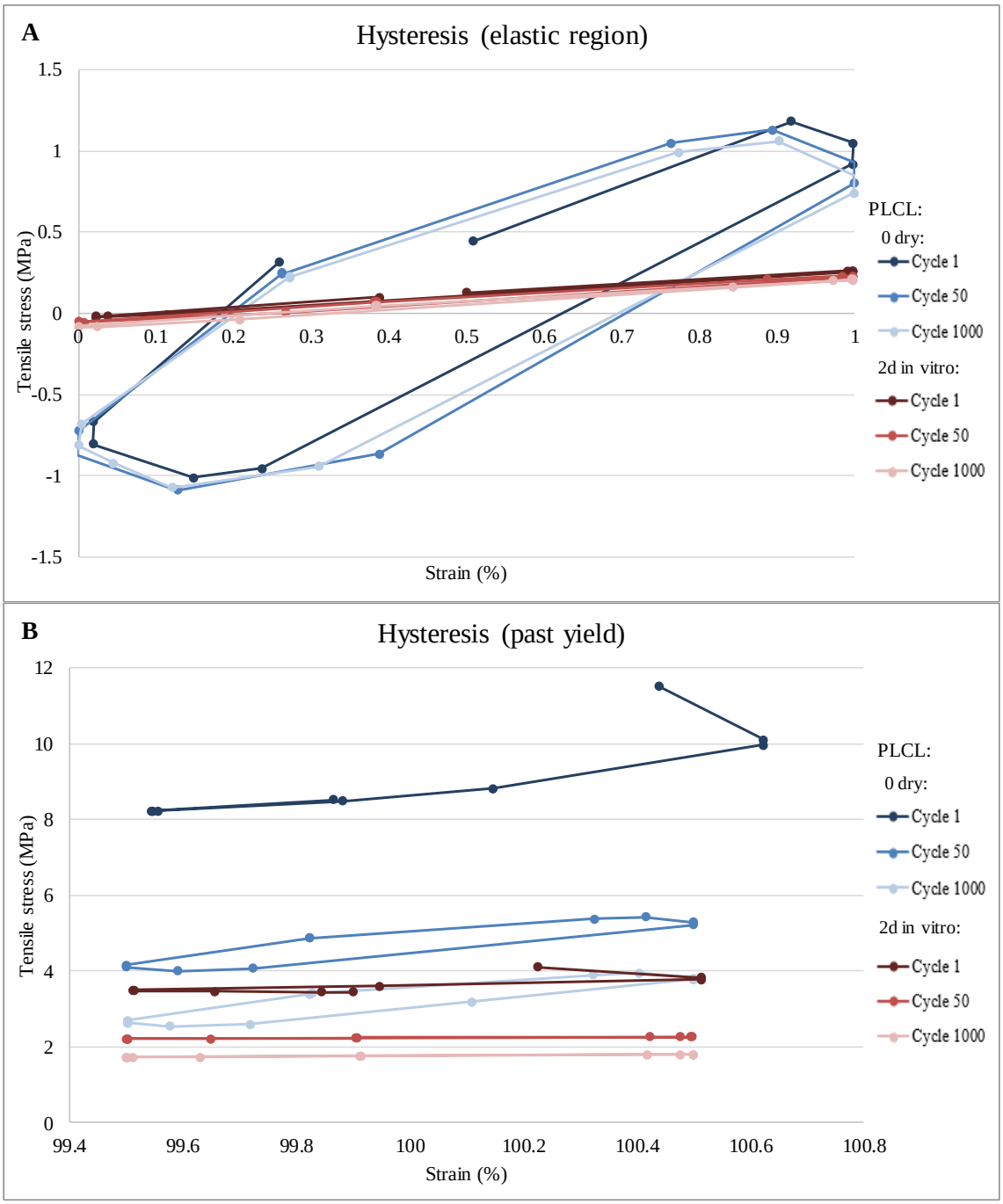

***Figure 45**. The stress-strain hysteresis graphs of PLCL dogbone A in the elastic region (n=4/6) B. past yield (n=3)*

The difference between the elastic region hysteresis curves obtained from the tests in dry and physiologically simulated conditions are easily recognized. While both materials had large dry hysteresis curves, meaning that the energy dissipation was more significant, the physiologically simulated hysteresis curves were much smaller, seemingly linear, suggesting more elastic behavior. Another difference between the two testing conditions is that during dry testing the samples experienced the same amount of negative and positive forces between the minimum and maximum strain, while the 2d in vitro samples stayed seemingly between zero and the maximum stress needed to

deform. Also, during the PLCL-TCP50 dry testing, the testing machine had difficulties in delivering the right amount of deformation during the first cycle.

While PLCL-TCP50 needed more forces in order to deform in the elastic region, the situation was reversed during testing past yield. Also, this time, during the testing of dry PLCL, the machine had also trouble delivering the right amount of strain in the first cycle, in addition to both conditions of PLCL-TCP50. Otherwise, the hysteresis curves were very similar between the two materials. In dry conditions the hysteresis curves were loops, while in physiologically simulated condition seemingly more linear, meaning that during dry testing the energy dissipation was more pronounced. Also, while the hysteresis curves from dynamic loading in the elastic region stayed in the same place as well as the same size, the different hysteresis curves from dynamic loading past yield were all distinctive, the drop between the first and the 10^{th} cycles more pronounced than the drop between the 10^{th} and the 1000^{th} cycles.

Generally, the results from the mechanical tests of the dogbones could indicate that at least the PLCL material could be used as sheets in biomedical applications such as hernia repair, or as a basis for urethral reconstruction. [100,101] The PLCL-TCP50 as thin sheets could be used in facial or cranial bone applications since the strains there during physiological activities are very low [102], so the material holds the initial stiffness.

7.3 Joint Scaffolds

A lot of previous studies have been conducted to similarly structured joint scaffolds or bioreconstructive small-joint prostheses as studied in this thesis [66,67,83,95]. Of the joint scaffolds tested here two were tested in simulated physiological conditions, the joint scaffold containing PEG and the Linvatec joint scaffold. Figure 46 shows the average water absorption of 2 and 14 days in vitro samples of PLA+PEG15 and 2 days in vitro samples of PLA 96/4 (Linvatec). The joint scaffold containing PEG had the largest average water absorption. The 2d in vitro samples absorbed 145 ± 40 % water and the 14d in vitro samples absorbed 160 ± 32 % water. The smaller joint scaffolds absorbed significantly less, 40 ± 11 %. The reason for the huge difference might be that, similarly to the porous polymer and composite scaffolds, the bigger structure held more liquid in the knit pores even though the top and bottom were tapped with paper and the bigger joint scaffold had bigger porosity. Overall, the water absorption was more structural water absorption.

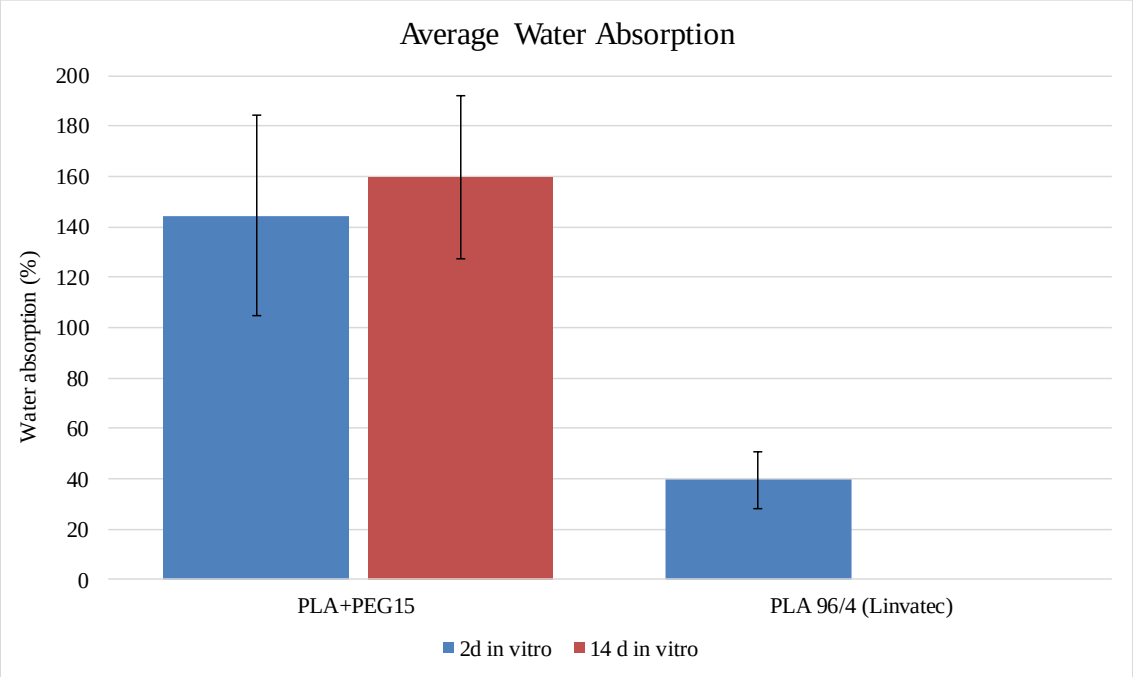

Figure 46. *The average water absorption of the joint scaffolds (PLA+PEG15 n=17/18 and PLA 96/4 n=7)*

The results from DSC tests showed that the joint scaffolds containing PEG had lower glass transition temperature (52 ± 1.0 °C, 53 ± 0.3°C and 52 ± 1.0 °C, for 0 dry, 2d and 14d in vitro, respectively) compared to the other two joint scaffolds (60 ± 0.3 °C and 60 ± 0.4 °C for Linvatec 0 dry and 2d in vitro respectively and 61 ± 0.8 °C for Bionx 0 dry. The PLA 96/4 joint scaffolds were also more crystalline than the joint scaffolds containing PEG. The crystallinity of PLA+PEG15 was 29.4 ± 0.9 J/g, 29.4 ± 0.8 J/g and 30.7 ± 0.6 J/g for 0dry, 2d and 14d in vitro, respectively while the crystallinity of PLA 96/4 (Linvatec) was 38.4 ± 0.5 J/g and 37.0 ± 1.7 J/g, and the crystallinity of PLA 96/4 (Bionx) 36.6 ± 1.6 J/g.

The compressibility of the joint scaffolds was tested by compressing until 500 N was reached. The stress-strain behavior was also observed from that test. The resulting stress-strain curves are presented in Figure 47. The different stress values are due to the different diameter sizes between the PLA+PEG15 scaffolds and the PLA 96/4 Linvatec and Bionx scaffolds, as well as due to dissimilar diameter sizes of parallel samples.

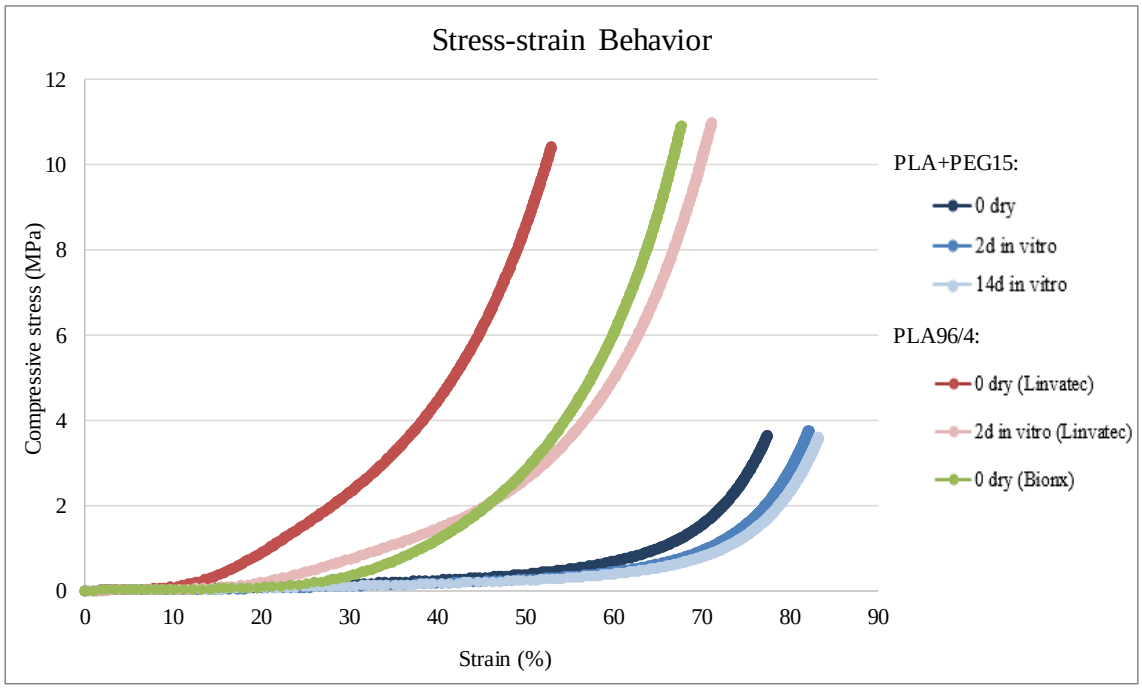

Figure 47. *The stress-strain behavior of the different joint scaffolds (PLA+PEG15 n=6 (standard deviation of strain ranged between 0 and ± 2.6 for 0 dry, between 0 and ± 6.8 for 2d in vitro and between 0 and ± 4.0 for 14d in vitro), PLA 96/4 (Linvatec) n=4 (deviation of strain ranged between 0 and ± 5.3 for 0 dry and between 0 and ± 5.5 for 2d), PLA 96/4 (Bionx) n=3 (deviation of strain ranged between 0 and ± 6.3 for 0 dry))*

The joint scaffolds had very similarly behaving stress-strain curves. At the beginning of the curves, compression occurred without significant increase in stress until at some point during the compression, a slight increase in stress can be observed before ultimate upsurge of stress. The samples tested dry were overall compressed less than the samples tested wet. Drily tested samples had the upsurge in stress earlier in the stress-strain curve than the samples tested wet, particularly the PLA 96/4 scaffolds.

The average maximum compression of dry PLA+PEG15 was 77.5 ± 2.6 % (7.3 ± 0.3 mm) whereas for samples tested after 2 days and 14 days in buffer solution the values were very similar with 82.2 ± 4.4 % (7.8 ± 0.4 mm) and 83.3 ± 3.2 % (7.9 ± 0.3 mm), respectively.

The dry PLA 96/4 (Linvatec) and dry PLA 96/4 (Bionx) had average maximum compression values of 52.9 ± 5.1 % (1.8 ± 0.2 mm) and 67.7 ± 5.4 % (2.7 ± 0.4 mm). The PLA 96/4 (Linvatec) scaffolds were also tested after two days in buffer solution and had average maximum compression of 71.1 ± 4.9 % (2.5 ± 0.2 mm).

From the curves it is easy to see the difference in sizes with the different scaffolds. The maximum stress of the PLA+PEG scaffolds was less than the maximum stresses of PLA 96/4 scaffolds, even though the loads were the same, because the surface areas were smaller with the PLA 96/4 scaffolds. On the other hand, the percentage compression was largest with the bigger scaffolds compared with the smaller ones, probably because

the smaller scaffolds had seemingly more rigid knitted structure due to the smaller height as well as the increased crystallinity, causing the predetermined load to be reached at smaller strains. When comparing the two PLA 96/4 (Linvatec) and PLA 96/4 (Bionx) joint scaffolds, the average stress-strain curve of 0 dry PLA 96/4 (Bionx) is more similar with the PLA 96/4 (Linvatec) curve resulting from tests after 2 days in buffer solution. It can be concluded that the Bionx scaffold was somewhat softer perhaps due to relaxation of the knitted structure as well as the slightly less crystalline structure.

Figure 48 compiles the average modulus values obtained from the stress-strain curves by tangent approximately between 10 and 20 % strain.

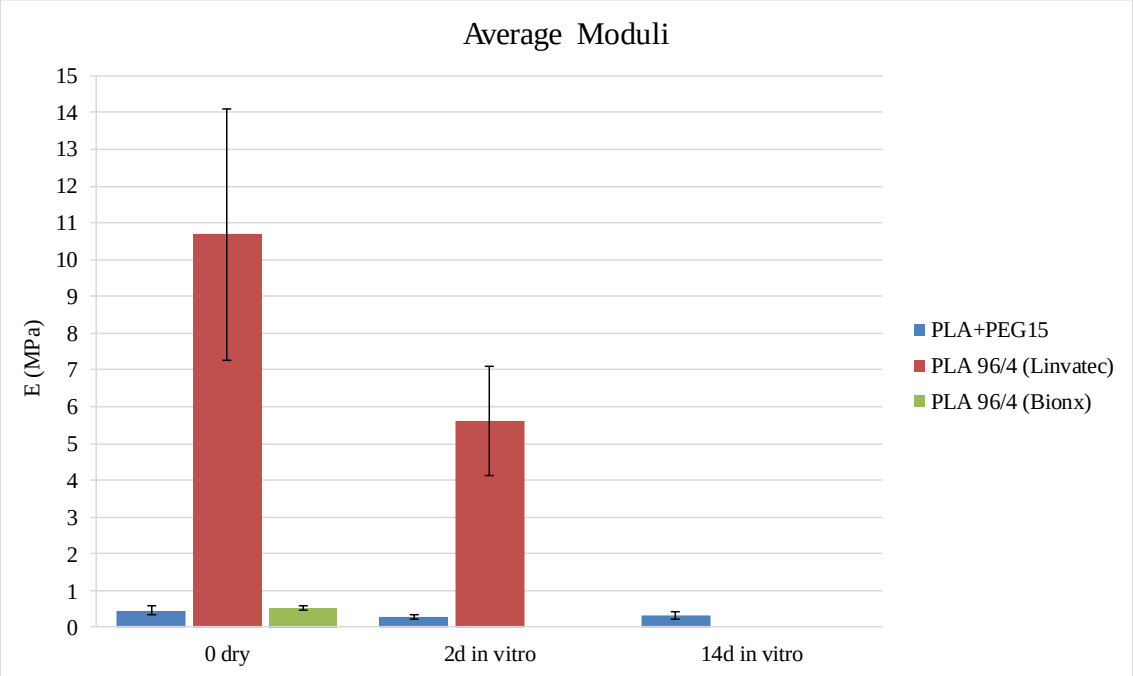

Figure 48. *The average moduli of the joint scaffolds (PLA+PEG15 n=6, PLA 96/4 (Linvatec) n=4, PLA 96/4 (Bionx) n=3)*

Of the joint scaffolds the PLA 96/4 (Linvatec) had the largest modulus value of 10.7 ± 3.4 MPa in dry condition and 5.6 ± 1.5 MPa in physiologically simulated condition. The next largest value of modulus 0.52 ± 0.07 MPa belonged to the other PLA 96/4 scaffold. The huge difference in the moduli confirm that the two scaffolds, even though made of the same material and the same knitted structure, must have some structural differences either physically and/or chemically as seen in the different crystallinities. The PLA + PEG15 scaffolds on the other hand, had the smallest modulus values. The 0 dry average modulus of 0.46 ± 0.11 MPa was the largest of the three, followed by the 14d in vitro with 0.32 ± 0.11 MPa and 2d in vitro with 0.28 ± 0.07 MPa. While the chemical structures were different with the two different sized scaffolds, higher crystallinity results usually in higher modulus values [103].

As mentioned before the compressibility of the joint scaffolds was tested by the compression to 500 N. Observations on how much different amounts of load caused the scaffolds to compress were made. As previously noted, the chosen load values were based on the previously studied approximate forces different individuals might experience in the MCP joint. Figure 49 A represents the average load-strain curves obtained from the tests, whereas the average compressibility values at 80 N, 220 N and 440 N are shown in graph B.

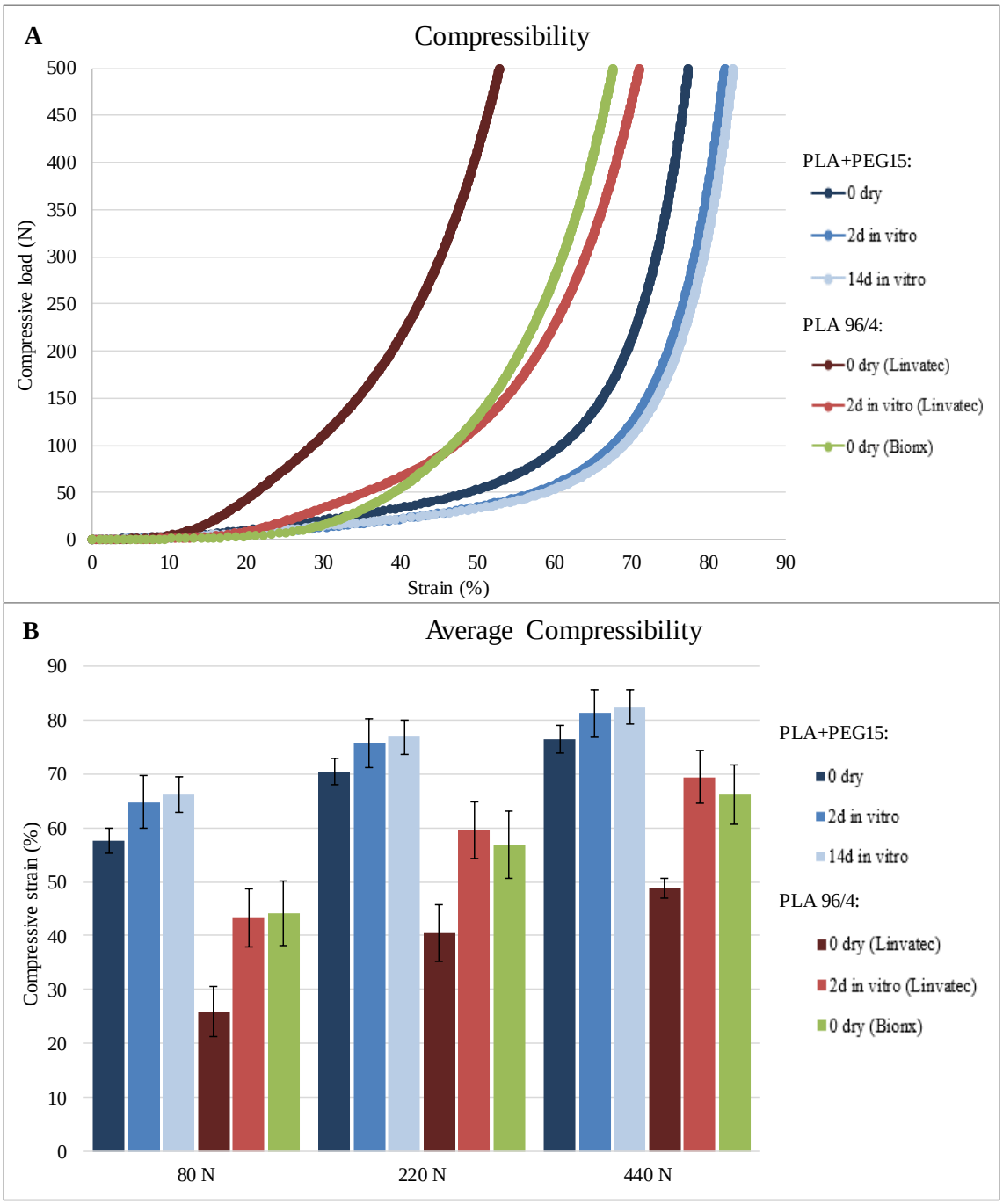

Figure 49. *The compressibility of the joint scaffolds: A. The average load-strain curves (same standard deviations as in Figure 44) B. The average compressibility at different loads (PLA+PEG15 n=6, PLA 96/4 (Linvatec) n=4, PLA 96/4 (Bionx) n=3)*

It can be observed from the load-strain curves that the PLA 96/4 (Linvatec) tested dry resisted compression the most starting from the beginning, and generally the PLA+PEG15 scaffolds resisted compression the least. However, it has to be noted that the PLA+PEG scaffolds, started to resist the compression significantly towards the end because the pores in the knitted structure were compressing together, even though the overall compression is very large.

The PLA 96/4 (Linvatec) had the biggest difference between the 0 dry and the 2d in vitro compressions while the PLA+PEG15 had the smallest with all three time points, meaning that the addition of water and warmer environment affected the Linvatec joint scaffolds the most. While the 2d in vitro behavior of PLA 96/4 (Bionx) is unknown, the scaffold behaved very similarly with the 2d in vitro PLA 96/4 (Linvatec). It could be speculated that had there been samples to test in physiologically simulated conditions, the load-strain curve might have been closer to the PLA+PEG15 curves from physiologically simulated conditions.

The average compressibility of PLA+PEG was at 80N load 57.6 ± 2.4 %, 64.7 ± 4.9 % and 66.2 ± 3.3 % for 0 dry, 2d in vitro and 14d in vitro, respectively. At 220 N, the values were 70.4 ± 2.5 %, 75.7 ± 4.5 % and 76.9 ± 3.2 % and finally at 440 N, 76.5 ± 2.6 %, 81.2 ± 4.4 % and 82.3 ± 3.2 %.

For 0 dry and 2d in vitro PLA 96/4 (Linvatec) scaffolds the values were at 80 N load 25.9 ± 4.7 % and 43.3 ± 5.4 %, at 220 N 40.4 ± 5.3 % and 59.5 ± 5.2 % and at 440 N 48.7 ± 1.9 % and 69.4 ± 4.9 %. Finally, the values for 0 dry PLA 96/4 (Bionx) were at 80 N 44.1 ± 6.0 %, at 220 N 56.9 ± 6.2 % and at 440 N 66.1 ± 5.5 %. After testing, all the scaffolds remained compressed and only little recovery to the original height occurred.

The scaffolds, with 8mm diameters, studied in the previous thesis had average compression values of approximately 40 %, 54 % and 63 % at 80 N, 220 N and 440 N, respectively, when tested in dry ambient conditions. [95] When comparing to the PLA 96/4 scaffolds, the values were most similar with the 2d in vitro 96/4 (Linvatec) and consequently the 0 dry PLA 96/4 (Bionx) scaffolds. Meaning that the previously studied scaffolds were softer and compressed more, while the 0 dry PLA 96/4 (Linvatec) scaffolds were tougher and compressed less, meaning that there must have occurred enough molecular changes in the smaller joint scaffolds during the storage period to decrease the mechanical properties, which might not happen during shorter storage time [83].

In addition to stress relaxation, creep is also experienced by polymers and biological tissues as viscoelastic materials [7]. A small-scale static creep test was performed with the PLA+PEG15 joint scaffolds. The scaffolds were compressed to 50N and held for 1000 seconds. The initial strain and displacement values were compared to the values

after the 1000 seconds. Figure 50 represents the strain-time curves obtained from the tests.

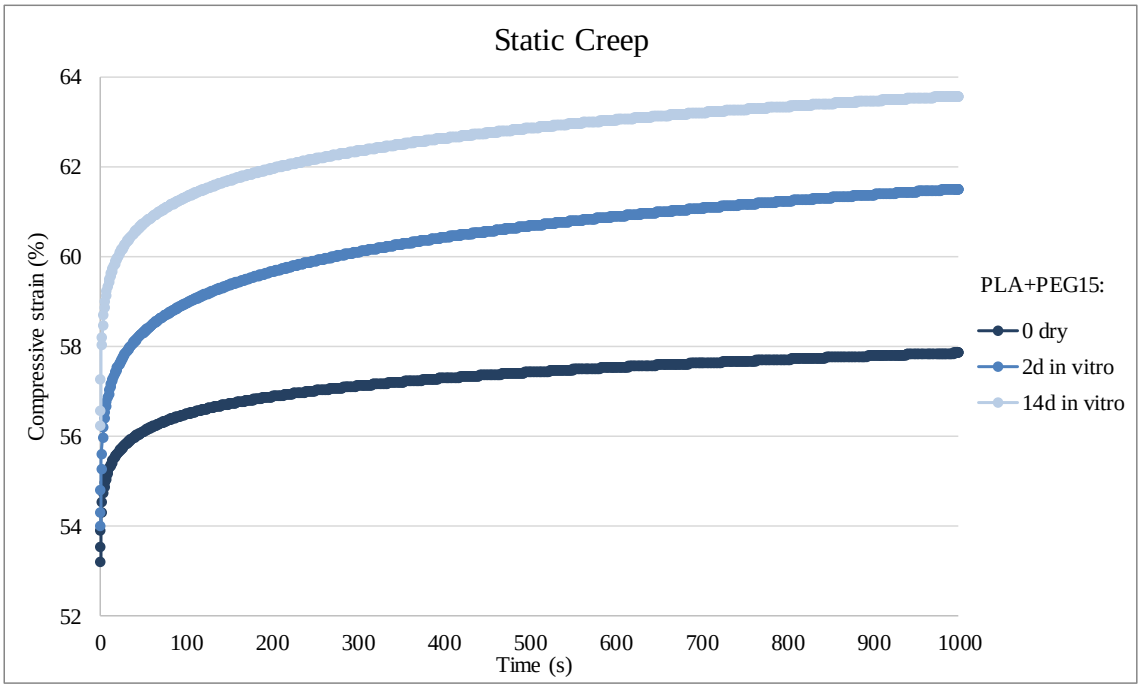

Figure 50. *The average creep curves of PLA+PEG15 joint scaffold (n=4/5, standard deviations of strain ranged between ± 2.2 and ± 2.7 for 0 dry, between ± 4.9 and ± 4.5 for 2d in vitro and between ± 3.7 and ± 3.2 for 14d in vitro)*

Just like with the relaxation curves, the creep curves also exhibit the biggest change in the beginning. While the relaxation curves start to drop due to decreases in compressive forces, the creep curves start to rise because the scaffold structures start to compress under the constant load. Like in the relaxation tests, the noticeable change in the curves occurred quite quickly, however the curves did not plateau towards the end, instead the increase in compressive strain slowed down. The curves also show clear difference between the 0 dry, 2d in vitro and 14d in vitro. The 0 dry joint scaffolds clearly resisted the deformation the most, while introducing water and warmer environment into the testing as well as increasing the amount of time in buffer solution prior to testing, resulted in more deformation occurring.

Figure 51 represents the obtained averages of displacements at initial compression and after the 1000 seconds hold and the average percentage creep between the compressions.

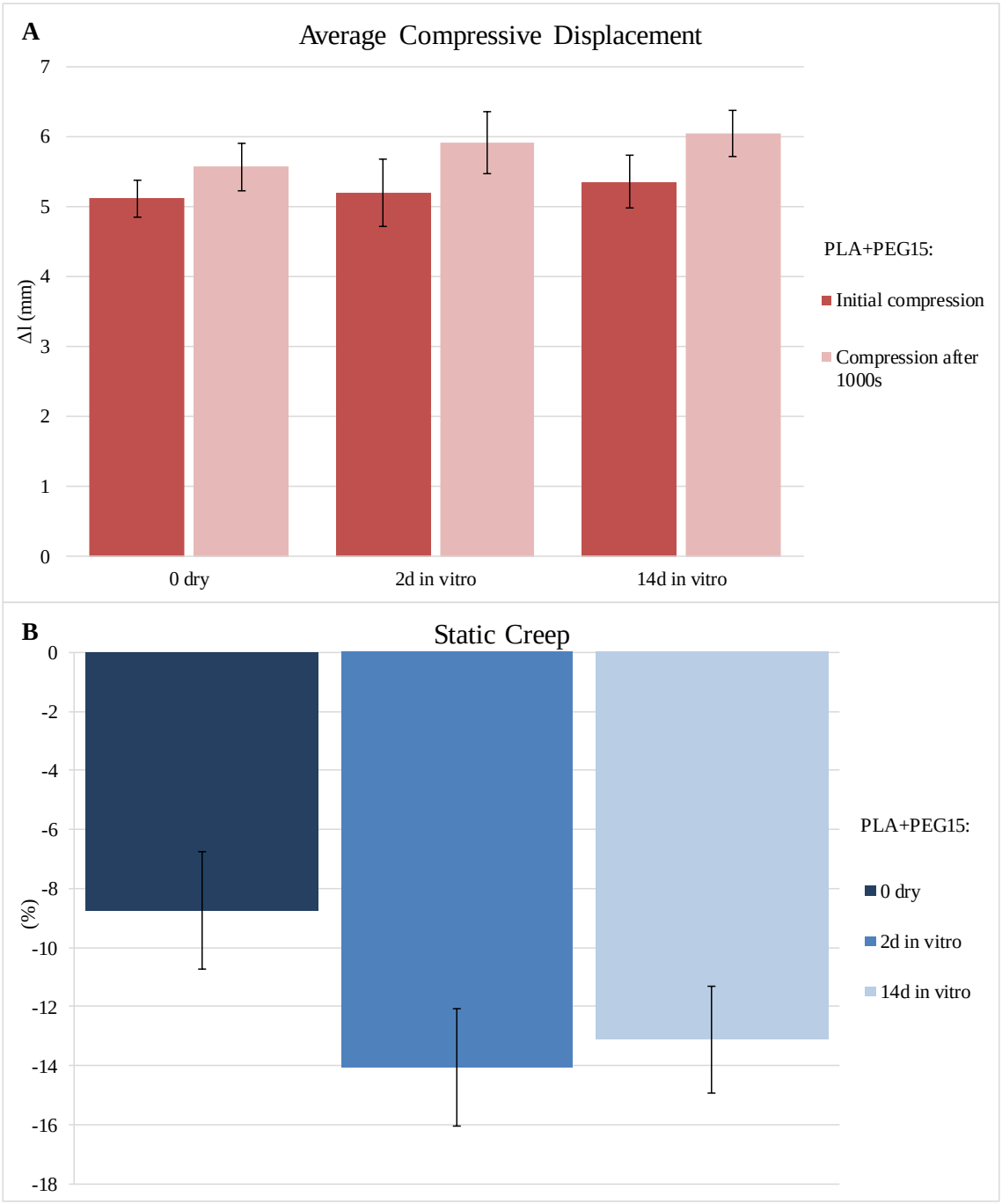

Figure 51. *The average displacement values of PLA+PEG15 joint scaffold at initial compression and after 1000 second hold B. The average percentage creep between the compressions (n=4/5)*

Graph A confirms that while the average deformation of the 14d in vitro scaffolds was the largest, from graph B it can be seen that actually the 2d in vitro samples deformed most compared to the initial deformation. The drily tested resisted the most deformation. Overall, while the initial compression due to the exerted 50 N is quite large at over 50 % strain and 5 mm displacement, the compression increases only 8.75 ± 2.0 %, 14.1 ± 2.0 % and 13.1 ± 1.8 % compared to the initial compression for 0 dry, 2d in vitro and 14d in vitro scaffolds.

The PLA+PEG15 and PLA 96/4 (Linvatec) joint scaffolds were dynamically compressed using 50N amplitude and the increase in compressive strain, i.e. dynamic creep, was observed during the testing. The resulting curves of strain with respect to cycles are presented in Figure 52.

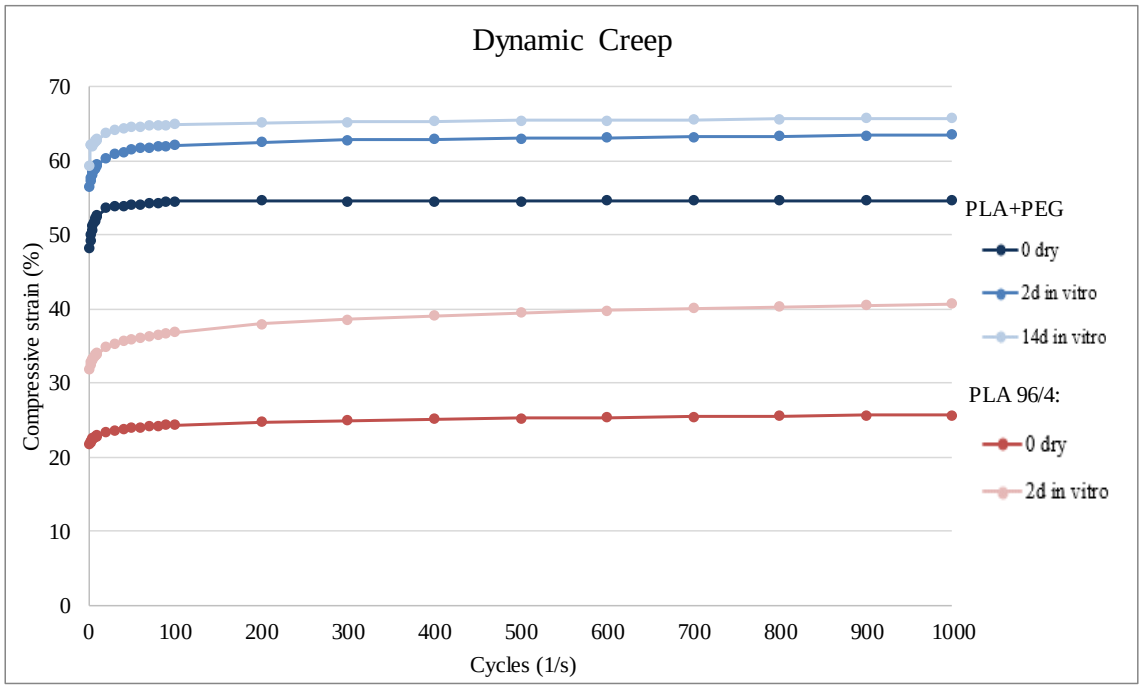

Figure 52. *The dynamic creep behavior of the joint scaffolds (PLA+PEG15 n=3/6/3, (standard deviation of strain ranges between ± 3.0 and ± 3.7 for 0 dry, between ± 5.3 and ± 3.8 for 2d in vitro and between ± 7.1 and ± 4.5 for 14d in vitro) and PLA 96/4 n=3 (standard deviation of strain ranges between ± 1.8 and ± 2.8 for 0 dry and between ± 5.9 and ± 7.8 for 2d in vitro)*

Familiarly by now, the dynamic creep behavior is very similar with the other relaxation behaviors, the fastest change from the original occurs at the very beginning of the test, the fastest of the curves being the 0 dry PLA+PEG15 curve. The 0 dry PLA+PEG15 curve also has the most evident plateauing towards the end, while the other curves do exhibit somewhat similar plateauing, it can be clearly seen in the graph that the curves do in fact continue rising, though slightly.

In Figure 53 the average displacement at first and last cycles are presented with the average percentage creep between those cycles.

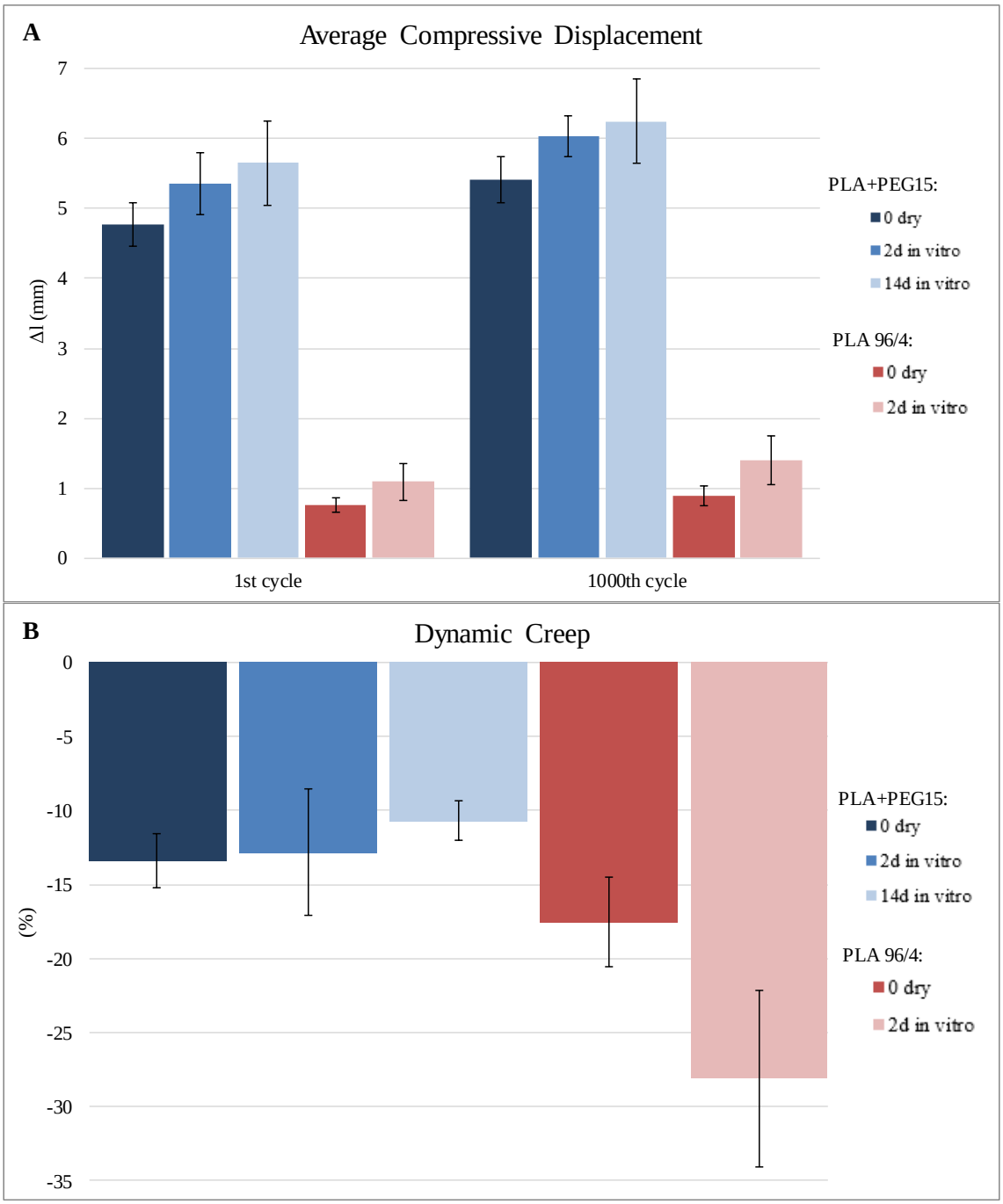

Figure 53. *A. The average displacement of the joint scaffolds at the first cycle and the last cycle. B. The average percentage creep between the cycles (PLA+PEG15 n=3/6/3, PLA 96/4 n=3)*

Overall, the 14d in vitro PLA+PEG15 scaffolds experienced the most deformation, while obviously the 0 dry PLA 96/4 scaffolds the least, partly because of their significant difference in heights. Interestingly, of the PLA 96/4 scaffolds, the physiologically simulated scaffolds exhibited the most percentage creep, while the 0 dry, though slightly, had the most percentage change of the PLA+PEG scaffolds, opposite to what occurred during the static creep test. Also compared to the static creep tests the 0 dry PLA+PEG15 scaffolds experienced more percentage creep during the

dynamic testing while the physiologically simulated scaffolds experienced more percentage creep during static testing. The 1 Hz testing speed was used because it is often used to represent speed experienced physiologically, however in further tests concerning joint scaffolds, faster speeds could be considered, such as 3 Hz to represents the average speed a person might use while tapping a keyboard [104].

During the dynamic testing, the mechanical testing device had some difficulties in delivering the right amount of load for some of the PLA + PEG15 parallel samples due to the scaffold materials compliance, so the amount of parallel samples of the scaffolds differed. The fix was to program the machine into thinking the scaffolds were much stiffer and the load was delivered more reliably. The smaller joint scaffolds were programmed the same way and the tests were successful. Another problem with the bigger joint scaffolds was also the size of the scaffolds. Due to the fact that the ratio between the height and the diameter was not the optimal 1:2, especially during the dynamic loading, some buckling of the samples could be seen from the bottom. The smaller joint scaffolds did not have any problems regarding buckling.

Figure 54 represents the stress-strain hysteresis curves of the dynamically tested joint scaffolds, PLA+PEG15 and PLA 96/4 (Linvatec). Because the samples were dynamically loaded using load amplitude, the appearance of the hysteresis curves differed from those dynamically loaded using strain control. While the strain hysteresis curves stayed in one place in the stress-strain graph or dropped in vertical direction from cycle to cycle due to less stress needed to deform, the load hysteresis curves move horizontally to the direction of further deformation, due to repeated bouts of loading.

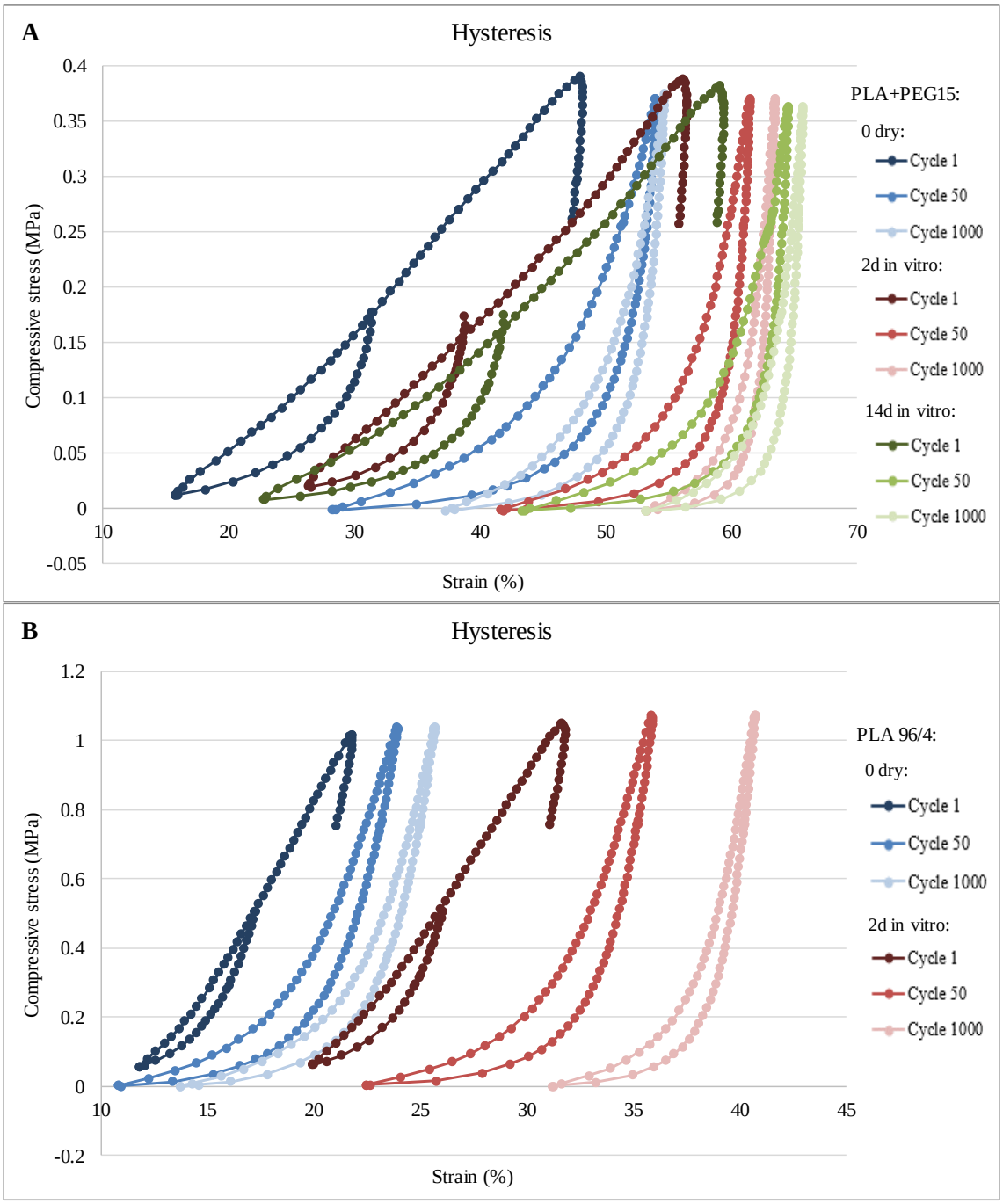

Figure 54. *The stress-strain hysteresis curves for the joint scaffolds. A. PLA+PEG15 (n=3/6/3) and B. PLA 96/4 (n=3)*

While the loops of the first cycles of the joint scaffolds look to be smaller than the following cycles, because of the ramp preceding the dynamic movement, in reality, the energy dissipation is much larger during the first cycles. The area under the first cycle loops is smaller than the first cycle loops but bigger than the areas under the following cycle loops, meaning that while some of the original shape of the scaffolds is retained after first cycles, further compression cycles increase the deformation and the scaffolds remain compressed. This is further demonstrated by the shapes of the hysteresis curves. During the first cycles, the behavior of stress is linear towards strain during loading

while in the following cycles, the scaffolds are deformed more with slower increase in stress up to a point when stress needed to deform starts to increase more quickly. The obvious difference between the joint scaffolds was the much bigger overall deformation of the PLA+PEG15 scaffolds.

7.4 Fibers

Producing fibers by melt spinning of polymers is a popular way of generating safe products to use as themselves as sutures or as other structures such as porous knitted structures in medical applications. [78,83]

The stress-strain behavior of three fibers was determined by straining until the fibers broke. Figure 55 represents the average stress-strain curves recorded up till the first parallel samples broke, in order to get a sensible graph. Instead, the average strain at break values calculated from each parallel sample can be found in Table 6 among other stress-strain characteristics of the parallel samples.

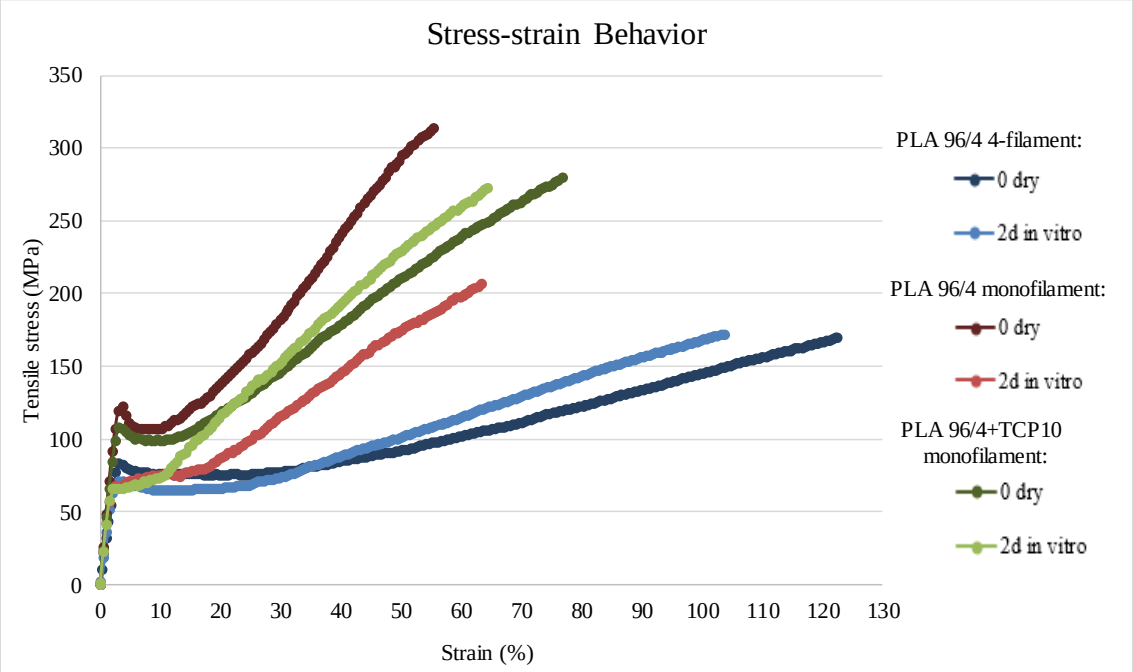

Figure 55. *The stress-strain behavior of the fibers (n=6, the standard deviation of stress ranged between 0 and ± 40 and between 0 and ± 23 for 0 dry and 2d in vitro PLA 96/4 multifilament, between 0 and ± 28 and between 0 and ± 39 for 0 dry and 2d in vitro PLA 96/4 monofilament and between 0 and ± 19 and between 0 and ± 48 for 0 dry and 2d in vitro PLA 96/4 +TCP10)*

Typical for tensile tests, the stress-strain curves start with recognizable elastic regions before yielding starts at around 2 and 3 % strains. Characteristically for polymers, two distinct yield points can be seen in the curves, first upper yield point (Yield in Table 6), followed by lower yield point. [31] Usually the second yield point occurs at a lower

stress value than the first yield point, however, from the graph above, it can be observed that the monofilaments tested in physiologically simulated conditions, have secondary yield points at higher stresses than the first yield points. After yielding, strain hardening region can be seen where steadily increasing amount of stress is needed to continue the straining. The stress-strain curves finally end in breakdown of the fibers, which is not seen in the curves above. While the monofilament samples broke suddenly, the 4-filament samples broke one filament at a time. After one filament broke, the stress suddenly dropped before starting to increase again until another filament broke resulting in the same drop and increase in stress until all the filaments had broken.

Table 6. *The average mechanical stress-strain characteristics (n=6)*

	Modulus (MPa)		**Stress at Yield (MPa)**		**Strain at Yield (%)**		**Stress at Break (MPa)**		**Load at Break (N)**		**Strain at Break (%)**	
	0 dry	2d in vitro	0 dry	2d in vitro	0 dry	2d in vitro	0 dry	2d in vitro	0 dry	2d in vitro	0 dry	2d in vitro
PLA 96/4 4-filament	3282.9 ±289.0	3424.8 ±368.8	83.9 ±8.5	73.9 ±12.4	3.2 ±0.6	3.1 ±0.5	187.4 ±28.2	200.6 ±20.8	8.1 ±1.0	5.6 ±0.5	147.0 ±23.8	131 ±16.2
PLA 96/4 monofilament	4544.5 ±201.4	4215.0 ±267.8	122.5 ±5.8	67.2 ±7.7	3.3 ±0.3	2.1 ±0.4	343.4 ±17.3	266.4 ±15.4	1.5 ±0.5	1.9 ±0.6	63.9 ±8.8	93.2 ±25.8
PLA 96/4 + TCP10 monofilament	4388.1 ±255.5	4040.7 ±246.6	108.7 ±3.9	68.2 ±8.9	3.2 ±0.4	2.2 ±0.4	287.0 ±19.7	293 ±31.2	2.0 ±0.07	1.5 ±0.2	80.1 ±4.1	73.0 ±12.9

The average modulus values were determined from the elastic region at the beginning of the stress-strain curves and while there were only little differences between 0 dry and 2d in vitro samples, the monofilaments had much higher moduli compared to the multifilament. And while the average moduli of the monofilaments decreased when tested in physiologically simulated conditions, the average modulus of the multifilament increased. The stresses needed to reach the first yield point were higher with the monofilaments, because their cross-sectional areas were smaller than the combined 4 filaments of the multifilament, however the yielding started in very similar points of deformation with all the fibers. Only one percent difference was between the 0 dry and 2d in vitro monofilaments. At the final stage of deformation, the breakdown, the highest stresses were yet again observed with the monofilaments while the overall deformation before failure was more significant with the multifilament.

The tested fibers were previously mechanically tested in different mechanical testing device, albeit using slightly higher testing speed and only in dry condition. Using higher testing speed had resulted in higher modulus and quite similar stresses at yield and at break but samples had yielded and broke at smaller strains compared to using slower test speed.

The three different fibers were dynamically tested in the elastic region, determined from the stress-strain curves. The dynamic relaxations of stress were observed and Figure 56 represents the dynamic stress relaxation curves.

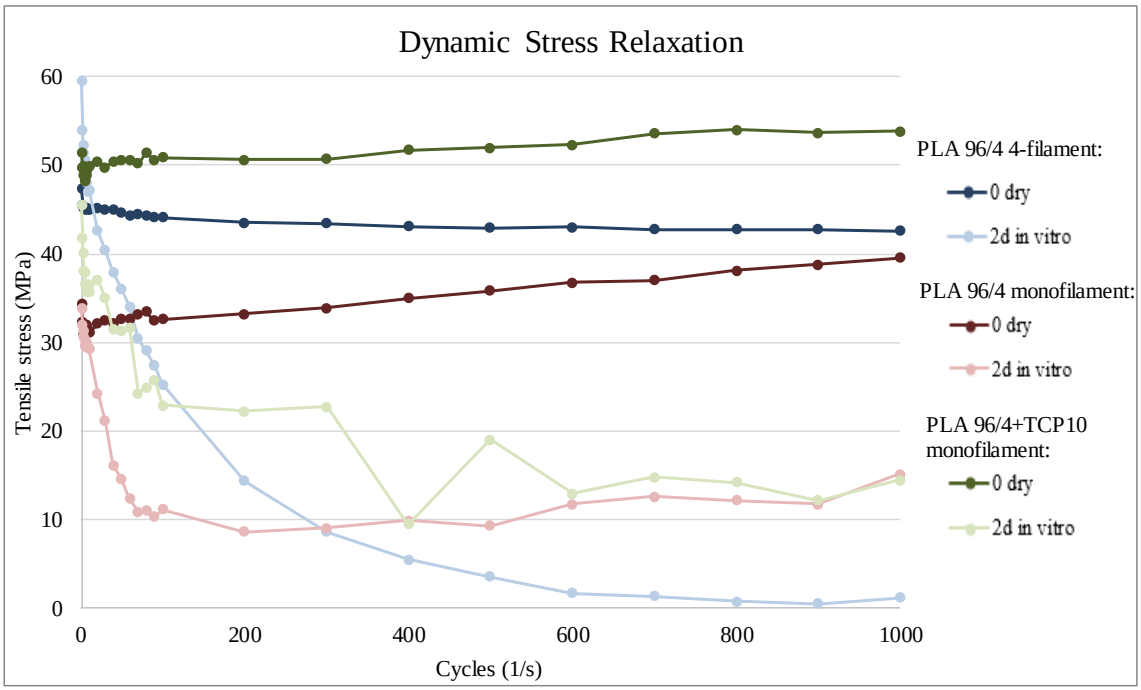

Figure 56. *The dynamic stress relaxation of the fibers (n=3, the standard deviation of strain ranged between ± 1.2 and ± 0.16 and between ± 10 and 0.55 for 0 dry and 2d in vitro PLA 96/4 multifilament, between ± 20 and ±16 and between ± 6.3 and ± 20 for 0 dry and 2d in vitro PLA 96/4 monofilament and between ± 2.0 and ± 0.27 and between ± 1.6 and ± 25 for 0 dry and 2d in vitro PLA 96/4+TCP10)*

The dynamic behavior of the fibers was very difficult to predict. While the 0 dry PLA 96/4 4-filament behaved as one would expect, by having a curve that starts to decrease first more quickly, then slower, the equivalent monofilaments on the other hand have curves that though start to decrease first, end up inclining towards the end. As for the physiologically simulated samples, the multifilament curve drop way below expected level and while the monofilament curves do drop quickly at the beginning as expected, towards the end the curves fluctuate, PLA 96/4 + TCP10 more severely.

In Figure 57, the average load values at the first and the last cycles are presented with the average percentage change between those cycles.

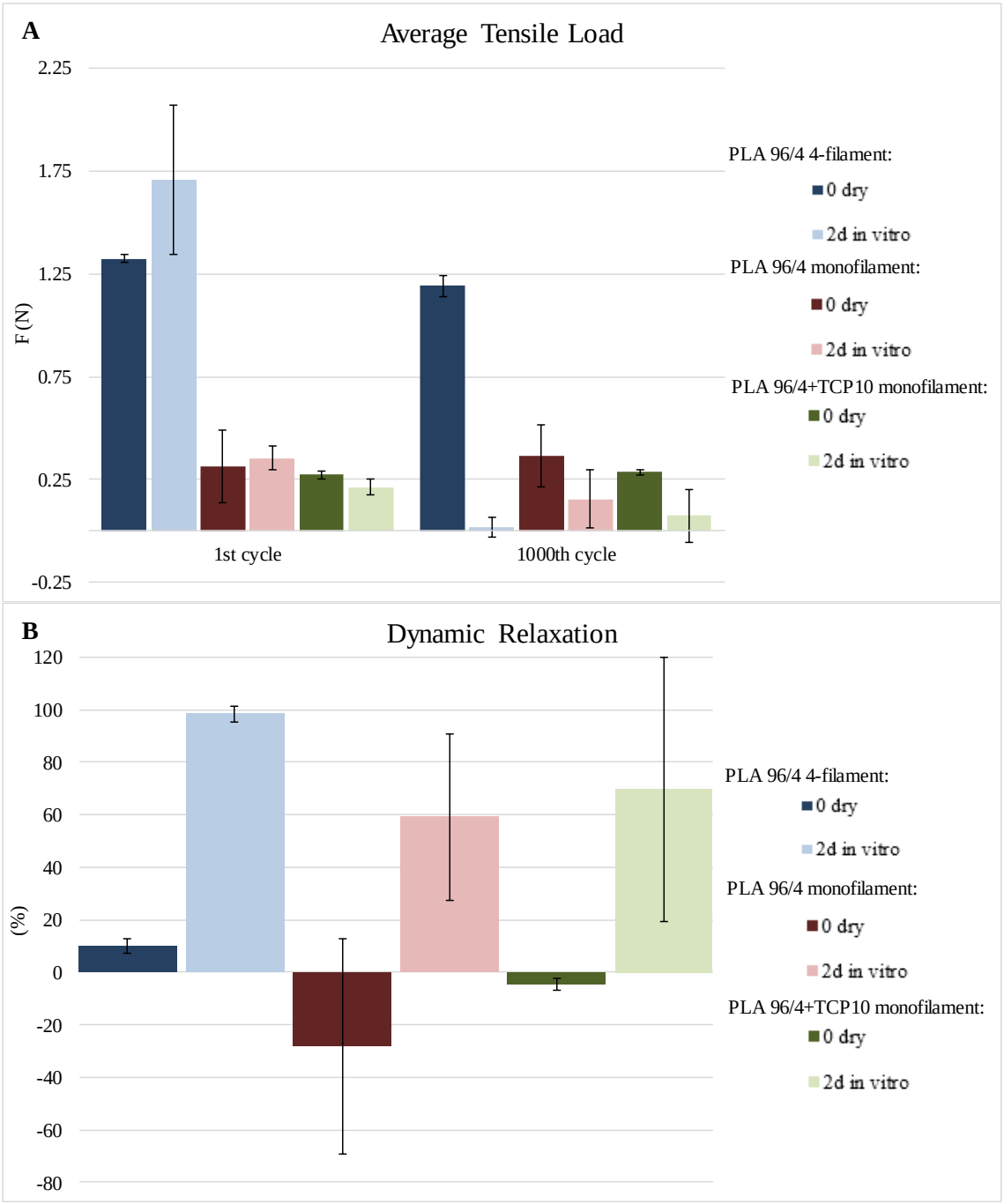

Figure 57. *Figure 51. A. The average load at first and last cycles and B. The average percentage change between the cycles (n=3)*

While the fibers are very difficult to compare to each other due to different sizes and chemical compositions, both PLA 96/4 4-filament and the monofilament with TCP had very slight difference in the load values at first and last cycles tested in dry conditions, however while the monofilament actually increased the values, the multifilament decreased. Overall, compared to the drily tested samples, the physiologically simulated samples experienced the most percentage relaxation. The standard deviations varied a lot across different fibers and testing conditions, suggesting that three parallel samples were not enough to give more reliable information of the fibers.

The dynamic testing of the fibers was originally intended to be performed using stress amplitude of 25 MPa, which is equal to a maximum tension of 50 MPa, still in the essentially elastic region. The idea was to observe how many cycles the fibers could withstand before failure, however, the compliance between the samples and the machine during testing was too great, so the machine had difficulties in delivering the correct stress amplitude. The programming of the machine into believing the samples were tougher was unsuccessful, so the testing was switched to one with strain amplitude. Perhaps another testing machine could be more suitable for the fibers, if fatigue failure of the fibers is of interest.

In Figure 58 three different hysteresis curves, obtained by dynamically loading the three different fibers between 0 and 2% strain are presented.

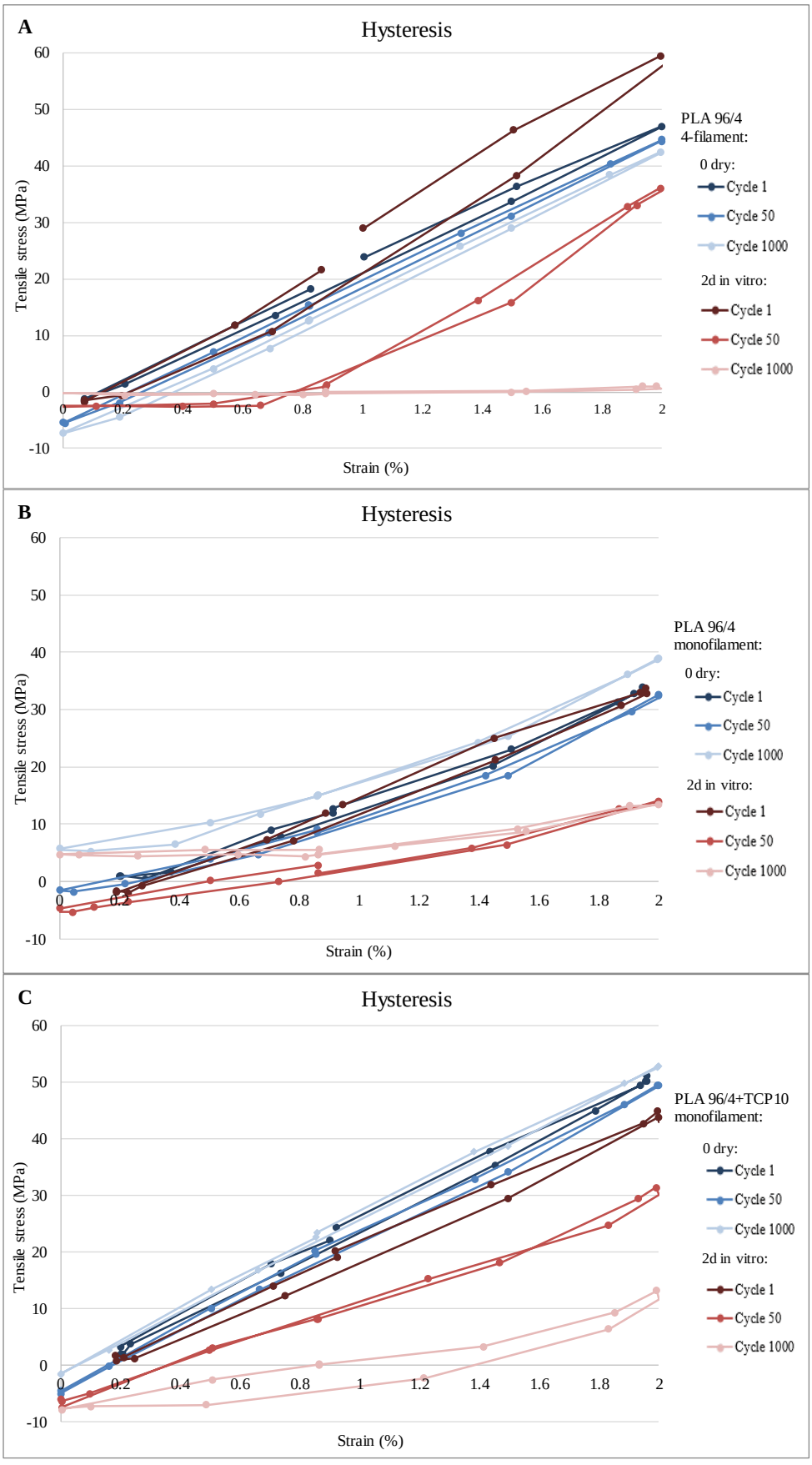

Figure 58. *The stress-strain hysteresis curves of A. PLA 96/4 4-filament (n=3), B. PLA 96/4 monofilament (n=3) and C. PLA 96/4 +TCP10 (n=3)*

As mentioned before, the fibers behaved unpredictably during dynamic testing. While the dry samples had rather clear shaped hysteresis loops that somewhat overlapped with each other, the samples tested in simulated physiological conditions had very irregular shaped hysteresis loops, clearly separate from each cycle. The multifilament PLA 96/4 even dropping to zero forces in the last cycle. Even though the physiologically simulated samples had drastically different hysteresis loops, during testing no difference could be seen with the naked eye compared to the dry samples.

As with other tested materials, the fibers also experienced the machine difficulties in delivering the right amount of deformation during the first cycles. From the graphs it can also be seen that while during the testing the samples experienced negative forces, they were not as drastic as experienced by the dry dogbones.

7.5 Cancellous Bone

The bone of a pig is commonly used as an animal model for testing orthopedic implants prior to clinical testing due to the similarities in bone anatomy, morphology, bone regeneration and densities etc. compared to humans. [105-107] Figure 59 represents a TGA result from a test on a cancellous bone sample showing the amount of inorganic material after all the organic material had been burned away. The average percentage of inorganic material was 33.2 ± 2.6 % tested from 8 samples. In contrast, the amount of inorganic matrix in human bone is reportedly between 60 to 70 % [39], significantly more than the bone samples tested had.

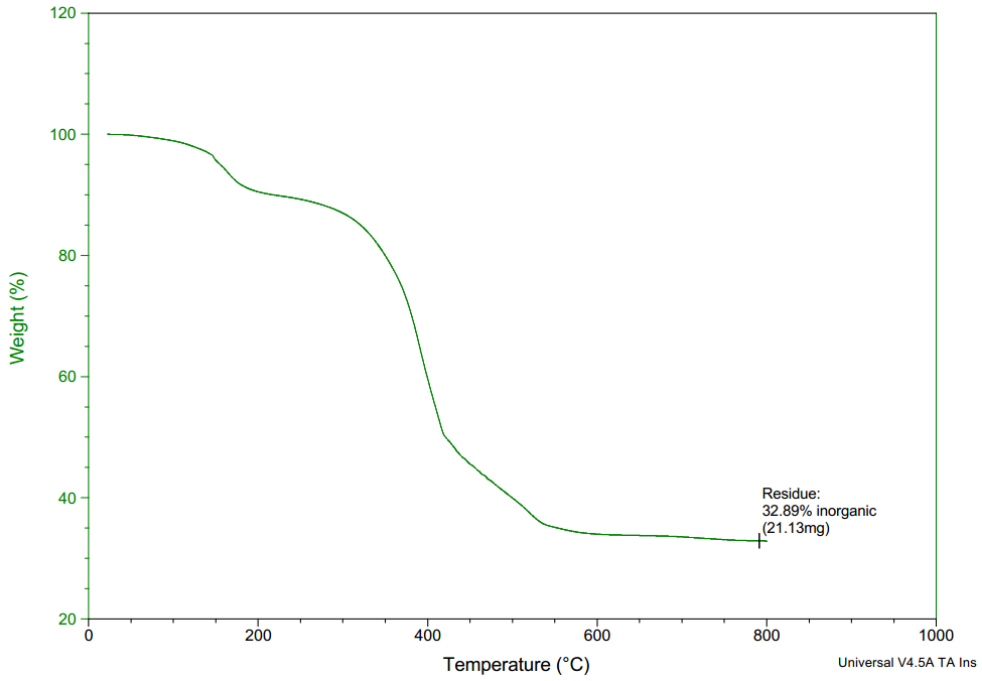

Figure 59. *The TGA results of the cancellous bone*

The cancellous bone samples were compressed to 20% strain in order to obtain a stress-strain curves were the moduli could be determined. Figure 60 represents the average stress-strain graph.

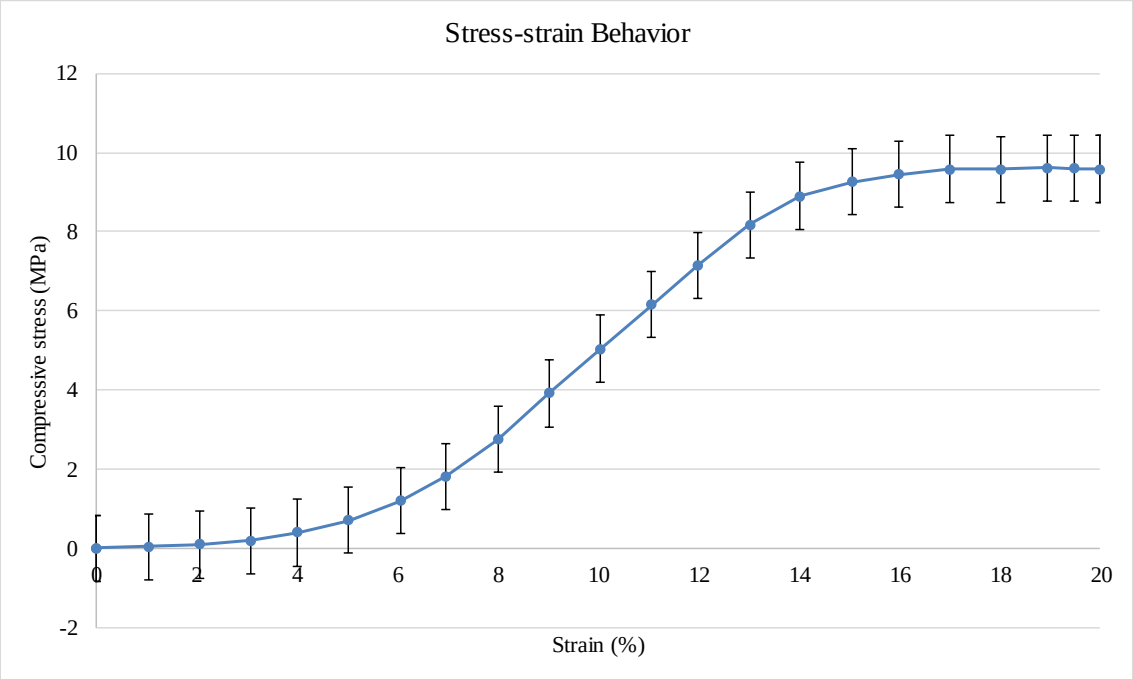

Figure 60. *The stress-strain behavior of cancellous bone (n=7)*

The stress-strain curve showed some similarities with the porous scaffolds, however the three regions were more easily detected and the loads and stresses were greater during the compression. At the start of the curve is a very distinct toe region, before stress started to rise linearly, resulting in an elastic region, finally ending in the plateau region. Unlike with the PLCL and PLCL-TCP50 scaffolds, further compression would have resulted in the fracture of the bone samples. The cancellous bone had an average modulus of 133.8 ± 38.2 MPa, obtained from the linear portion generally between 5 and 15 % strain. Other publications give modulus value of 4.9 GPa to cancellous bone of a pig taken from femur [41], however without knowing the exact testing conditions and parameters as well as the bone quality, those values are hard to compare. However, one reason for the somewhat low modulus could be the low amount of inorganic material compared to what might have been expected. Compared to the porous polymer and polymer-ceramic composite, the modulus was higher. Though more reliable comparison could have been made, had the bone samples also been tested in simulated physiological conditions.

The cancellous bone samples were tested dynamically using two different testing speeds. Samples were dynamically tested with 0.5 Hz frequency for 500 cycles and with 1Hz frequency for 1000 cycles. Both tests had the overall duration of 1000 seconds. The amount of compressive load and stress was monitored. Figure 61 shows the decrease in stress with respect to the increasing cycles.

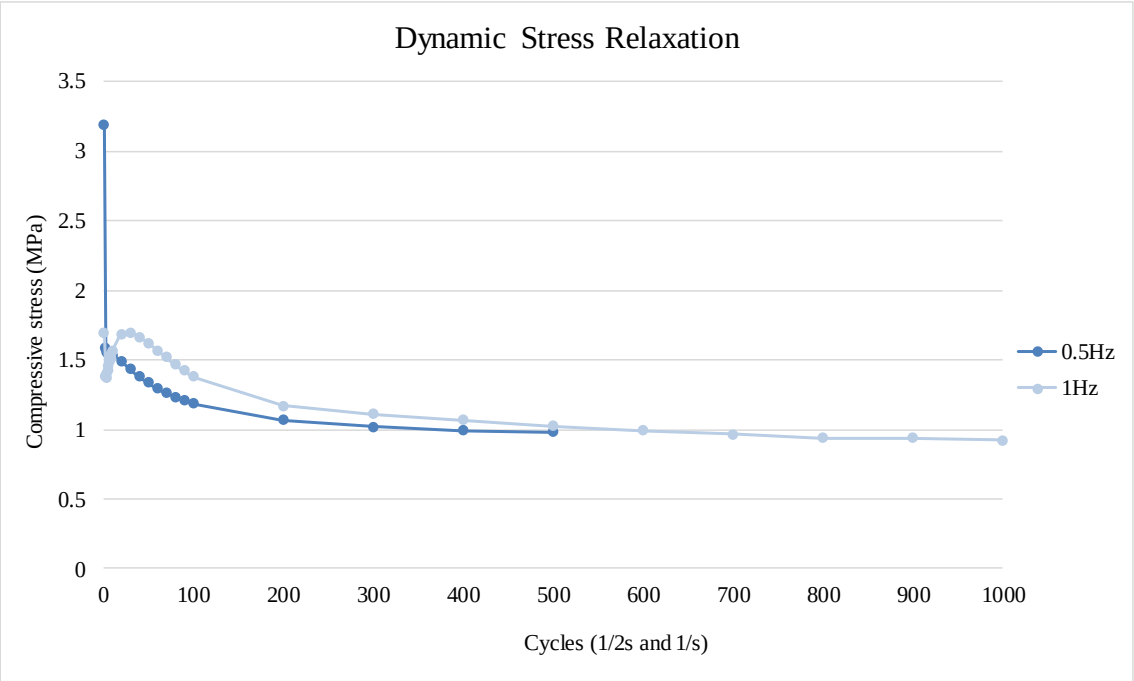

Figure 61. *The average dynamic stress relaxation of cancellous bone samples (0.5Hz n=4 (the standard deviation of stress range between ± 2.7 and ± 0.68)) and 1Hz n=3 (the standard deviation of stress range between ± 1.8 and ± 0.91))*

The outward appearance of the two different curves were very similar to the same curves by the dry porous scaffolds. The 0.5 Hz curve shape resembled that of PLCL, whereas the 1Hz resembled somewhat the PLCL-TCP50 curve. While, the 0.5 Hz curve experienced a steady decrease in the compressive forces, resulting in drop of the curve, that ultimately slowed down to a somewhat of a plateau, the 1Hz curve had an increase in the compressive forces that did not continue steadily, instead, the compressive forces returned to the initial amount in 20 cycles, after which the curve followed the same behavior as the 0.5 Hz.

While the slower testing speed resulted in higher compressive forces at the beginning, and 1 Hz had higher almost throughout the rest of the tests, in the end the compressive forces were practically the same as seen in Figure 62. Both test methods had large standard deviations with the parallel samples, most likely because the samples were taken from different locations from the femur.

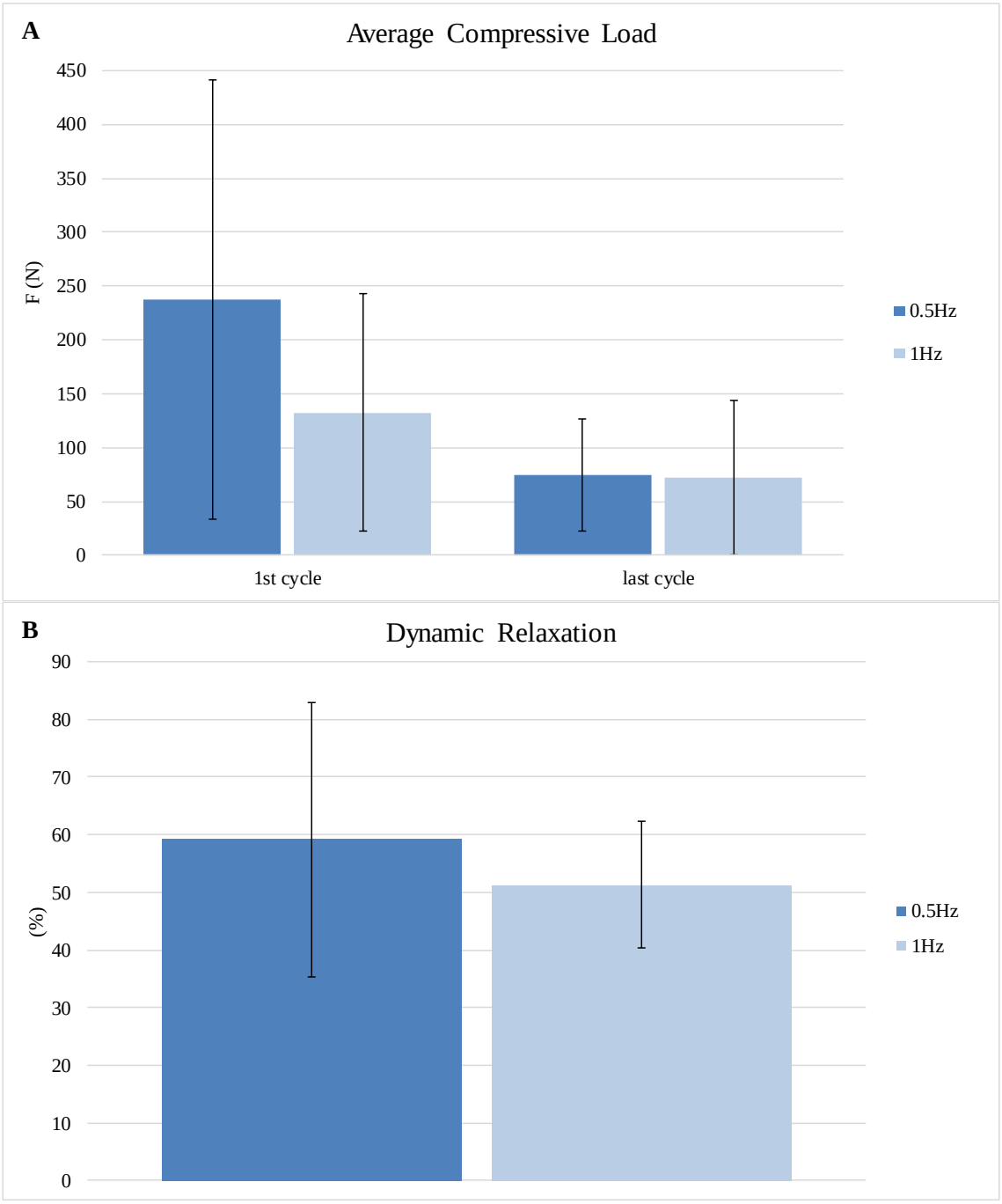

Figure 62. *The average load at first and last cycles and B. The average percentage change between the cycles (0.5Hz n=4, 1Hz n=3)*

Due to the fact that the initial stress and load was larger with the slower testing speed, the average percentage relaxation was also greater. The average percentage relaxation between the first and last cycle was 59.1 ± 23.8 % and 51.3 ± 11.1 % for 0.5 Hz and 1 Hz samples, respectively.

The results from the dynamic loading were also presented as stress-strain hysteresis curves (Figure 63) The loops were between 0 and 10 % strain.

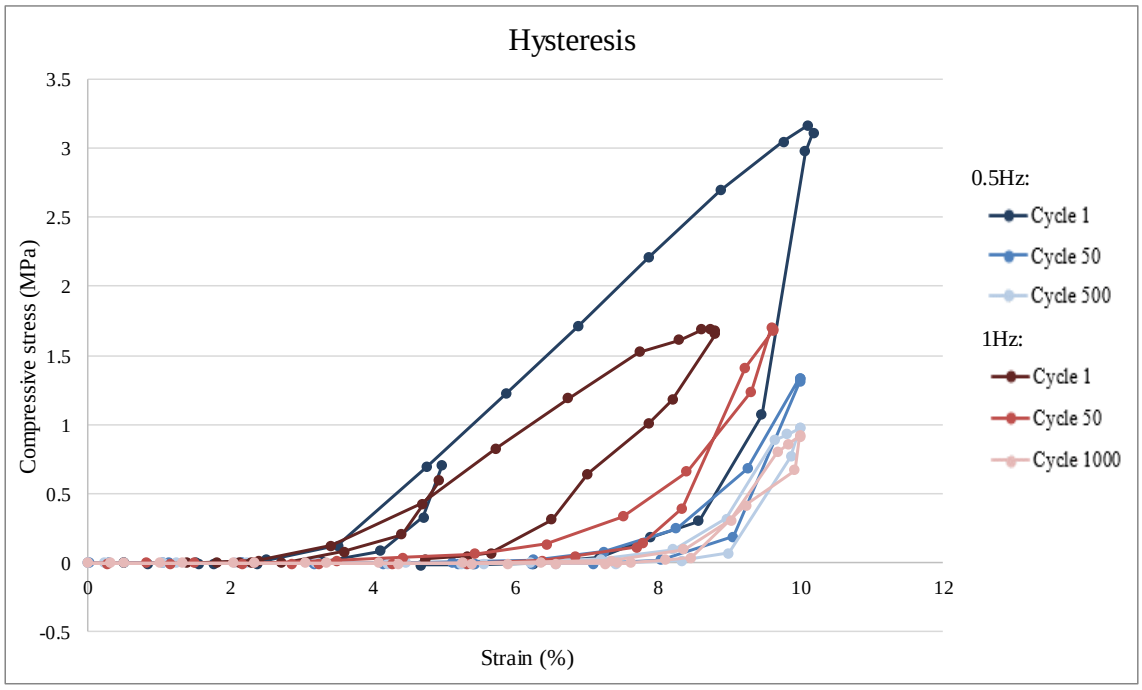

Figure 63. *The hysteresis curves of the cancellous bone (0.5Hz n=4 and 1Hz n=3)*

The biggest hysteresis loop was formed from the first cycle of the slower testing speed, meaning that the energy dissipation was greatest and more force was needed to compress to 10 % strain. It would also seem that the samples tested with 1 Hz retain more energy after the first cycle. Then again both first cycle hysteresis loops start after 2 % indicating that the initial ramp to 5 % before dynamic loading might have caused some initial permanent deformation. While the initial hysteresis loops can be distinguished, the final loops of the different testing speeds are practically the same, indicating that after 1000 seconds of testing bone might behave similarly independent of the testing speed.

Unlike in the other material tests, the machine had no problem delivering the wanted amount of deformation, indicating that the stiffer the material the easier it is for the testing machine to function.

8. CONCLUSIONS

The aim of this thesis was to study the static and dynamic mechanical behavior of polymer based biomaterials as scaffold constructs and as materials, as well as cancellous bone as a representative of biological tissue. The idea was also to test the samples in dry and simulated physiological conditions. The biomaterials were tested dry and after 2 days and/or 14 days in buffer solution, while the bone samples were tested only in dry environment but as moist by keeping them in buffer solution prior to testing.

Overall, the different mechanical tests showed that there is a difference between results obtained from dry environment and more physiologically simulated environment, making it clear that in order to test the mechanical behavior of materials and constructs intended to be used in the human body, normal laboratory environment is not enough to make reliable assumptions of the material behavior in the human body. The combination of aqueous and warmer environment result in softer and elastically behaving materials compared to the same materials in dry ambient laboratory environment.

While static mechanical tests can be used to determine basic mechanical properties as seen in the tests performed in this thesis, adding tests on dynamic mechanical behavior is vital when testing materials and constructs intended inside the human body. While the dynamic tests in this thesis were very basic, future considerations of testing should take into account the actual mechanical environment of the body and the different repeated loads a biomaterial implant experiences, be it in the MCP joint, the femur or in the hip. Instead of the simplified waveform used in this thesis, determining the correct fluctuations of load could be helpful when determining mechanical properties. Thus in the future, in addition to using simulated physiological condition of aqueous and 37 °C environment, using simulated mechanical environment should be considered.

In addition, the thesis also revealed that careful designing of test methods is important. While the testing machine can show some limitations due to the softness of polymer based materials, when testing viscoelastic materials, the test speed should be considered carefully. Also when comparing biomaterials to biological tissues, testing tissue samples should be considered instead of using values found in literature since test parameters are more comparable then and thus the results.

REFERENCES

[1] Callister WDJ. Mechanical Properties of Metals. Materials Science and Engineering - An Introduction. 7th ed.: John Wiley & Sons, Inc.; 2007. p. 131-173.

[2] Hosford WF. Stress and strain. Mechanical Behavior of Materials: Cambridge University Press; 2005. p. 1-20.

[3] Huang J, Guo ZX. Biomechanical and biochemical compatibility in innovative biomaterials. In: Boutrand J, editor. Biocompatibility and performance of medical devices: Woodhead Publishing Limited; 2012. p. 37-61.

[4] Chen Q, Thouas GA. Metallic implant biomaterials. Materials Science and Engineering: R: Reports 2015 1;87:1-57.

[5] Nakano T. Mechanical properties of metallic biomaterials. In: Niinomi M, editor. Metals for Biomedical Devices: Woodhead Publishing Limited; 2010. p. 71-98.

[6] Ong KL, Lovald S, Black J. Mechanical properties. Orthopaedic Biomaterials in Research and Practice. 2nd ed.: CRC Press; 2014. p. 53-76.

[7] Roeder RK. Mechanical Characterization of Biomaterials. In: Bandhyopadhya A, Bose S, editors. Characterization of Biomaterials: Elsevier Inc.; 2013. p. 49-109.

[8] Mano JF, Neves NM, Reis RL. Mechanical Characterization of Biomaterials. In: Reis RL, Román JS, editors. Biodegradable Systems in Tissue Engineering and Regenerative Medicine: CRC Press; 2004.

[9] Kaddick C. Mechanical testing for soft and hard tissue implants. In: Boutrand J, editor. Biocompatibility and performance of medical devices: Woodhead Publishing Limited; 2012. p. 362-380.

[10] Njeh CF, Nicholson PH, Rho J. Mechanical testing. In: Langton CM, Njeh CF, editors. The physical measurement of bone: Taylor & Francis; 2003.

[11] Ashby M, Shercliff H, Cebon D. Stiffness and weight: density and elastic modulus. Materials - engineering, sciense, processing and design: Elsevier Ltd; 2007. p. 48-79.

[12] Callister WDJ. Materials Selection and Design Considerations. Materials Science and Engineering - An Introduction. 7th ed.: John Wiley & Sons, Inc.; 2007. p. 143-191 (first pages).

[13] An YH, Bensen CV. General Considerations of Mechanical Testing. In: An YH, Draughn RA, editors. Mechanical Testing of Bone and the Bone Implant Interface: CRC Press; 2000. p. 119-132.

[14] An YH, Zioupos P, Smith CW. Factors Affecting Mechanical Properties of Bone. In: An YH, Draughn RA, editors. Mechanical testing of bone and the bone-implant interface: CRC Press LLC; 2000. p. 65-86.

[15] Hosford WF. Tensile testing. Mechanical Behaviour of Materials: Cambridge University Press; 2005. p. 39-52.

[16] Park J, Lakes RS. Characterization of Materials --- I. Biomaterials - an Introduction. 3rd ed. New York, NY: Springer New York; 2007. p. 42-81.

[17] Dieter GE. Mechanical Behavior Under Tensile and Compressive Loads. In: Kuhn H, Medlin D, editors. Mechanical testing and evaluation: ASM International; 2000.

[18] An YH. Mechanical Properties of Bone. In: An YH, Draughn RA, editors. Mechanical testing of bone and the bone-implant interface: CRC Press LLC; 2000. p. 41-64.

[19] Hutmacher DW, Schantz T, Zein I, Ng KW, Teoh SH, Tan KC. Mechanical properties and cell cultural response of polycaprolactone scaffolds designed and fabricated via fused deposition modeling. J Biomed Mater Res 2001;55(2):203-216.

[20] Ebewele RO. Chapter 13. Mechanical Properties of Polymers. Polymer Science and Technology: CRC Press; 2000.

[21] An YH, Barfield W, R., Draughn RA. Basic Concepts of Mechanical Property Measurement and Bone Biomechanics. In: An YH, Draughn RA, editors. Mechanical Testing of Bone and the Bone Implant Interface: CRC Press; 2000. p. 23-40.

[22] Ong KL, Lovald S, Black J. Viscoelasticity. Orthopaedic Biomaterials in Research and Practice. 2nd ed.: CRC Press; 2014. p. 77-99.

[23] Zhou Y, Yang L, Huang Y. Mechanical Properties of Polymer Materials. Micro- and Macromechanical Properties of Materials: CRC Press; 2013. p. 451-490.

[24] Chanda M, Roy SK. Plastics Properties and Testing. Plastics Technology Handbook. 4th ed.: CRC Press; 2006. p. 3-1-1-104.

[25] Thomopoulos S, Genin GM. Tendon and Ligament Biomechanics. : CRC Press; 2012. p. 49-74.

[26] Callister WDJ. Failure. Materials Science and Engineering - An Introduction. 7th ed.: John Wiley & Sons, Inc.; 2007. p. 207-251.

[27] Callister WDJ. Structures and Properties of Ceramics. Materials Science and Engineering - An Introduction. 7th ed.: John Wiley & Sons, Inc.; 2007. p. 414-459.

[28] Debski RE, Moore SM, Rainis EJ. Tendons and Ligaments, Mechanical Testing of. In: Wnek GE, Bowlin GL, editors. Encyclopedia of Biomaterials and Biomedical Engineering. 2nd ed.: CRC Press; 2008. p. 2588-2600.

[29] Woo SL, Nguyen TD, Liang R, Papas N. Tissue mechanics of ligaments and tendons. In: Kumar S, editor. Biomechanics in Ergonomics. 2nd ed.: CRC Press; 2007.

[30] Kieser J, Taylor M, Carr D. Developments in Forensic Science: Forensic Biomechanics. 1st ed.: John Wiley & Sons; 2012.

[31] Hosford WF. Fatigue. Mechanical Behaviour of Materials: Cambridge University Press; 2005. p. 279-309.

[32] Brown RB. Handbook of Polymer Testing: Short-Term Mechanical Tests. : Rapra Technology Limited; 2002.

[33] Jiles DC. Mechanical Testing Methods. Introduction to the Principles of Materials Evaluation: CRC Press; 2007. p. 99-122.

[34] O'Brien FJ. Biomaterials & scaffolds for tissue engineering. Materials Today 2011 3;14(3):88-95.

[35] Caeiro JR, González P, Guede D. Biomechanics and bone (&II): Trials in different hierarchical levels of bone and alternative tools for the determination of bone strength. Journal of Osteoporosis & Mineral Metabolism / Revista de Osteop 2013;5(2):99-108.

[36] Rho J, Kuhn-Spearing L, Zioupos P. Mechanical properties and the hierarchical structure of bone. Medical Engineering & Physics 1998;20:92-102.

[37] Huston RL. Tissue biomechanics. Principles of biomechanics: CRC Press; 2008.

[38] Martini F, H., Nath J, L. Fundamentals of Anatomy and Physiology. 8th ed. San Francisco: Pearson/Benjamin Cummings; 2009.

[39] Burgess EA, Hollinger JO. Options for Engineering Bone. In: Patrick CW, Mikos AG, McIntire LV, editors. Frontiers in Tissue Engineering: Pergamon; 1998. p. 383-399.

[40] Hutmacher DW, Schantz JT, Lam CX, Tan KC, Lim TC. State of the art and future directions of scaffold-based bone engineering from a biomaterials perspective. Journal of Tissue Engineering and Regenerative Medicine 2007;1(4):245-260.

[41] Pal S. Mechanical Properties of Biological Materials. Design of Artificial Human Joints & Organs. 1st ed.: Springer US; 2014. p. 23-40.

[42] Qin Q. Introduction to Bone Materials. Mechanics of Cellular Bone Remodeling Coupled Thermal, Electrical, and Mechanical Field Effects: CRC Press; 2013. p. 1-24.

[43] Spauwen PHM, Jansen JA, Ruhe PQ, Wolke JGC. Calcium Phosphate Ceramics for Bone Tissue Engineering. : CRC Press; 2007. p. 9-1-9-18.

[44] Hart R, Natali A, Pavan P, Knets I. Mechanics of bone tissue. In: Natali A, editor. Dental Biomechanics: CRC Press; 2003. p. 1-19.

[45] Ong KL, Lovald S, Black J. Properties of Natural Materials. Orthopaedic Biomaterials in Research and Practice. 2nd ed.: CRC Press; 2014. p. 101-130.

[46] Shore SW, Unnikrishnan GU, Hussein AI, Morgan EF. Bone Biomechanics. In: Winkelstein BA, editor. Othopaedic biomechanics: CRC Press; 2012. p. 3-47.

[47] Pruitt LA, Chakravartula AM. Mechanical behaviour of structural tissues. Mechanics of Biomaterials - Fundamental Principles for Implant Design: Cambridge University Press; 2012. p. 129-163.

[48] Laasanen MS, Töyräs J, Korhonen RK, Rieppo J, Saarakkala S, Nieminen MT, et al. Biomechanical properties of knee articular cartilage. Biorheology 2003;40:133-140.

[49] Morrell KC, Hodge WA, Krebs DE, Mann RW. Corroboration of in vivo cartilage pressures with implications for synovial joint tribology and osteoarthritis causation. Proc Natl Acad Sci U S A 2005 10/03;102(41):14819-14824.

[50] Kennedy FE, Van Citters DW. Natural and Artificial Human Joints. In: Bruce RW, editor. Handbook of Lubrication and Tribology, Volume II Theory and Design. 2nd ed.: CRC Press; 2012. p. 1-20.

[51] Wayne JS. Articular cartilage biomechanics. In: Wnek GE, Bowlin GL, editors. Encyclopedia of biomaterials and biomedical engineering. 2nd ed.: CRC Press; 2008. p. 85-94.

[52] Mow VC, Gu WY, Chen FH. Structure and function of articular cartilage and meniscus. In: Mow VC, Huiskes R, editors. Basic Orthopaedic Biomechanics and Mechano-Biology. 3rd ed.: Wolters Kluwer; 2004. p. 181.

[53] Schinagl RM, Gurskis D, Chen AC, Sah RL. Depth-dependent confined compression modulus of full-thickness bovine articular cartilage. Journal of Orthopaedic Research 1997;15(4):499-506.

[54] Athanasiou KA, Rosenwasser MP, Buckwalter JA, Malinin TI, Mow VC. Interspecies comparisons of in situ intrinsic mechanical properties of distal femoral cartilage. Journal of Orthopaedic Research 1991;9(3):330-340.

[55] Haut RC, Powlison AC. The effects of test environment and cyclic stretching on the failure properties of human patellar tendons. Journal of Orthopaedic Research 1990;8(4):532-540.

[56] Guo C, Spector M. Tissue Engineering of Tendons and Ligaments. In: Ma PX, Elisseeff J, editors. Scaffolding in Tissue Engineering: CRC Press; 2005. p. 385-411.

[57] Woo SL, Lee TQ, Abramowitch SD, Gilbert TW. Structure and function of ligaments and tendons. In: Mow VC, Huiskes R, editors. Basic Orthopaedic Biomechanics and Mechano-Biology. 3rd ed.: Wolters Kluwer; 2004. p. 301.

[58] Johnson GA, Tramaglini DM, Levine RE, Ohno K, Choi N, L-Y. Woo S. Tensile and viscoelastic properties of human patellar tendon. Journal of Orthopaedic Research 1994;12(6):796-803.

[59] Wren TAL, Yerby SA, Beaupré GS, Carter DR. Mechanical properties of the human achilles tendon. Clin Biomech 2001 3;16(3):245-251.

[60] Woo SL, Orlando CA, Gomez MA, Frank CB, Akeson WH. Tensile properties of the medial collateral ligament as a function of age. Journal of Orthopaedic Research 1986;4(2):133-141.

[61] Pioletti DP, Rakotomanana LR, Leyvraz P-. Strain rate effect on the mechanical behavior of the anterior cruciate ligament–bone complex. Med Eng Phys 1999 3;21(2):95-100.

[62] Pal S. The Finger Joint and its Artificial Replacement. Design of Artificial Human Joints & Organs. 1st ed.: Springer US; 2014. p. 167-175.

[63] Ash HA, Joyce TJ, Unsworth A. Biomechanics of the distal upper limb. Current Orthopaedics 1996 1;10(1):25-36.

[64] Gibson I, Chow PS, Lam WK, Lu WW, Ngan WAH, Yip YW, et al. The Development of an Artificial Finger Joint. In: Bartolo P, Bidanda B, editors. Bio-Materials and Prototyping Applications in Medicine Boston, MA: Springer US; 2008. p. 157-190.

[65] Joyce TJ, Unsworth A. A test procedure for artificial finger joints. Proceedings of the Institution of Mechanical Engineers, Part H: Journal of Engineering in Medicine 2002 February 01;216(2):105-110.

[66] Waris E, Ashammakhi N, Lehtimäki M, Tulamo R, Kellomäki M, Törmälä P, et al. The use of biodegradable scaffold as an alternative to silicone implant arthroplasty for small joint reconstruction: An experimental study in minipigs. Biomaterials 2008 2;29(6):683-691.

[67] Honkanen PB, Kellomäki M, Lehtimäki MY, Törmälä P, Mäkelä S, Lehto MKU. Bioreconstructive Joint Scaffold Implant arthroplasty in Metacarpophalangeal Joints: Short-term Results of a New Treatment Concept in Rheumatoid Arthritis Patients. Tissue engineering 2004;9(5):957-965.

[68] Honkanen PB, Kellomäki M, Konttinen YT, Mäkelä S, Lehto MUK. A Midterm Follow-Up Study of Bioreconstructive Polylactide Scaffold Implants in Metacarpophalangeal Joint Arthroplasty in Rheumatoid Arthritis Patients. Journal of Hand Surgery (European Volume) 2009 April 01;34(2):179-185.

[69] Bergmann G, Deuretzbacher G, Heller M, Graichen F, Rohlmann A, Strauss J, et al. Hip contact forces and gait patterns from routine activities. J Biomech 2001 7;34(7):859-871.

[70] Stewart TD, Hall RM. (iv) Basic biomechanics of human joints: Hips, knees and the spine. Current Orthopaedics 2006 2;20(1):23-31.

[71] Hashimoto N, Ando M, Yayama T, Uchida K, Kobayashi S, Negoro K, et al. Dynamic Analysis of the Resultant Force Acting on the Hip Joint During Level Walking. Artif Organs 2005;29(5):387-392.

[72] Lunn DE, Lampropoulos A, Stewart TD. Basic biomechanics of the hip. Orthopaedics and Trauma 2016 6;30(3):239-246.

[73] Kutzner I, Heinlein B, Graichen F, Bender A, Rohlmann A, Halder A, et al. Loading of the knee joint during activities of daily living measured in vivo in five subjects. J Biomech 2010 8/10;43(11):2164-2173.

[74] Bergmann G, Bender A, Graichen F, Dymke J, Rohlmann A, Trepczynski A, et al. Standardized Loads Acting in Knee Implants. PLoS ONE 2014 01/23;9(1):1-12.

[75] Shelburne KB, Torry MR, Pandy MG. Muscle, Ligament, and Joint-Contact Forces at the Knee during Walking. Medicine & Science in Sports & Exercise 2005;37(11):1948-1956.

[76] Eckstein F, Lemberger B, Gratzke C, Hudelmaier M, Glaser C, Englmeier K, et al. In vivo cartilage deformation after different types of activity and its dependence on physical training status. Annals of the Rheumatic Diseases 2005;64(2):291-295.

[77] Roddy E, Zhang W, Doherty M. Aerobic walking or strengthening exercise for osteoarthritis of the knee? A systematic review. Annals of the Rheumatic Diseases 2005 April 01;64(4):544-548.

[78] Paakinaho K. Processing Derived Control of Hydrolytic degradation and Generation of Shape-Memory in Lactide Copolymers; 2013.

[79] Ahola N, Männistö N, Veiranto M, Karp M, Rich J, Efimov A, et al. An in vitro study of composites of poly(L-lactide-co-e-caprolactone), b-tricalcium phosphate and ciprofloxacin intended for local treatment of osteomyelitis. Biomatter 2012 12/07;3(2):e23162-1-e23162-13.

[80] Malin M, Hiljanen-Vainio M, Karjalainen T, Seppälä J. Biodegradable lactone copolymers. II. Hydrolytic study of ε-caprolactone and lactide copolymers. J Appl Polym Sci 1996;59(8):1289-1298.

[81] Södergård A, Stolt M. Properties of lactic acid based polymers and their correlation with composition. Progress in Polymer Science 2002 7;27(6):1123-1163.

[82] Freeman JW, Woods MD, Laurencin CT. Tissue Engineering of the Anterior Cruciate Ligament Using a Braid-Twist Scaffold Design. J Biomech 2006 11/13;40(9):2029-2036.

[83] Ellä V, Annala T, Länsman S, Nurminen M, Kellomäki M. Knitted polylactide 96/4 L/D structures and scaffolds for tissue engineering: Shelf life, in vitro and in vivo studies. Biomatter 2011 07/01;1(1):102-113.

[84] Ellä V, Gomes ME, Reis RL, Törmälä P, Kellomäki M. Studies of P(L/D)LA 96/4 non-woven scaffolds and fibres; properties, wettability and cell spreading before and after intrusive treatment methods. J Mater Sci Mater Med 2007;18(6):1253-1261.

[85] Wang X, Han C, Hu X, Sun H, You C, Gao C, et al. Applications of knitted mesh fabrication techniques to scaffolds for tissue engineering and regenerative medicine. Journal of the Mechanical Behavior of Biomedical Materials 2011 10;4(7):922-932.

[86] Laurent CP, Durville D, Mainard D, Ganghoffer J, Rahouadj R. A multilayer braided scaffold for Anterior Cruciate Ligament: Mechanical modeling at the fiber scale. Journal of the Mechanical Behavior of Biomedical Materials 2012 8;12:184-196.

[87] Haaparanta A, Haimi S, Ellä V, Hopper N, Miettinen S, Suuronen R, et al. Porous polylactide/β-tricalcium phosphate composite scaffolds for tissue engineering applications. Journal of Tissue Engineering and Regenerative Medicine 2010;4(5):366-373.

[88] Arahira T, Maruta M, Matsuya S, Todo M. Development and characterization of a novel porous β-TCP scaffold with a three-dimensional PLLA network structure for use in bone tissue engineering. Mater Lett 2015 8/1;152:148-150.

[89] Viswanath B, Raghavan R, Gurao NP, Ramamurty U, Ravishankar N. Mechanical properties of tricalcium phosphate single crystals grown by molten salt synthesis. Acta Biomaterialia 2008 9;4(5):1448-1454.

[90] Lin F, Chen T, Lin C, Lee C. The Merit of Sintered PDLLA/TCP Composites in Management of Bone Fracture Internal Fixation. Artif Organs 1999;23(2):186-194.

[91] Yang Y, Zhao Y, Tang G, Li H, Yuan X, Fan Y. In vitro degradation of porous poly(l-lactide-co-glycolide)/β-tricalcium phosphate (PLGA/β-TCP) scaffolds under dynamic and static conditions. Polym Degrad Stab 2008 10;93(10):1838-1845.

[92] Liu C, Abedian R, Meister R, Haasper C, Hurschler C, Krettek C, et al. Influence of perfusion and compression on the proliferation and differentiation of bone mesenchymal stromal cells seeded on polyurethane scaffolds. Biomaterials 2012 2;33(4):1052-1064.

[93] Kang Y, Yao Y, Yin G, Huang Z, Liao X, Xu X, et al. A study on the in vitro degradation properties of poly(l-lactic acid)/β-tricalcuim phosphate(PLLA/β-TCP) scaffold under dynamic loading. Med Eng Phys 2009 6;31(5):589-594.

[94] Ramakrishna S, Mayer J, Wintermantel E, Leong KW. Biomedical applications of polymer-composite materials: a review. Composites Sci Technol 2001 7;61(9):1189-1224.

[95] Mutanen M . Studies of Bioreconstructive Small-Joint Prostheses; 2004.

[96] Ahola N, Veiranto M, Rich J, Efimov A, Hannula M, Seppälä J, et al. Hydrolytic degradation of composites of poly(L-lactide-co-ε-caprolactone) 70/30 and β-tricalcium phosphate. Journal of Biomaterials Applications 2013 November 01;28(4):529-543.

[97] Paakinaho K, Heino H, Pelto M, Hannula M, Törmälä P, Kellomäki M. Programmed water-induced shape-memory of bioabsorbable poly(d,l-lactide): activation and properties in physiological temperature. J Mater Sci Mater Med 2012;23(3):613-621.

[98] Paakinaho K, Hukka TI, Kastinen T, Kellomäki M. Demonstrating the Mechanism and Efficacy of Water-Induced Shape-Memory and the Influence of Water on the Thermal Properties of Oriented Poly(D,L-lactide). J Mater Sci Mater Med 2013;130(6):4209-4218.

[99] Sasaki N. Viscoelastic properties of bone and testing methods. In: An YH, Draughn RA, editors. Mechanical Testing of Bone and the Bone Implant Interface: CRC Press; 2000. p. 329-348.

[100] Kalaba S, Gerhard E, Winder JS, Pauli EM, Haluck RS, Yang J. Design strategies and applications of biomaterials and devices for Hernia repair. Bioactive Materials 2016 9;1(1):2-17.

[101] Sartoneva R, Haaparanta A, Lahdes-Vasama T, Mannerström B, Kellomäki M, Salomäki M, et al. Characterizing and optimizing poly-l-lactide-co-e-caprolactone membranes for urothelial tissue engineering. Journal of The Royal Society Interface 2012;9(77):3444-3454.

[102] Hillam RA, Goodship AE, Skerry TM. Peak strain magnitudes and rates in the tibia exceed greatly those in the skull: An in vivo study in a human subject. J Biomech 2015 9/18;48(12):3292-3298.

[103] Hiljanen-Vainio M, Karjalainen T, Seppälä J. Biodegradable lactone copolymers. I. Characterization and mechanical behavior of ε-caprolactone and lactide copolymers. J Appl Polym Sci 1996;59(8):1281-1288.

[104] Dennerlein JT, Kingma I, Visser B, van Dieën JH. The contribution of the wrist, elbow and shoulder joints to single-finger tapping. J Biomech 2007;40(13):3013-3022.

[105] Thorwarth M, Schultze-Mosgau S, Kessler P, Wiltfang J, Schlegel KA. Bone Regeneration in Osseous Defects Using a Resorbable Nanoparticular Hydroxyapatite. Journal of Oral and Maxillofacial Surgery 2005 11;63(11):1626-1633.

[106] Li Y, Chen S, Li L, Qin L, Wang X, Lai Y. Bone defect animal models for testing efficacy of bone substitute biomaterials. Journal of Orthopaedic Translation 2015 7;3(3):95-104.

[107] Pearce AI, Richards RG, Milz S, Schneider E, Pearce SG. Animal Models for Implant Biomaterial Research in Bone: A Review. European Cells and Materials 2007;13:1-10.